MASTER'S THESIS

Experimental methods to study the process of snow-ice formation induced by saltwater rise

Presented by

Yannick Kern

Supervisors

Dr. Chris Borstad, The University Centre in Svalbard, Longyearbyen, Norway

Dr. Dirk Notz, Max Planck Institut für Meteorologie, Hamburg, Germany

Prof. Dr. Frank Nilsen, The University Centre in Svalbard, Longyearbyen, Norway

Master's Programme in Meteorology and Oceanography

Specialisation in Physical Oceanography

Geophysical Institute

UNIVERSITY OF BERGEN

September 2018

The presented research in this thesis is part of my master studies in the Geophysical Institute of the University of Bergen and was performed in the Geophysics Department of The University Centre in Svalbard between September 2017 and September 2018. All presented work is my own and this thesis does not contain any work of other people without being appropriately stated and provided in the bibliography. None of the content in this thesis has been used in other examinations and has not been submitted or published before at UiB or at any other educational institutions in Norway or abroad.

Abstract

The Arctic region is experiencing a change from thick multiyear to much younger and thinner sea ice. In many places, increasing precipitation is leading to higher snow loads on young sea ice. Hence seawater can infiltrate the snow layer through pathways in the ice from below or from the side. Consequently parts of the snow layer may form a slushy layer that can freeze and form so called "snow ice". Involved processes have substantial impacts on sea ice and snow in terms of salinity and temperature. The spatial and temporal evolution of these is still only poorly understood. In this context my study concentrates on the establishment of unique measurement methods to investigate thermodynamics, temperature evolution and salt rejection during snow-ice formation. For the investigation of saltwater rise in snow and subsequent freezing I adapt existing methods from sea-ice investigations to the application in snow. I developed two new cost-efficient experimental setups in the cold laboratory environment at the University Centre in Svalbard to first, investigate saltwater rise in snow and second, realistically represent floating ice and vertical flooding. The salinity harp installed in snow and sea ice provides a non-destructive method to measure the impedance and temperature at high temporal and spatial resolution. Within the scope of 14 experiments at different parameter setups I find salinity of the flooding water to be the predominant driver of water rise and freezing. Results suggest a transition with time and height from capillary rise to freezing and brine drainage in the initial 24 h after flooding if initial temperatures between flooding water and pre-existing snow differ. Furthermore, first results of vertical flooding of floating ice highlight the capability of the new experimental setup. Characteristics indicate that ocean water displaces brine in sea ice which is pushed to the ice-snow interface and wets the snow. The presented methods provide a promising foundation for further investigations of vertical rise of water through sea ice and subsequent snow-ice formation.

Contents

List of Figures

List of Tables

1 Motivation

The effects of the ongoing global warming on the cryosphere are subject to many present scientific studies and play an important role in the understanding of the earth system. In the Arctic regions sea-ice retreat and sea-ice thinning are leading to a prevalence of younger and thinner sea ice (e.g. *Lindsay and Schweiger*, 2015). A much thicker cover of snow on sea ice has been found in recent measurements compared to what is assumed in most models so far and snow is found to contribute more to sea-ice mass balance than originally thought (*Granskog et al.*, 2017).

Usually the role of snow on sea ice is related to its insulating role and its high albedo. It prevents ice growth in winter and melt in summer. However, if distinct precipitation events coincide with the prevalent presence of thin ice (e.g. young ice) large areas of sea ice gain a negative freeboard and seawater can flood the ice. Brine and seawater may infiltrate the snow from below through available pathways in the sea ice or horizontally from the side. Meltwater and precipitation at the snow surface can enter the snow from the top. Hence, a slushy wet snow layer may form on top of the sea ice, which can freeze and thereby contribute to ice growth as so called "snow ice".

In the Arctic regions like the Barents Sea, *Saloranta* (2000) observed that 10–30 % of the sea ice was composed of snow ice. In 2015 a contribution of snow up to on average 7.5–9.7 % on sea-ice mass balance was measured from ice cores in the drift ice north of Svalbard (*Granskog et al.*, 2017). Recent studies like the N-ICE2015 field campaign (e.g. *Provost et al.* (2017); *Granskog et al.* (2017) and *Rösel et al.* (2018)) highlight the existence of snow ice, its increasing contribution to sea-ice mass and illustrate the importance of understanding involved processes in snow-ice formation in the Arctic.

Relevant literature based on laboratory experiments is provided by *Matt* (2014) who studied the movement of a waterfront through snow on ice as a result of horizontal flooding and *Coléou et al.* (1999) who studied the capillary rise of freshwater in wet snow. Since sea ice does not usually crack under thermally induced stress, flooding must depend on brine channels in the ice (*Crocker and Wadhams*, 1989). On the other hand results by *Matt* (2014) suggest the hypothesis that close to the sea-ice edge, and on smaller sheets of ice, horizontal flooding and movement of seawater as result of a negative freeboard would be the dominant process.

From a thermodynamic point of view snow on sea ice is currently still rather crudely represented in coupled sea-ice models and improved measurements are needed to increase the understanding of the fundamental functioning of today's sea-ice cover (*Notz*, 2012). *Jutras et al.* (2016) realised laboratory experiments that confirm an appropriate implementation of the energetics of slush and snow-ice formation in most sea-ice models. However, according to the authors large uncertainties are still related to the lack of information about the salinity of the flooding water. They emphasise

the further need of laboratory work to improve the understanding of the contribution of brine and seawater to flooding. Moreover, *Jutras et al.* (2016) suggests the use of non-destructive measurements as proposed by *Notz et al.* (2005) to improve the understanding of the spatial and temporal salt and temperature evolution of snow-ice formation after flooding.

In my project I follow up on work of *Jutras et al.* (2016) using the suggested non-destructive methods (*Notz et al.*, 2005) to answer the scientific question of how salinity and temperature change, spatially and temporally during the process of flooding, formation of a slushy layer and freezing. First, I introduce relevant background (Sec. 2) and present the utilised instruments for my study (Sec. 3). I am focusing on the investigation of vertical flooding to address snow-ice formation further away of the sea-ice edge and representative for large sheets of ice. Therefore, I am introducing a new set of methods (Sec. 4) and experimental setups to investigate saltwater rise in snow (Sec. 5) and to represent flooding on floating sea ice (Sec. 6) in a cold laboratory environment. My work is providing a foundation for future in-deph investigations of water rise and snow-ice formation. In the end a draw conclusions on the presented work and provide an outlook for follow-up studies (Sec. 7).

2 Background

In my study I am referring to the physical properties of snow, sea ice and seawater. Within this section I am presenting an overview of equations and properties of these mediums relevant for my studies. My focus lays on the snow-ice interaction rather than providing an overall detailed background.

2.1 Seawater

One of the main quantities describing the properties of seawater is its salt content. The so called salinity S describes the fraction of dissolved salt within water. It is the fraction of mass of salt m_s (mainly NaCl) relative to the total mass of the seawater and it is defined by

$$S = \frac{m_\mathrm{s}}{m_\mathrm{s} + m_\mathrm{f}} \tag{2.1}$$

where m_f is the mass of fresh water. Salinity is usually given in $\mathrm{g\,kg^{-1}}$. Exemplary values at the surface in the Arctic Ocean are around $32\,\mathrm{g\,kg^{-1}}$ (*Aagaard et al.*, 1981).

In winter, when air temperatures are below the ocean temperatures heat is lost into the atmosphere. Subsequently, the temperature of seawater is decreasing until it eventually reaches its freezing temperature $T_\mathrm{f,sw}$. In literature the freezing temperature of saltwater is often referred to as liquidus temperature which is a physically more appropriate description. It defines the temperature of a multi-component medium at which crystals start to form (*Notz*, 2005). For seawater $T_\mathrm{f,sw}$ can be calculated by

$$T_\mathrm{f,sw} = -0.0575S + 1.710523 \cdot 10^{-3} S^{\frac{3}{2}} - 2.154996 \cdot 10^{-4} S^2 - 7.53 \cdot 10^{-4} p \tag{2.2}$$

where p is the atmospheric pressure in decibar. The equation is given by *Fofonoff and Millard Jr* (1983) and was originally proposed by *Millero and Leung* (1976) who derived it based on measurements by *Doherty and Kester* (1974) for salinities between $4\,\mathrm{g\,kg^{-1}}$ and $40\,\mathrm{g\,kg^{-1}}$. Within this range Eq. 2.2 fits measurements by $\pm 0.0003\,\mathrm{K}$ on average (*Millero and Leung*, 1976).

In laboratory environment it is often not possible to use seawater. Typically a NaCl solution is used instead (e.g. *Notz et al.* (2005); *Jutras et al.* (2016) and *Fuchs* (2017)). *Notz* (2005) defined a polynomial fit to measurements by *Weast et al.* (1989) to describe the liquidus temperature of NaCl solutions

$$T_\mathrm{f,NaCl} = -0.0592S - 9.37 \cdot 10^{-6} S^2 - 5.33 \cdot 10^{-7} S^3 \tag{2.3}$$

where $T_\mathrm{f,NaCl}$ is in °C and S is the concentration of NaCl in ppt.

2.2 Sea ice

As soon as seawater reaches its freezing temperature at approximately −1.8 °C sea ice starts to form. If air temperatures stay below the freezing point, heat from the ice-ocean interface is conducted through the ice and released into the air. Imbalances in case of a lower ocean heat flux and a higher upwards heat flux are compensated by further sea-ice formation and ice thickness increases (*Notz*, 2005). Different to freshwater ice, sea ice is a very complex medium. It is defined by a mixture of solid ice and liquid brine (*Notz*, 2005). The fraction of the ice, the so called solid fraction is always salt free. Thus, salt released during the freezing of ocean water increases the salinity of the liquid fraction i.e. brine.

The boundary between the liquid brine and the solid ice is described by a dynamic equilibrium (*Kim and Yethiraj*, 2008). According to *Notz* (2005), in sea ice the freezing temperature of the brine always equals the local temperature because brine and ice must always be in phase equilibrium. Hence, if the local temperature changes it also affects the brine salinity. In case of cooling, parts of the water of brine freeze, forming more pure ice and releasing salt. Therefore, the brine salinity increases, leading to a lower freezing temperature of the brine which equals the colder local temperature. Accordingly, increasing temperatures are related to freshening of the brine and increasing its freezing temperature. *Notz* (2005) further describes the re-establishment of the equilibrium to be almost simultaneous. To find a relation between the brine salinity S_br and temperature T he fitted an equation to measurements by *Assur* (1958) to receive the relation

$$S_{\mathrm{br,sw}} = -1.20 - 21.8T - 0.919T^2 - 0.0178T^3. \tag{2.4}$$

The brine concentration in sea ice $S_{\mathrm{br,sw}}$ is given in $\mathrm{g\,kg^{-1}}$ and the sea-ice temperature T is in °C with a validity of the equation in the range between −2 °C and −22.9 °C. Eq. 2.3 can be numerically inverted to obtain an equation for the concentration (in $\mathrm{g\,kg^{-1}}$) of the interstitial brine of NaCl ice

$$S_{\mathrm{br,NaCl}} = -17.6T - 0.388T^2 - 0.00361T^3 \tag{2.5}$$

where T is the ice temperature in °C (*Notz*, 2005). Both relationships, Eq. 2.4 and Eq. 2.5 can be combined with measurements of the liquid mass fraction ϕ_{l} to receive the bulk salinity

$$S_{\mathrm{bu}} = S_{\mathrm{br}} \cdot \phi_{\mathrm{l}} \tag{2.6}$$

in sea ice (*Notz et al.*, 2005). The bulk salinity describes the salt within a defined ice volume i.e. the salinity of the volume after it is completely melted. If no salt or liquid is taken out, the bulk salinity stays constant during freezing or melting. A higher liquid fraction is related to less saline brine and vice versa in case of lower liquid fraction which is in accordance to the described freezing

temperature and salinity relation above.

In case the bulk salinity changes so-called desalination processes lead to redistribution or brine release from the ice. *Notz and Worster* (2009) discuss five processes, mainly named in literature in connection with desalination: brine diffusion, initial brine entrapment, brine expulsion, flushing and gravity drainage. They show that only gravity drainage and flushing by surface meltwater show measurable net loss of salt.

Gravity drainage is related to the brine densities increasing with salinity (*Fuchs*, 2017). If ice is cooled from above the density profile of brine becomes unstable due to the maintained phase equilibrium (*Notz and Worster*, 2009). The density is highest at the top of the ice. If the permeability of the ice increases a convective overturn may lead to some of the more dense brine replaced with underlying seawater. Consequently, the bulk salinity decreases. *Martin* (1979) describe growing brine channels in warming ice which leads to such a change of permeability of ice for instance.

Flushing is related to the presence of meltwater on top of the ice. The effect is similar to gravity drainage but here the meltwater causes the pressure overhead on the brine from the top (*Notz*, 2005). Such features may be present during summer when air temperatures increase and melting is induced from the top. Then also sea ice is warmer and more permeable. Consequently, meltwater flushes brine out of the ice, replacing it and thus decreasing the bulk salinity of the sea ice.

According to *Notz* (2005) the relation Eq. 2.6 is strictly valid for the liquid mass fraction. He provides an equation to transfer the solid volume fraction $\phi_{\mathrm{s,v}}$ into the solid mass fraction $\phi_{\mathrm{s,m}}$ by

$$\phi_{\mathrm{s,m}} = \frac{1}{1 + \left(\frac{1}{\phi_{\mathrm{s,v}}} - 1\right) \frac{\rho_{\mathrm{l}}}{\rho_{\mathrm{s}}}}. \tag{2.7}$$

By using $\phi_{\mathrm{s}} = 1 - \phi_{\mathrm{l}}$ the same relationship can be defined for the liquid mass fraction

$$\phi_{\mathrm{l,m}} = \frac{1}{1 + \left(\frac{1}{\phi_{\mathrm{l,v}}} - 1\right) \frac{\rho_{\mathrm{s}}}{\rho_{\mathrm{l}}}}. \tag{2.8}$$

Here ρ_{s} and ρ_{l} is the density of the solid or liquid.

2.3 Snow

After or during the growth of ice snow may accumulate on top of sea ice. Several processes like metamorphism, more accumulation, intermittent meltwater or brine migration lead to a formation of a complex snow pack on top of sea ice (*Massom et al.*, 2001). Furthermore, snow on top of sea ice is isolating. It conducts heat at lower rates compared to sea ice. Consequently, the vertical temperature gradient in snow is stronger compared to the one in sea ice. This results in warming of

sea ice if snow accumulates on sea ice which has been exposed to cold air temperatures before. As already mentioned above this leads to a growth of brine channels and increase of the permeability of the sea ice.

A standard snow profile on top of sea ice is usually characterised by a depth hoar layer close to the ice-snow interface, a wind slab with intermittent icy layers and the snow surface (*Massom et al.*, 2001). To classify different layers in snow it is important to understand the process of metamorphism. *Sommerfeld and LaChapelle* (1970) proposes the division of different types based on (I) mechanical damage, (II) water vapour transport at constant temperature, (III) water vapour transport along a thermal gradient and (IV) firnification (Fig. A.1). Based on these processes snow grains change their original shape over time and the structure of the snow profile changes. I used this classification to identify different types of used snow grains in my experiments. Snow is further characterised by the properties grain size (or grain size distribution), density, temperature, wetness and bonding. The latter is related to the strength of the snow i.e. building bond between crystals (*Massom et al.*, 2001).

If distinct precipitation events coincide with the prevalent presence of thin ice (e.g. young ice) large areas of sea ice gain a negative freeboard. As a result brine and seawater can flood the ice where brine channels or cracks connect the ice surface and ocean (*Massom et al.*, 2001). Consequently, brine and seawater infiltrates the snow. Depending on the pathways flooding occurs vertically or horizontally or at a combination of both. Close to the sea-ice edge or along large cracks horizontal is dominant as described by *Matt* (2014). He finds the horizontal movement of snow dependent on rates of refreezing which slow down further penetration of water into snow. Furthermore, capillary suction is the reason for water rising in snow. *Coléou et al.* (1999) investigated the rise of freshwater in snow and observed decreasing liquid fractions of the pore volume with height. Furthermore, meltwater and precipitation at the snow surface can enter the snow from the top. In either case a slushy wet snow layer may form on top of the sea ice which can freeze and form snow ice.

3 Instruments

A various amount of different types of instruments is available to investigate properties of seawater, sea ice and snow. For the purpose of my study I mainly used one specific instrument the so called salinity harp. In this section I present the fundamental theory the instrument is based on and explain operating procedures. Additionally, I introduce a new light harp instrument that I tested for my objectives and give an overview to the other instruments I used during my study either as reference or to capture additional quantities.

3.1 The salinity harp

The salinity harp (Fig. 3.1a) is based on an instrument by *Shirtcliffe et al.* (1991). It was established by *Notz et al.* (2005) and further developed by the *Sea ice in the Earth system* working group at the Max-Planck Institute for Meteorology (MPI-M). By a non-destructive technique the instrument allows to measure the impedance of a measurement volume like sea ice with high temporal and spatial resolution. Furthermore, based on those impedance measurements it is possible to infer the solid and liquid fraction of the volume and estimate the evolution of the bulk salinity (*Notz et al.*, 2005). In the following I recapitulate the measurement principle of the harp and the related theory (cf. *Shirtcliffe et al.* (1991); *Notz et al.* (2005) and *Fuchs* (2017)).

Every 2 cm the harp has two horizontal parallel titanium wires with a length of 16 cm. Between each pair of wires the impedance is measured, allowing to draw conclusions on sea-ice properties averaged along wires. A sketch of the electrical circuit is illustrated in Fig. 3.1b. The voltage drop V_S of a sinusoidal signal over a reference resistor and the voltage drop V over each titanium pair is recorded. The impedance Z of the measurement volume is then calculated by using $|V| = Z \cdot |I|$ and $|V_\mathrm{S}| = R_\mathrm{S} \cdot |I|$ where I is the electrical current through the system, V and V_S are d.c. voltages and R is the resistance of a reference resistor. For a more detailed and technical explanation I want to point to the description by *Notz et al.* (2005). Though, measurements above around 17 000 Ω have to be defined as noise or unreliable (based on personal communication with Leif Riemenschneider, the designing engineer of the instrument). Furthermore, at each wire pair the temperature is recorded. It is required for the determination of the brine salinity (Eq. 2.4 or Eq. 2.5) and thus the bulk salinity (Eq. 2.6).

Notz et al. (2005) measured the impedance of a NaCl-solution at various temperatures above and below the freezing point of the solution. They found that the impedance is strongly dependant on the solid fraction of the ice that is surrounding the wires. Based on this they establish a theory to calculate the liquid volume fraction $\phi_{\mathrm{l,v}}$ of a measurement volume from its impedance. If Z_0 is the impedance at the time $t = 0$ when ice starts to form and Z is the impedance at a time t_1 with

(a) (b)

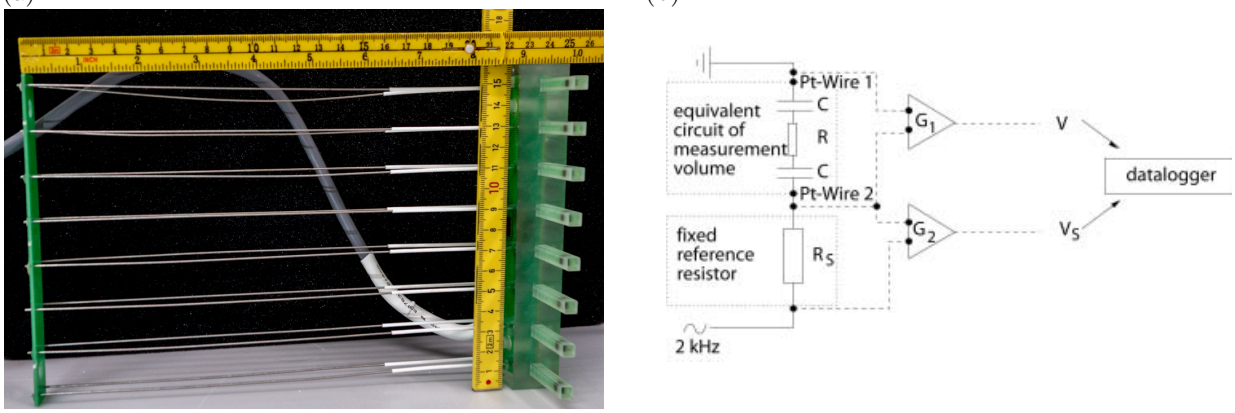

Figure 3.1 *a) Salinity harp and scales. b) Circuit that is used for the impedance measurement between one wire pair Pt-Wire 1 and Pt-Wire 2. C is a capacitor, R and R_S are resistors and G1 and G2 each represent a unit out of amplifiers, filters and rectifiers. V and V_S are d.c. voltages. Their ratio determines the impedance of the measurement volume (*Notz et al.*, 2005).*

$t_1 > 0$ and measured at a lower temperature both values can be set into relation to determine the liquid volume fraction

$$\phi_{l,v} = \frac{\gamma_0}{\gamma(T,S)} \cdot \frac{Z_0}{Z(t)}. \tag{3.1}$$

Here the conductivity of the interstitial brine at time $t = 0$ is γ_0 and γ at t_1 with T being the temperature and S is the salt concentration of the brine. To find Z_0 *Fuchs* (2017) suggests a value that is $\beta = 1.03$ times the impedance measured when the water reaches its freezing point.

The retrieved impedance is assumed to be ohmic, even if that is technically not correct (*Fuchs*, 2017). Pure ice is a good electrical isolator, liquid brine instead forms an inductive cell. Depending on the used AC frequency both influence the conductivity measurements differently. *Fuchs* (2017) studied the application of higher frequencies and was aiming to reduce inductive effects so that the impedance Z can be clarified as an ohmic resistance. However, he figured out that at higher salinities the liquid fraction and thus the bulk salinity gets underestimated at higher frequencies. The salinity harp records values at two frequencies, 2 kHz and 16 kHz. Based on his findings *Fuchs* (2017) suggests to use 2 kHz as the appropriate frequency. This frequency was also originally used by *Notz et al.* (2005).

The term γ_0/γ in Eq. 3.1 can be referred to as brine sensitivity (*Fuchs*, 2017). Brine salinity is strongly dependant on temperature. On one hand decreasing temperatures go along with lower conductivities in brine channels. On the other hand lower temperatures lead to an increase in brine salinity which contrariwise increase the conductivity (*Fuchs*, 2017). Similar to the work of *Fuchs* (2017) the latter is the dominating effect for the temperature ranges I use in this work.

Notz et al. (2005) find the salinity dependency of the conductivity to be non-linear, described by

the power-law fit

$$\gamma_{20}(S) = 0.05 S^{0.33} \tag{3.2}$$

at the fixed reference temperature $T_{\mathrm{ref}} = 20\,^{\circ}\mathrm{C}$. The temperature dependency is well represented by the linear relationship

$$\gamma = \gamma_{20} - 0.0015 \Delta T \tag{3.3}$$

where ΔT is the difference between the reference temperature at 20 °C and the measured temperature T. This equation is valid within the range of temperatures and salt concentrations that are relevant for the solidification of sea water. However, both equations depend on the used harp model and the coefficients found by *Notz et al.* (2005) refer to an older version of the instrument. Thus, *Fuchs* (2017) suggests to determine new coefficients for a different model of the salinity harp which I present in Sec. 4.1. Moreover he uses a different non-linear relation for the dependency of conductivity on salinity

$$\gamma_{0.5}(S) = 0.101 - 0.101 \cdot e^{-0.102 \cdot S} \tag{3.4}$$

at a different reference temperature $T_{\mathrm{ref}} = 0.5\,^{\circ}\mathrm{C}$ and for a similar model of the salinity harp that I use in this work.

With the here presented method to calculate the liquid volume fraction *Notz et al.* (2005) finds the maximum error for the so obtained bulk salinity to be 15 %. Although, the main advantage compared to the commonly used alternative method of ice coring is the high spatial and temporal resolution and the fact that the usage of the salinity harp is non-destructive. Aside from that, alternative methods like ice coring often come along with large errors due to brine drainage during sampling (*Fuchs*, 2017).

3.2 Other

In table Tab. 3.1 I present a list of other instruments I used to measure boundary conditions in the experiments described below (Sec. 5; Sec. 6). Further informations to the blade hardness gauge can be found by *Borstad and McClung* (2011).

Table 3.1 *All other instruments that were used in this study.*

Sensor	**Measurement**	**Accuracy**	**Location**
WTW	Salinity [$\mathrm{g\,kg^{-1}}$]	±0.1 (5 °C ... 25 °C	Water
		±0.2 (25 °C ... 30 °C	Water
	Temperature [°C]	±0.1 (5 °C ... 25 °C	Water
TinyTag TGP-4520	Temperature [°C]	±0.35 – ±0.5	Air
Blade hardness gauge	Hardness [N]	–	Snow

4 Salinity harp adaptions

Within this section I first determine updated brine sensitivity equations for the salinity harp models I use. In the second part I present newly developed principles that provide the necessary theoretical background for the operation of the salinity harp in snow which eventually is flooded by brine.

4.1 Brine sensitivity

As already mentioned earlier the equations for brine sensitivity (Eq. 3.2 and Eq. 3.3) depend on the version of the instrument. To determine new coefficients for the temperature dependency I installed one salinity harp in seawater with a salinity of $34.45 \pm 0.25\,\mathrm{g\,kg^{-1}}$ during the realisation of the experiment. The initial temperature was at approximately 5 °C and the water was cooled from the top down to its freezing point while it was constantly mixed. From measured resistances I used the relation $Z = \gamma^{-1}$ to retrieve the conductivity dependant on temperature in the given range (Fig. A.2). For the salinity harps that I used I find the linear relation

$$\gamma = \gamma_{T_{\mathrm{ref}}} - 0.00196(T_{\mathrm{ref}} - T) \tag{4.1}$$

with almost the same slope as proposed by *Notz et al.* (2005) and *Fuchs* (2017). Here the slope is the average over the slope coefficients of the linear fit I determined for each wire pair (Tab. A.1). The brine sensitivity is defined by the change of γ relative to γ_0. Therefore, and due to the linkage of Eq. 3.2 and Eq. 3.3 the absolute values of the different wire pairs are negligible and only the slope of the linear fit is of interest for the temperature dependency. Hence, it was sufficient to only use one instrument for the determination. Both harps are constructed identically and recorded impedance values theoretically mainly differ due to external impacts like the wire spacing or impurities.

The absolute values are more important for the determination of the salinity dependency. I rather averaged the impedance measurements over all wire pairs per instrument similarly to *Fuchs* (2017) than calculating one single average over all wire pairs independently of the instrument. Thus, the retrieved absolute values for each salinity harp still contain any potential instrument related systematic differences. Furthermore, the above mentioned external impacts on impedance values are eliminated. I placed both harps into a box with seawater at a temperature of $T_{\mathrm{ref}} = 8\,°\mathrm{C}$ whereas *Notz et al.* (2005) used $T_{\mathrm{ref}} = 20\,°\mathrm{C}$ and *Fuchs* (2017) $T_{\mathrm{ref}} = 0.5\,°\mathrm{C}$. The salinity ranges from the initial salinity of the seawater with $34.2\,\mathrm{g\,kg^{-1}}$ and up to the maximum concentration of $69.8\,\mathrm{g\,kg^{-1}}$. To increase the salinity I added salt (NaCl) and ensured that it was completely mixed and evenly distributed by stirring before I took the measurements with the harps at each particular concentration. I measured the respective salinity with the WTW Mulit 340i hand-held salinometer. The measurements for both harps are illustrated in Fig. 4.1. *Notz et al.* (2005) suggest

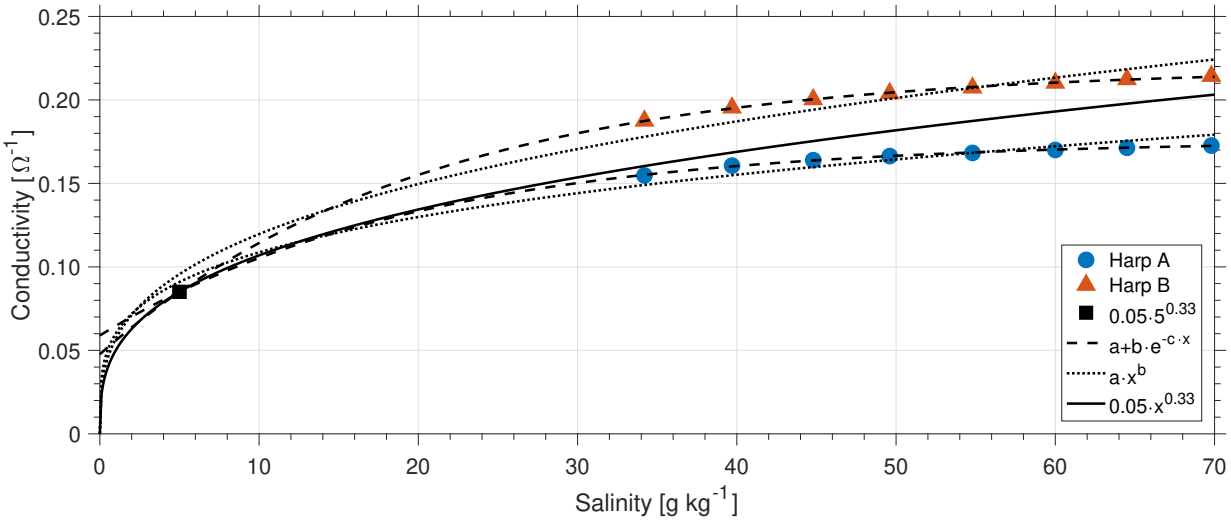

Figure 4.1 *The conductivity as a function of salinity at* $T_{\mathrm{ref}} = 8\,°C$ *for salinity Harp A and B and respective non-linear fits. The black square is an artificial data point based on Eq. 3.2.*

the power-law fit

$$\gamma_8(S) = a \cdot S^b \tag{4.2}$$

whereas *Fuchs* (2017) proposes another non-linear fit of the form

$$\gamma_8(S) = a + b \cdot e^{-c \cdot S} \tag{4.3}$$

to describe the conductivity dependency on salinity where a, b and c are the fitting coefficients. Due to some logistical problems I was not able to conduct more experiments at lower salinities to improve the quality of the non-linear fit. Hence, I decided to add one artificial data point at $S = 5\,\mathrm{g\,kg^{-1}}$ using the originally proposed fit Eq. 3.2 by *Notz et al.* (2005). In doing so I was able to determine the coefficients for Eq. 4.2 and Eq. 4.3 (listed in Tab. 4.1). The values are in the same dimension as found by *Notz et al.* (2005) and *Fuchs* (2017) for the respective equation.

Both Eq. 4.2 and Eq. 4.3 are appropriate to use and describe a similar shape. For higher salt concentrations above $30\,\mathrm{g\,kg^{-1}}$ the effect of salinity on conductivity doesn't change significantly and a correction could be neglected if values stay in that range. Instead, if salinities drop below $20\,\mathrm{g\,kg^{-1}}$ both equations highlight the importance of the conductivity correction. Otherwise errors of the factor two or even larger are likely during the calculation of the solid fraction.

In my study the fit proposed by *Fuchs* (2017) is the most suitable for the measured data points. Though, at lower salinities below $5\,\mathrm{g\,kg^{-1}}$ the fit doesn't decrease towards $Z = 0\,\Omega^{-1}$ for $S = 0\,\mathrm{g\,kg^{-1}}$ compared to the fit originally suggested by *Notz et al.* (2005). The curves for both fits intersect at $14.4\,\mathrm{g\,kg^{-1}}$. Hence, for values above this point I use Eq. 4.3 and for values below Eq. 4.2 to correct for the conductivity dependency on salinity.

Table 4.1 *The coefficients of the non-linear fits (Eq. 4.2 and Eq. 4.3) to the conductivity values of salinity harp A and B shown in Fig. 4.1.*

Harp	Equation	a	b	c
Harp A	Eq. 4.2	0.060	0.257	–
	Eq. 4.3	0.176	-0.117	0.051
Harp B	Eq. 4.2	0.057	0.323	–
	Eq. 4.3	0.219	-0.172	0.049

4.2 From sea ice into snow

So far the salinity harp was solely used for the application in sea ice (*Notz*, 2005; *Notz et al.*, 2005; *Notz and Worster*, 2008; *Notz and Worster*, 2009 and *Fuchs*, 2017). It was installed into seawater before freezing so that sea ice forms around it. On the one hand, this is an essential step to capture the moment of freezing as the resistance measured at this point Z_0 is required for further calculations as stated in Sec. 3.1. On the other hand, it is not possible to install the harp in a pre-existing mushy layer (*Notz et al.*, 2005). In fact, a later installation is technically possible but would be destructive and even after refreezing measurements may not be representative for the measuring site.

One of the aims of my study is the development of methods to install the instrument not in sea ice but in snow to investigate the process of flooding from below and subsequent freezing. That means I have to adapt the measurement procedure and extend the theory to meet the new conditions. Similar to the installation of the salinity harp in already existing sea ice the installation into a pre-existing snow cover would be destructive. It would be difficult to recreate the same snow properties around the instrument as prior to the interference with the snow cover. Therefore the harp needs to installed before the deployment of snow. In the field this is not always possible. However, if deployed later into an already existing snow cover measurements may still be representative for the field site after a sufficient time. Snow is a changing medium *Massom et al.* (2001) and with time the disturbed installation site may build up the same profile as before. The chances of that to happen depend mostly on the characteristics of the pre-existing snow cover. The more complex the original cover was the more unlikely it is to gain a snow profile with the same conditions. For example if the snow cover was characterised by several intermediate icy layers linked to rain events during its formation it is unlikely to get this complex profile again.

4.2.1 Determination of Z_0

The main difference to the installation in sea ice is the identification of the Z_0 values. If snow is flooded by saltwater subsequently it is not possible to find the point of freezing for each wire pair like it was done by *Fuchs* (2017). However, technically it is the same as if the harp was installed in the saltwater that floods the snow and the snow is added to the system afterwards. Thus, I developed a method to determine Z_0 based on the same theory that is used for the sea ice case which I presented earlier (Sec. 3.1).

First of all impedance values for different salinity solutions and corresponding temperatures are required such as the measurements I used for the calculation of the conductivity dependency on salinity (Sec. 4.1). For each solution the freezing temperature can be calculated using Eq. 2.2 or Eq. 2.3. By using the fact that $\gamma = Z^{-1}$ and with the calculated freezing temperature T_f, Eq. 4.1 can be rewritten to

$$\gamma_\mathrm{f}(S) = \gamma + 0.00196 \cdot (T_\mathrm{f} - T). \tag{4.4}$$

Here γ_f is the conductivity at the freezing point of the solution with the salinity S and the temperature T. As already mentioned above, *Fuchs* (2017) defines $Z_0 = \beta \cdot Z_\mathrm{f}$ with $\beta = 1.03$ and Z_f the impedance value when the solution reaches its freezing temperature. Similar to this suggestion I propose to calculate γ_0 by

$$\gamma_0 = \frac{\gamma_\mathrm{f}}{\beta}. \tag{4.5}$$

For the so retrieved γ_0 values of each solution it is possible to find a non-linear fit of the form

$$\gamma_0(S) = a + b \cdot e^{-c \cdot S} \tag{4.6}$$

similar to Eq. 4.3 whereas here the index of γ_0 does not refer to the temperature but to the same moment as Z_0. Values for a, b and c I determined the same way as for Eq. 4.3. Although, instead of using one set of coefficients for all wire pairs of one harp (like Tab. 4.1) I calculated a, b and c for each respective wire pair (**??**). Finally, Eq. 4.6 enables the determination of γ_0 for any salinity S which can then be inverted back to impedance by $Z_0 = \gamma_0^{-1}$.

This method holds if snow is flooded with saltwater at known salt concentration. In case of snow on sea ice the flooding water has not necessarily the same salinity as the underlying seawater. Either saltier brine, the underlying seawater or a mixture of both might find a way to the ice-snow interface and wet the snow (*Massom et al.*, 2001). Hence, it is essential to find a reliable method to measure the brine salinity of the rising water. One possibility is to measure the temperature at the ice-snow interface and use Eq. 2.4 or Eq. 2.5 to calculate the brine salinity of the ice as an estimation of the salt concentration of the flooding water.

4.2.2 Consideration of the gas fraction and respective density profiles

The estimation of the liquid fraction from impedance measurements is based on the assumption that sea ice mainly consists of liquid brine and solid ice. However, flooded snow or snow ice may contain inclusions of air in form of small bubbles that got trapped during the flooding and refreezing (Fig. 4.2). As already outlined above the salinity harp is used to estimate the liquid volume fraction (Eq. 3.1). To calculate the bulk salinity (Eq. 2.6) the liquid volume fraction needs to be transfered into the liquid mass fraction via Eq. 2.8. The equation is based on the assumption that the gas content is negligible so that $\phi_\mathrm{s} + \phi_\mathrm{l} = 1$. Instead, if it is necessary to account for the gas content, the relation becomes $\phi_\mathrm{s} + \phi_\mathrm{l} + \phi_\mathrm{g} = 1$ where ϕ_g is the gas fraction. Hence, Eq. 2.8 is not valid anymore and would break the theory of the bulk salinity retrieval.

Snow is a complex porous medium and consists of solid snow grains out of ice and air in between (*Massom et al.*, 2001). If it is flooded by saltwater and transformed into slush and potentially refreezes, it becomes a combination of ice, brine and air inclusions. Saltwater is a good conductor compared to dry snow. Measured direct-current electrical conductivities show differences of up to seven magnitudes between snow and seawater (*Evans*, 1965). Hence, in terms of impedance measurements using the salinity harp, ice and snow grains with the volume fraction $\phi_\mathrm{s,v}$ and air and gas inclusions with the volume fraction $\phi_\mathrm{g,v}$ both act as a good isolator. Based on this, I suggest to use a combined isolating fraction ϕ_iso like indicated in Fig. 4.3 so that

$$\phi_\mathrm{iso} = \phi_\mathrm{s} + \phi_\mathrm{g}. \tag{4.7}$$

It is connected to the liquid fraction by $\phi_\mathrm{l} = 1 - \phi_\mathrm{iso}$. As a result, it is possible to derive the isolating mass fraction $\phi_\mathrm{iso,m}$ from the isolating volume fraction $\phi_\mathrm{iso,v}$ by considering the relation of the densities of the liquid and the isolating fraction. The derivation is similar to the one presented by *Notz* (2005) for Eq. 2.7 and I will demonstrate it below.

The solid volume fraction is defined as

$$\phi_\mathrm{s,v} = \frac{V_\mathrm{s}}{V} \tag{4.8}$$

with V_s the volume of the solid and V the total volume. The equation for the isolating volume fraction is defined accordingly. Thus, the respective densities can be written as

$$\rho_\mathrm{s} = \frac{m_\mathrm{s}}{\phi_\mathrm{s,v} V} \text{and} \quad \rho_\mathrm{iso} = \frac{m_\mathrm{g}}{\phi_\mathrm{g,v} V}$$

where m is the mass and ρ the density of the solid (s) and the isolating fraction (iso) respectively.

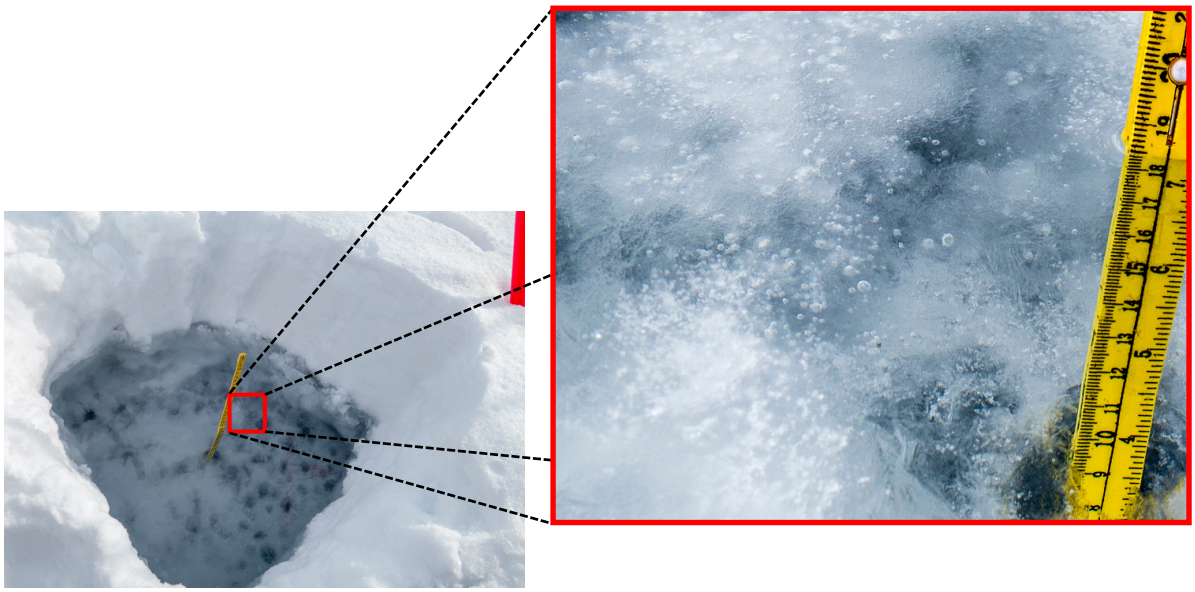

Figure 4.2 *Enclosed air bubbles in snow ice inside a snow pit on sea ice of Van Mijenfjorden, Svalbard on 01.05.2018.*

This can further be used to calculate the mean density of the volume

$$\begin{aligned}\bar{\rho} &= \frac{m_{\mathrm{iso}} + m_{\mathrm{l}}}{V} \\ &= \phi_{\mathrm{iso,v}} \rho_{\mathrm{iso,v}} + (1 - \phi_{\mathrm{iso,v}})\, \rho_{\mathrm{l}}. \end{aligned} \tag{4.9}$$

Following the derivations by *Notz* (2005) the liquid mass fraction is described by

$$\phi_{\mathrm{l,m}} = \frac{1}{1 + \left(\frac{1}{\phi_{\mathrm{l,v}}} - 1\right) \frac{\rho_{\mathrm{iso}}}{\rho_{\mathrm{l}}}} \tag{4.10}$$

similar to Eq. 2.8. Hence, the gas and solid fraction are represented by one combined fraction and it is not necessary to find them separately but to find one suitable density ρ_{iso} for both. Though, ρ_{iso} may not be the same at each wire pair. Therefore, it is necessary to find a density profile that specifies an appropriate density value ρ_{iso} at each wire pair for the calculation of the correct liquid mass fraction via Eq. 4.10.

On the one hand, the liquid density ρ_{l} does not vary much for the upper ocean, relevant for sea ice. Densities for the surface of the ocean range from $1022\,\mathrm{kg\,m^{-3}}$ up to $1028\,\mathrm{kg\,m^{-3}}$ (*Talley*, 2011). On the other hand, for small liquid fractions the effect of the density on the calculated liquid mass fraction can be up to the factor of two if $400\,\mathrm{kg\,m^{-3}} \leq \rho_{\mathrm{iso}} \leq 900\,\mathrm{kg\,m^{-3}}$ for instance. Therefore, it is essential to find an appropriate density profile that links the usually lower density values for snow at the top with the expected higher values at the ice-snow interface. For this I present two approaches.

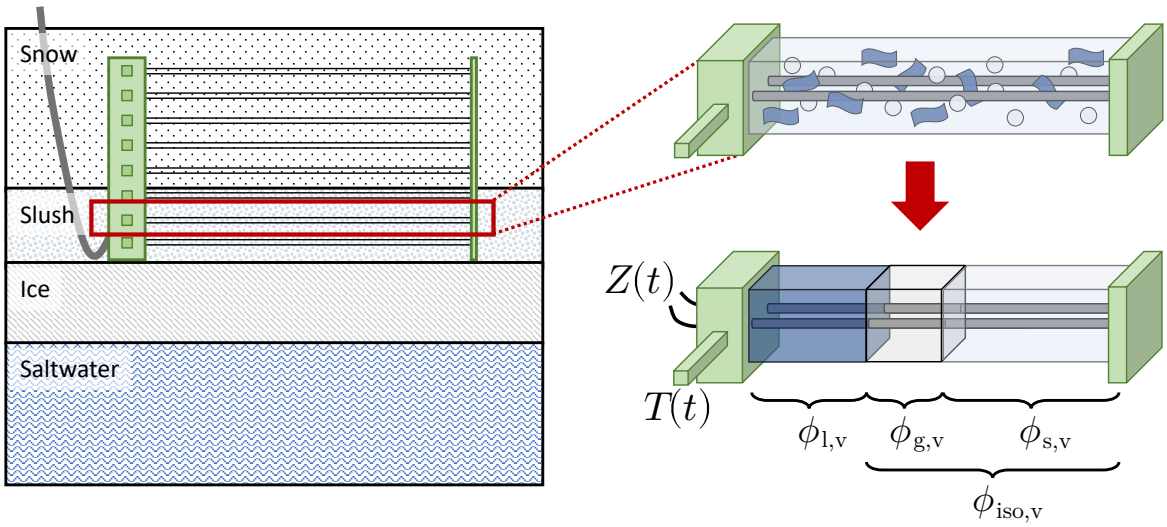

Figure 4.3 *An illustration of the measurement principle of the salinity harp. The instrument is mounted in snow on ice that eventually is flooded by saltwater. The resulting slush or snow ice is composed of solid ice and snow grains with a volume fraction $\phi_{s,v}$, brine inclusions and brine channels with a volume fraction $\phi_{l,v}$ and air inclusions with a volume fraction $\phi_{g,v}$. The fractions can in theory be splitted like illustrated for the measurement volume. For each titanium wire pair the instrument records the impedance $Z(t)$ and the temperature $T(t)$ at the time t. The sketch is based on a similar version for only sea ice by* Fuchs *(2017).*

First of all, if no density measurements are available suitable values for the uppermost wire pair in snow and the lowermost wire pair at the ice-snow interface are needed. The former can be estimated by typical density values for snow. Based on measurements by *Eicken et al.* (1994), *Massom et al.* (2001) and my own (e.g. Sec. 5) reliable snow density values are in the range from $250\,\mathrm{kg\,m^{-3}}$ up to $500\,\mathrm{kg\,m^{-3}}$. For the exemplary demonstration of discussed density profiles later I use $\rho_{iso} = 450\,\mathrm{kg\,m^{-3}}$ as the value for the uppermost wire pair in snow.

If the snow was already flooded by saltwater and refroze, I expect values close to those of sea ice for the density value at the lowermost wire pair at the ice-snow interface. *Timco and Frederking* (1996) report a mean density around $900\,\mathrm{kg\,m^{-3}}$ for sea ice. Thus, I suggest this value as an appropriate estimation for the density value at the lowermost wire pair.

Maybe the least complex method to link both density values is to assume a linear decrease with height as illustrated in Fig. 4.4a. A linear profile for ρ_{iso} can be described by the relation

$$h(\rho_{iso}) = a \cdot \rho_{iso} + b \tag{4.11}$$

where h is the height above the ice-snow interface and a and b are coefficients depending on the chosen density values of the profile.

However, I expect a more complex density profile to be present in flooded snow. For the layers in snow that were flooded by dense saltwater I would assume density values close to the one at the ice-snow interface. In contrast, the snow that is not reached by saltwater remains close to its

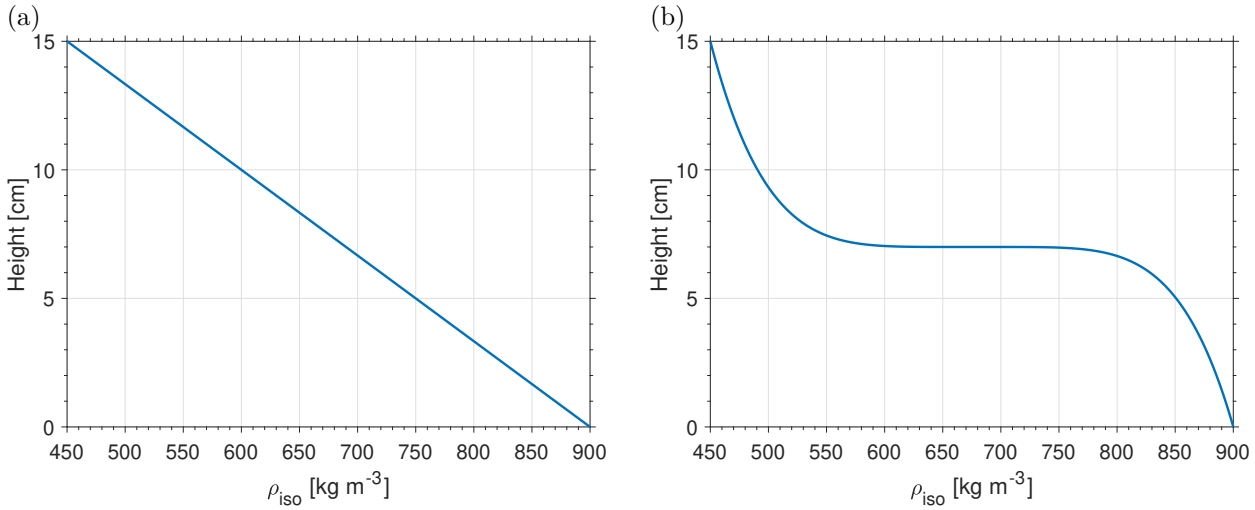

Figure 4.4 *Exemplary a) linear and b) quintic density profiles in flooded snow based on the discussed exemplary values for the minimum and maximum density and the height of saltwater rise in snow. The profile in a) is based on Eq. 4.11 and the profile in b) on Eq. 4.12.*

original density. Hence, I propose a profile described by the quintic relationship

$$h(\rho_{\mathrm{iso}}) = -a \cdot (\rho_{\mathrm{iso}} - b)^5 + c. \tag{4.12}$$

Here a is a constant in the dimension of 10^{-11} (if $400\,\mathrm{kg\,m^{-3}} \leq \rho_{\mathrm{iso}} \leq 900\,\mathrm{kg\,m^{-3}}$), b is the average between the assumed density maximum at the ice-snow interface and the presumed density minimum at the upper most wire pair and c is the height the water gets soaked up into the snow above the ice-snow interface. An example for the discussed values is shown in Fig. 4.4b. Based on my experiments I found c in the range of 6–8 cm which also agrees with observations by *Massom et al.* (2001). For the illustration of Eq. 4.12 in Fig. 4.4b I used an exemplary value of 7 cm. For the application of this theory to the later use in Sec. 5 and Sec. 6 I define b and c as already indicated and use the built-in non linear least square fitting method in Matlab to receive a.

4.3 Data handling

Besides the theory I presented above, I used further assumptions for the processing of the salinity harp data. In case of wire pairs are surrounded by a medium with high resistance the harp is not able to log reasonable impedance data. As a result values fluctuate and the time series feature huge jumps and peaks in the magnitude of more than one dimension. Hence, I corrected all data in a way that if the difference between a previous value and the subsequent value is more than 25 % the latter value is removed.

The saltwater I used for the cold laboratory experiments was always from Adventfjorden, Svalbard. Salt concentrations for this kind of water were around $34 \pm 1\,\mathrm{g\,kg^{-1}}$. If I wanted to get higher concentrations I added salt (NaCl) to the water. Hence, the seawater equations for the so retrieved NaCl solution were not valid anymore. Consequently, as soon as the salinity of the solution above $40\,\mathrm{g\,kg^{-1}}$ I used the NaCl equations for the calculation of the brine salinity and the freezing point instead.

For the processing and calculations of the harp data I used Matlab. I developed a Matlab tool (Fig. A.3) that combines all the assumptions, given theory and data handling concerning the salinity harp in one graphical user interface. After finishing my thesis I hope to make the tool online available as open source.

4.4 Summary

In this section I presented updated brine sensitivity equations for the salinity harp models I used in my work. Obtained coefficients are similar to the ones used in work by *Notz et al.* (2005) and *Fuchs* (2017). In both works they use the same linear equation for the conductivity dependency on temperature which I adopted with a corrected slope. For the salinity dependence their proposed non-linear equations vary slightly but were both useful to represent my data. Below the salinity of $14.4\,\mathrm{g\,kg^{-1}}$ of the interstitial brine I use Eq. 4.2 and above I use Eq. 4.3 to correct for the conductivity dependency on salinity.

Furthermore I demonstrated an adaption of the salinity harp theory to be suitable for the use in studying the flooding of snow. If the salinity of the infiltrating water is known I found a method to estimate Z_0 values similar to the procedure in sea ice. In snow the liquid fraction is not only dependant on the solid fraction but the gas fraction may also be relevant. Thus, I introduced the theoretical background to account for this. In terms of salinity harp measurements the solid and gas fraction are better isolators than the liquid fraction. Hence, I introduce the isolating fraction ϕ_{iso} as a combination of the solid and gas fraction and a respective common density ρ_{iso}. The new variables allow to correct and redefine the calculations for the liquid mass fraction from

harp measurements. While the density of the liquid is almost constant it is necessary to find an appropriate density value of the isolating fraction for each wire pair. To estimate adequate density profiles I proposed a linear and a more complex quintic approach.

Concerning the processing and handling of the salinity harp data I applied a filter to remove jumps above 25 % in the impedance time series. In terms of brine salinity and freezing point calculations of the used seawater in laboratory experiments I used the NaCl equations as soon as I manually increased the salinity above $40\,\mathrm{g\,kg^{-1}}$.

5 A new laboratory method to study the rise and refreezing of water in snow

As to my knowledge no in depth investigations at high resolutions of the salinity and temperature evolution during the flooding of snow have been made yet. Hence, I developed a new laboratory method for the application of the salinity harp in snow and to study those processes. My idea was to develop an experimental setup that serves as basis for various experiments to understand how controlled changes affect the measured variables temperature and resistance. I designed the experimental setup with as less uncontrolled side effects as possible and with a set of well defined boundary conditions (Sec. 5.1). Results (Sec. 5.2, Sec. 5.3 and Sec. 5.4) establish the foundation for more complex experiments like the one presented in Sec. 6. I hereafter refer to the experiments I introduce in this section as "snow frame" experiments.

5.1 Experimental setup

In order to investigate the rise of saltwater in snow I developed a setup where I deployed snow on a grid which I surrounded by a Lexan frame and placed into a box (Fig. 5.1). After the snow stabilised, I filled the box with water to create a negative freeboard respective to the height of the grid-snow interface. Consequently, water floods the snow. To measure the characteristics during the rise I placed a salinity harp inside the frame prior to the deployment of snow. It measures the temperature and impedance in the snow profile during the realisation of the experiment. In addition, a TinyTag temperature sensor records the air temperature above the snow surface.

Detailed description

In order to enable water to equally rise in snow the experimental setup needs to fulfill three main criteria. First of all a frame is required to keep the snow in one place. Secondly, this frame has to allow water entering from below and thirdly, I needed to guarantee a steady water supply from below. To satisfy the first criterion I built a frame out of Lexanglas (Fig. 5.2a) with a wall thickness of 6 mm. This enables to still trace ongoing processes visually and furthermore it keeps the impact of heat exchange between snow and the frame boundary low. Lexan is a polycarbonate and has a very low thermal conductivity of around $0.2\,\mathrm{W\,m^{-1}\,K^{-1}}$ (e.g. *SABIC* (2018)). It features similar values to snow, which has average values for thermal conductivity from $0.078\,\mathrm{W\,m^{-1}\,K^{-1}}$ for new snow up to $0.290\,\mathrm{W\,m^{-1}\,K^{-1}}$ for wind slab snow (*Sturm et al.*, 2002). Thus from a thermal perspective, Lexan takes the same insulating role as snow. By leaving the bottom of the frame open and keeping a stand in every corner of the frame I was able to install a grid. For this I used a plastic grid with a rectangular grid size of about 0.5 cm x 4 cm which I cut out of a plastic box. Plastic serves the role

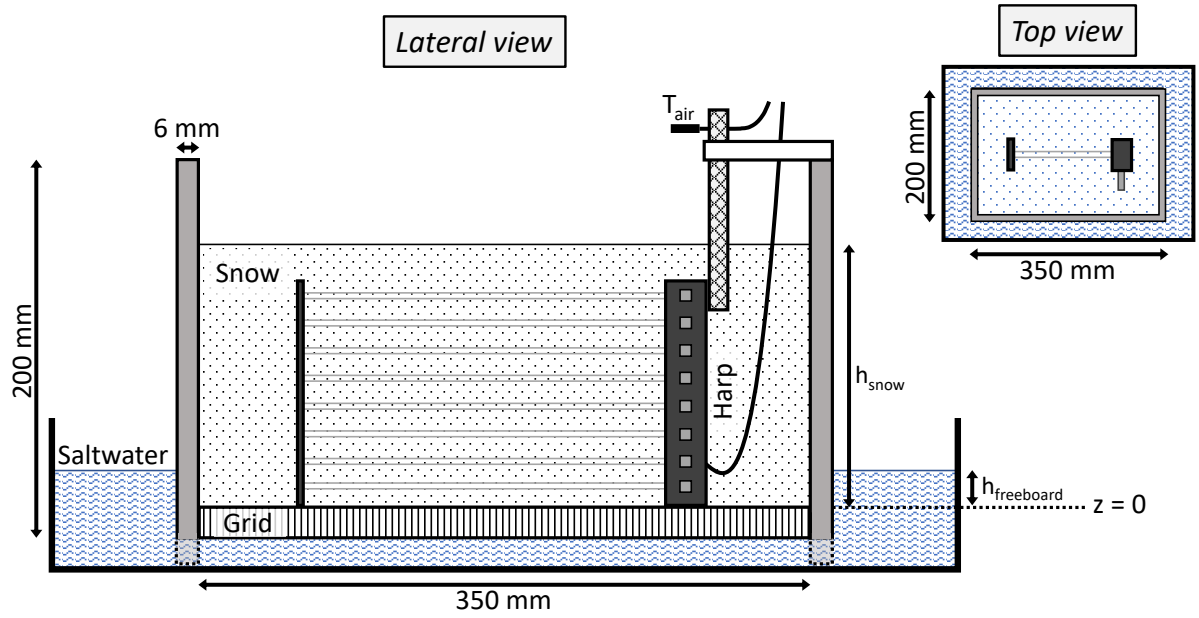

Figure 5.1 *Sketch of the experimental setup for the snow frame experiment. Note that dimensions are not true to scale.*

of minimising any thermal effects during the process of flooding. Furthermore the big mesh size allows the water to easily rise without blocking the path by freezing as it could happen by using a smaller mesh size. To prevent snow from filling up the grid I used an old nylon sock around the grid. Thus, the level for $z = 0$ is assured to be horizontal consistent. Next I placed the frame with grid inside a plastic box. Because of the stands of the frame there is an empty space below the grid. This fulfils the last criterion as it is now possible to fill the box with water such that it can spread evenly below the frame. When the water level reaches the grid and eventually the bottom of the snow it can evenly wet the snow. In addition, I surrounded the box with styrofoam from the sides and from below to reduce the process of cooling to the top only.

Finally, I placed the instruments in the middle of the frame (Fig. 5.1; Fig. 5.2a,b) to minimise any remaining boundary effects. Afterwards I switched on the cold laboratory to cool it down to the desired temperature. As soon as the temperature is stable I filled the the frame with snow (Fig. 5.2c). I recommend to use snow from outside and sieve it through a grid with desired mesh and grain size as this is a common method (e.g. *Sturm* (1991)). After the instruments are completely covered in snow I waited at least 24 h before the actual experiment can start. This time is required to let the snow grains bond together and settle during the so called metamorphosis. Thereby, effects of this process are insignificant for the flooding experiment and the state of the snow is more similar to how it would be in the field. In addition I took a smaller frame that I filled with the same snow. By that I am able to characterise the snow each time before flooding without disturbing the experiment itself. To start the actual experiment I filled water at desired salinity

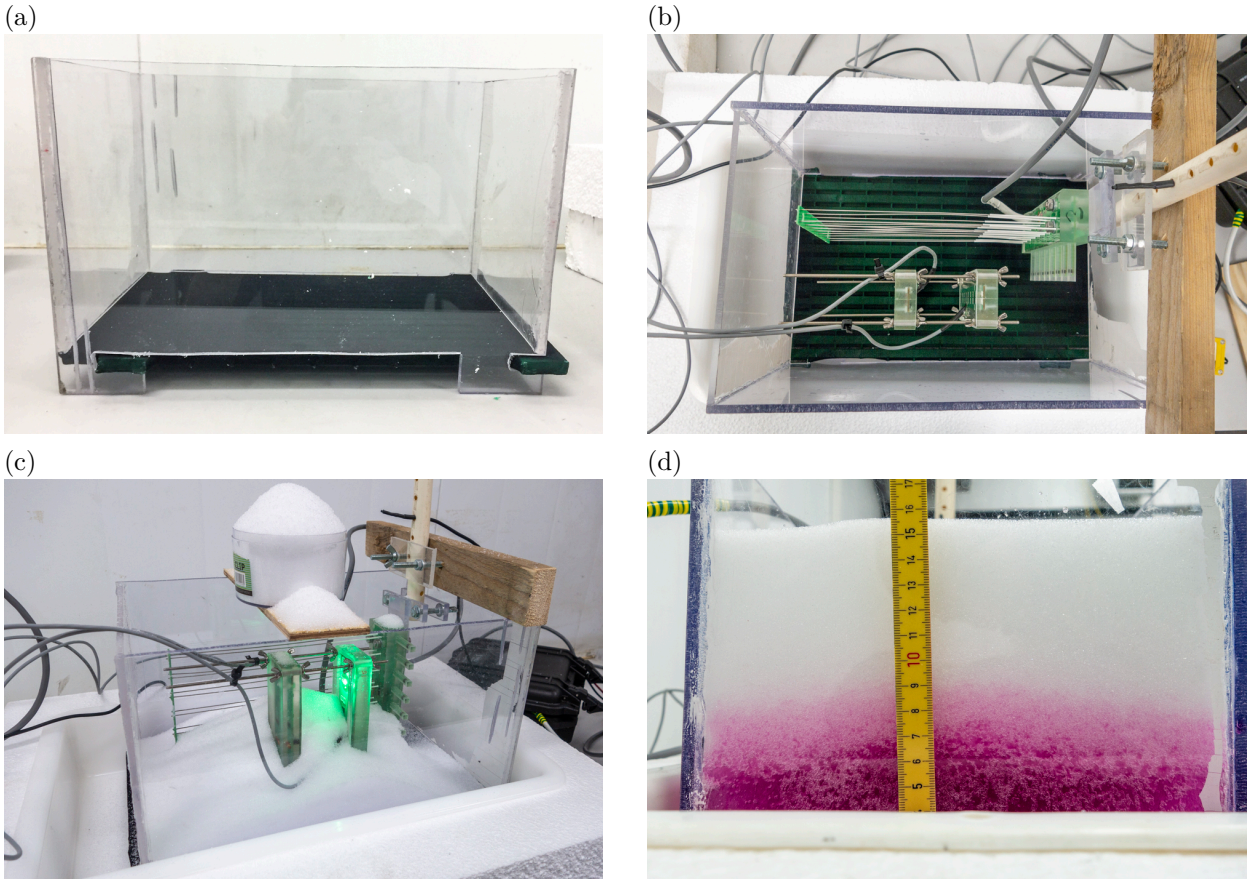

Figure 5.2 *(a) Lexan frame with grid. (b) Light harp and salinity harp installed together in one frame inside an isolated box. (c) Frame during filling with snow and extra container to measure snow characteristics. (d) Snow flooded with coloured (beetroot juice) saltwater from below with constant freeboard (refers to Experiment* $7_{5\mathrm{L(i)}}$ *in Tab. 5.1). The picture was taken after 72 h.*

into the box around the frame up to the intended freeboard. As water gets soaked into the snow and thereby decreasing the freeboard it has to be maintained until the process slows down and a stable freeboard is reached. This takes approximately 20–30 min. Additionally the water has to be at freezing temperature depending on its salinity to match the situation in the field. In normal case sea ice would be situated below the snow and water that rises through the ice, no matter if brine or seawater from below the ice, would always be at freezing temperature. In order to optically trace the flooding I used beetroot juice to colour the water (Fig. 5.2d) in some of the experiments. Now the whole setup can be left for a desired time. I figured out that leaving it for around 72 h covers the most important part of the ongoing processes.

Since I had two salinity harps and one light harp available I decided to build two identical experiment setups. Therefore, for each set temperature I was able to run two independent experiments at the same time and compare them. The described experimental setup allows to control the four variables air and initial snow temperature, salinity of the water, the freeboard and snow grain size. All conducted experiments are listed in Tab. 5.1. I used the same type of snow for sieving

Table 5.1 *An overview of all conducted snow frame experiments where ρ_{sn} is the density of the used snow, D the dominating grain sizes of the snow, T_{air} the air temperature, h_f the freeboard, $S_{w,A}$ and $S_{w,B}$ the salinity of the flooding water for frame A and B with respective measured freezing temperatures T_A and T_B.*

Nr.	ρ_{sn}[g kg^{-1}]	D [mm]	T_{air} [°C]	h_f [cm]	$S_{w,L}$ [g kg^{-1}]	T_A [°C]	$S_{w,B}$ [g kg^{-1}]	T_B [°C]
1	454	1–2	-5	-1	33.5	-1.9	65.8	-3.7
2	486	1–2	-10	-1	34.4	-1.9	67.7	-3.8
3	439	0.5–1	-5	-1	33.1	-1.8	62.0	-3.4
4	456	0.5–1	-10	-1	33.3	-1.9	68.4	-3.8
5	468	0.5–1	-5	-2	34.5	-2.0	67.5	-3.7
6	469	0.5–1	-10	-2	34.7	-1.9	69.1	-3.9
7	450	0.5–1	-5	-1	44.9	-2.5	54.9	-3.0

in Experiment 1 and 2 (type III-A-1) and in Experiment 3–7 (type II-B-2) (according to Fig. A.1). For D = 1–2 mm I used snow originally taken from the depth hoar layer and for D = 0.5–1 mm snow from the adjacent layer in a naturally deposited snowpack. To transport the snow from the field site to the cold storage I used airtight or isolated boxes. I had to store the boxes in a cold storage until using the snow in each experiment. Storing temperatures were around −3 °C to mimic similar temperatures like in the field. However, when using in the lab the snow was warmer than the air temperatures in all the experiments. Hence, when sieving snow into the frame both types experienced the same change in temperature. Consequently, I expect that the original properties of typical less bonding and lower density of depth hoar snow compared to snow from further up in the snowpack disappeared. In fact, both had a similar density in the end (Tab. 5.1). Furthermore, comparing this to work by *Borstad and McClung* (2011) I assume that both types of snow have approximately the same hardness and strength in bonding. Hence, hereafter I only refer to the differences in the grain size.

The experimental setup is designed to represent the process of saltwater rising in snow on thin ice as that is one of the main processes for snow-ice formation. However, due to the simplifications within the setup it has some limitations to keep in mind for the interpretation of experiments. The harp instrument samples data with a vertical resolution of 2 cm. Thus, this defines the accuracy for the interpretation of effects due to water rise. Furthermore, as discussed below (see Sec. 5.2), the setup is lacking a heat source from below. Therefore here, the initial snow profile is not representing the real scenario where snow is on top of sea ice with warmer seawater underneath. Moreover, the bottom grid takes over the role of the sea ice. It enables an unlimited water supply with instant availability and differs to the way sea ice is dividing snow and seawater in reality.

Hereafter, I refer to Experiments at $T_{air} = -5$ °C as high temperature experiments and at $T_{air} = -10$ °C as low temperature experiments. Additionally, experiments with 33.1 g kg^{-1} $\leq S_w \leq$ 34.7 g kg^{-1} are hereafter referred to as low-saline experiments and respectively experiments with

$62.0\,\mathrm{g\,kg^{-1}} \leq S_\mathrm{w} \leq 69.1\,\mathrm{g\,kg^{-1}}$ are referred to as high-saline experiments. My intention was to have an ocean comparable concentration and one with approximately double its salt content like brine salinities in ice. Due to some technical difficulties the used saltwater solutions didn't exactly fit this approach. However, the aim of my work is not to investigate the effect small changes in salt concentration in the dimension of $1\,\mathrm{g\,kg^{-1}}$ but to study larger effects in dimensions of double the concentration. Hence, by splitting the experiments into the two mentioned groups comparisons become comprehensible. Furthermore, if referring to single experiments I use the denomination like "Experiment $1_{5\mathrm{L}}$" or "Experiment $2_{10\mathrm{H}}$" linked to the respective experiment number (1–6), air temperature (5: high temperature or 10: low temperature) and salinity (L: low saline or H: high saline). In addtion, Experiment 7A and 7B are refereed to as Experiment $7_{5\mathrm{L(i)}}$ and $7_{5\mathrm{H(i)}}$ where (i) denotes the fact that the experiments are at intermediate salinities and thus different to all other experiments.

5.2 Temperature evolution in flooded snow

In this section I compare temperature measurements by the salinity harp in the upper layers of the snow to measurements by the TinyTag sensors in the air. Afterwards, I present and discuss the results of four exemplary experiments with varying air temperatures and salinities. In all experiments temperature evolution and development of gradients show strong dependencies on the air temperature and the salinity of the flooding water which I describe in more detail below.

5.2.1 Results

During the different experiments the temperature evolution of the air was captured at a temporal resolution of 10 min by TinyTag sensors installed 5 cm above the snow surface. The temperature profile within the snow was measured by the salinity harps placed in the middle of each frame as described above. The profile starts 1 cm above the snow-grid interface due to the technical configuration of the salinity harp. From this point a vertical temperature profile was measured at a spatial resolution of 2 cm up to the uppermost sensor at 15 cm and at a temporal resolution of approximately 40 s.

I defined the start of each experiment when the salinity harp was covered in snow and initiated flooding after at least 24 h. In case of Experiment $1_{5\mathrm{L}}$ and $1_{5\mathrm{H}}$ (Fig. 5.3a,b) I flooded the snow around 28 h after the start of the experiment. Fig. 5.3 shows the time series of the air temperature T_air and the effective air temperature $T_\mathrm{air,eff}$ during both experiments. Additionally, the temperatures for the upper two wire pairs at 13 cm and 15 cm of the respective salinity harp are illustrated. Disregarding T_air, the residual time series show a wave pattern with temperatures varying by up to 0.5 °C with a frequency of approximately 4 times per 24 h. Minimum and maximum turning points appear around 1 h earlier in the air temperature time series compared to those of the salinity harp

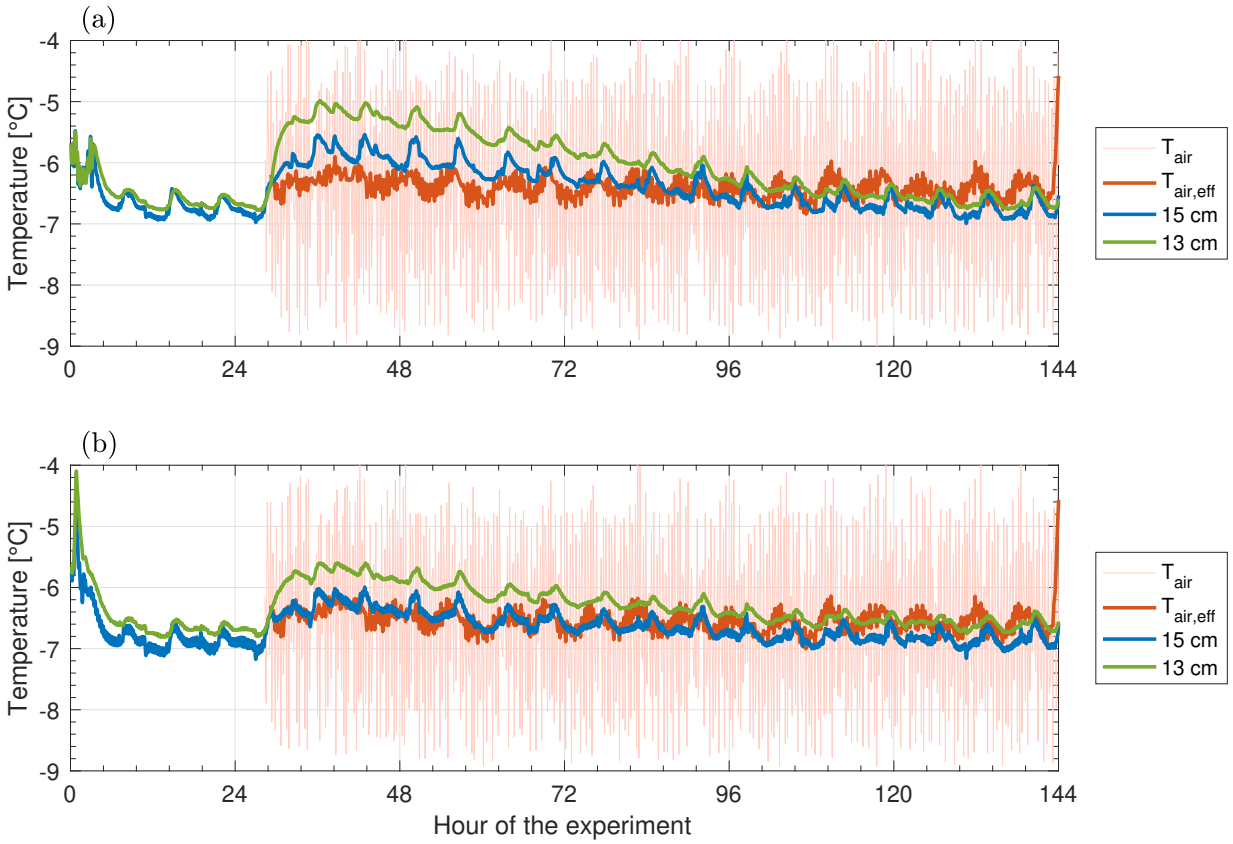

Figure 5.3 *The air temperature T_{air} (10 min temporal resolution) of a) Experiment $1_{5\mathrm{L}}$ and b) Experiment $1_{5\mathrm{H}}$ and the temperature measured by the salinity harps (approx. 40 s temporal resolution) in the snow at the 15 cm and 13 cm level. $T_{\mathrm{air,eff}}$ is the effective air temperature of T_{air} smoothed by a running mean over 10 data points. For reasons of better readability the time series of the salinity harp measurements are also smoothed by a running mean over 20 data points. The time of the experiment after setting $T_{\mathrm{air}} = 15\,°C$ is not shown in this figure.*

in snow. There is also a small offset of about 7–8 min between the turning points at the 13 cm and 15 cm level where the signal appears first at 15 cm.

Due to technical reasons the TinyTag logger started logging around 28 h after the start of the experiment for both Experiment $1_{5\mathrm{L}}$ and Experiment $1_{5\mathrm{H}}$. Values fluctuate around $-6.5 \pm 2.5\,°\mathrm{C}$ for both experiments. The effective air temperature $T_{\mathrm{air,eff}}$ is the air temperature averaged by a running mean over 10 data points. The averaging reduces the fluctuation to $\pm 0.25\,\mathrm{K}$. Both time series of $T_{\mathrm{air,eff}}$ for Experiment $1_{5\mathrm{L}}$ and Experiment $1_{5\mathrm{H}}$ keep constantly fluctuating around the level of $-6.5\,°\mathrm{C}$ during the rest of the experiment. In the end temperatures of all time series considerably rise above $-4\,°\mathrm{C}$ but are not shown within this figure.

Within the initial 28 h of Experiment $1_{5\mathrm{L}}$ (Fig. 5.3a) the temperature at 13 cm and 15 cm stabilises at $-6.75 \pm 0.25\,°\mathrm{C}$. At the point of flooding temperatures increase significantly up to $-5.25 \pm 0.25\,°\mathrm{C}$ at 13 cm and up to $-5.75 \pm 0.25\,°\mathrm{C}$ at 15 cm. Subsequently, the temperatures at both levels drop steadily until hour 120 of the experiment. Then they level out at approximately the same values

of $-6.75 \pm 0.25\,°C$ like in the beginning of the experiment.

A similar pattern appears for Experiment 1_{5H} (Fig. 5.3b). The temperature at 13 cm and 15 cm in the beginning stabilise at the same value of $-6.75 \pm 0.25\,°C$ within the initial 28 h. After initiating flooding, at both levels 13 cm and 15 cm temperatures significantly increase up to $-5.75 \pm 0.25\,°C$ for the former and up to $-6.25 \pm 0.25\,°C$ for the latter level. The rise is similar but in total 0.5 K smaller than the rise in Experiment 1_{5L} at each level respectively. Afterwards, temperatures also steadily decrease back to the initial temperature of $-6.75 \pm 0.25\,°C$ like it was in the beginning of the experiment. However, the decline takes place over 96 h which is 24 h less compared to Experiment 1_{5L}.

Based on measurements at all wire pairs the temperature evolution of the whole snow profile for both experiments is shown in Fig. 5.4. The upper panel (Fig. 5.4a) represents Experiment 1_{5L} and the lower panel (Fig. 5.4b) Experiment 1_{5H}. Data between two neighbouring wire pairs is linear interpolated. Besides a wave pattern in the upper levels similar to the one described above the temperature profile is almost constant for both experiments until flooding around hour 30. After that, a strong anomaly of higher temperatures appears at the bottom in both setups creating a vertical temperature gradient. The anomaly shows higher temperatures and the consequential temperature gradient is stronger in the experiment flooded with low saline water (Experiment 1_{5L}) compared to the high saline experiment (Experiment 1_{5H}). In both experiments the gradient starts to weaken after approximately hour 36. Whereas in the former experiment the temperature gradient completely dispersed at about 108 h it takes only 84 h in the latter experiment. After 144 h I increased the temperature in the laboratory to $T_{air} = 15\,°C$. Both experiments record high temperatures from the top reaching down to the bottom within 5 h. The onward warming of the lowermost level is more effective in Experiment 1_{5L} compared to Experiment 1_{5H}.

If changing the temperature to $T_{air} = -10\,°C$ (Fig. 5.5) the same characteristics in terms of lower (Fig. 5.5a) and higher ((Fig. 5.5)b) salinity of the flooding water appear. However, at a lower air temperature vertical gradients are stronger after the moment of flooding. Furthermore, the weakening of the gradient over time is at higher rates compared to the experiment at $T_{air} = -10\,°C$ (Fig. 5.4).

5.2.2 Discussion

First of all, the general wave pattern of the time series originates from the cooling system of the cold laboratory. In case of Experiment 1 I set the laboratory temperature to $-5\,°C$. Based on temperature sensors installed at different heights on the wall three refrigerators at the ceiling cool down the air in the room. Each cooling unit has its own internal cycle of cooling and defrosting. Thus, the room temperature is not constant and temporary below or above the set temperature. This creates the repetitive fluctuating pattern with a time period around 6 h and is common in cold

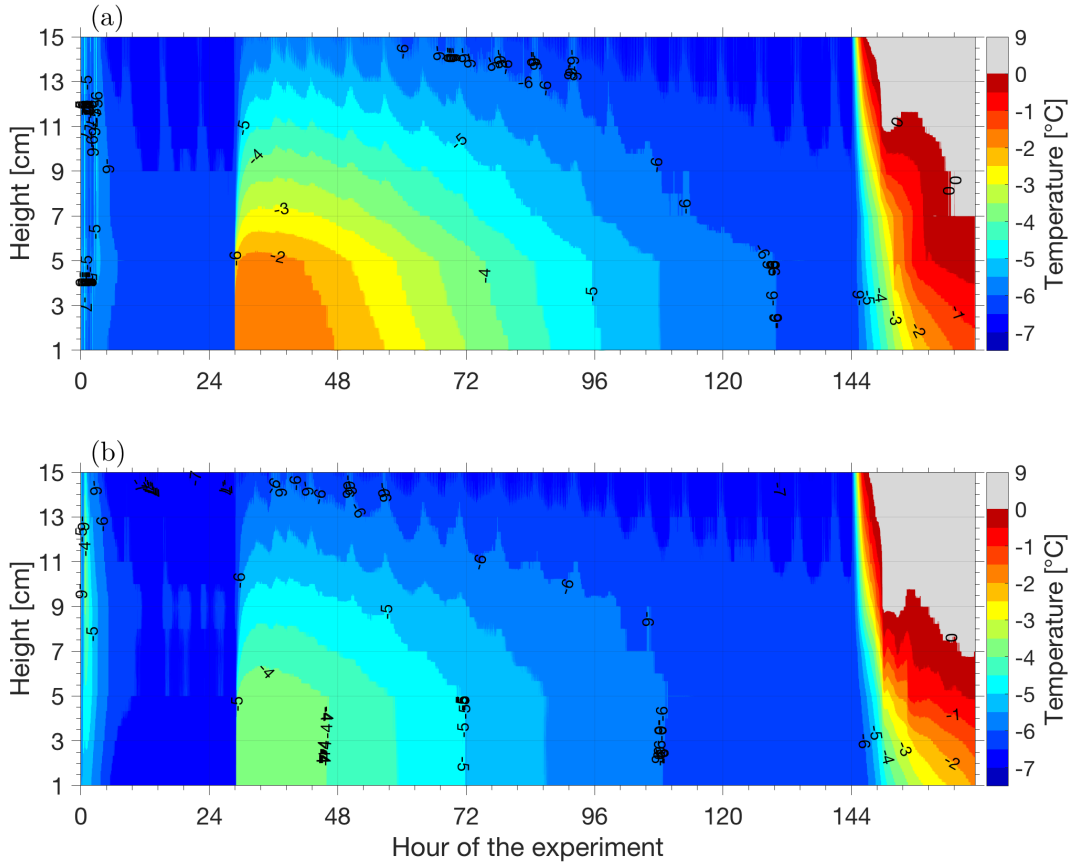

Figure 5.4 *The temperature evolution of a) Experiment* 1_{5L} *and b) Experiment* 1_{5H} *measured by the salinity harp instrument at a vertical resolution of 2 cm and a temporal resolution of approximately 40 s. By reason of comparability values above 0 °C are shown in grey.*

laboratory experiments (e.g. *Fuchs* (2017)). To get a better idea of the effective air temperature change I averaged the time series by a running mean over 10 data points (≡ 100 min) and the harp measurements over 20 data points (≈ 13.5 min). The periodic signal is still preserved because the steps for the averaging are smaller than 6 h. Hence, by application of the smoothing I rather receive more distinct effective temperature time series. If comparing those, the periodic signal first appears in the air temperature time series before it penetrates into the snow and reaches the sensors at 13 cm and 15 cm (Fig. 5.3) with an offset of around 1 h. One explanation for the delay is the result of the strong fluctuations of the air temperature by ±2.5 K. The alternating temperature signal at the snow surface changes on a high temporal resolution to be relatively warmer or colder than the snow. Therefore, an effective change in the mean of the adjacent air temperature signal is only slowly applied to the snow. They may even occur on a higher temporal resolution and are likely to be related with air flow patterns in the lab. However, at this point I don't want to go into further detail as this is not relevant for the scope of my study. There is also a delay of approximately 8 min from the signal reaching the 15 cm and afterwards the 13 cm level. The explanation for this is the

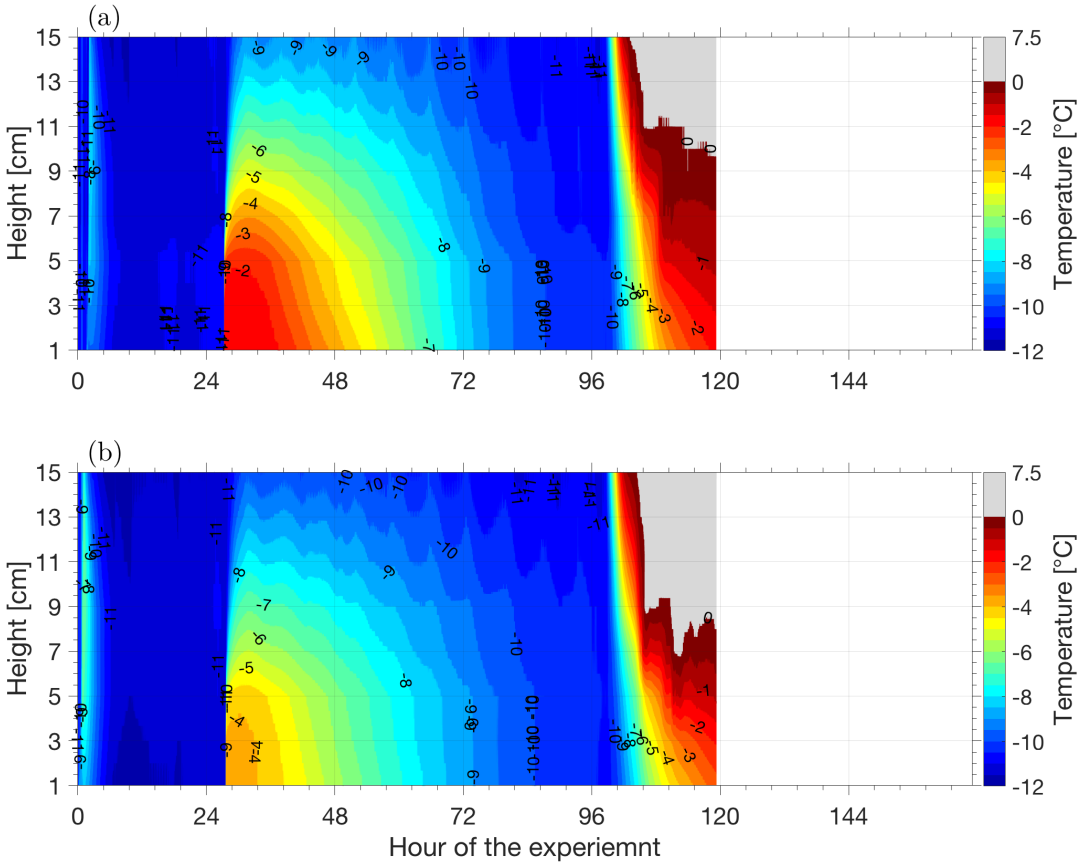

Figure 5.5 *The temperature evolution of a) Experiment* $2_{10\mathrm{L}}$ *and b) Experiment* $2_{10\mathrm{H}}$ *measured by the salinity harp instrument at a vertical resolution of 2 cm and a temporal resolution of approximately 40 s. By reason of comparability values above 0 °C are shown in grey and to increase comparability the time axis after the end of the experiment at 120 h is extended to fit the illustration in Fig. 5.4.*

heat conductivity of snow such as for a warm signal from the top it takes time before the heat is conducted downwards which first increases the temperature of the upper level.

Furthermore, the air temperature is 1–1.5 K colder than the value set for the cold lab. The experiments were situated on a table and the refrigerators are installed on the ceiling. Cold air is heavier than warm air and as a result it sinks to the bottom of the room. Hence, the temperatures in the lower levels of the room are colder than the preset temperature.

Following the description of snow properties by *Massom et al.* (2001) I assumed a linear temperature gradient in snow. Consequently, I linearly interpolated between the temperature measurements at each wire-pair level to obtain the temperature evolution of the covered profile in the snow (Fig. 5.4). For every experiment I waited at least 24 h from the start to let the snow adjust to the prevailing surrounding conditions and to let the snow profile stabilise. The experimental setup lacks any heat source from below like sea ice and underlying seawater. As a result the snow is equally tempered and no major vertical differences are visible in that time (e.g. Fig. 5.3; Fig. 5.4). The

moment of flooding at around 28 h from below with saltwater at its freezing temperature creates a temporary heat source at the bottom. Water at higher temperatures compared to the surrounding wets the lower levels of the snow and establishes a vertical linear temperature gradient along the whole profile (Fig. 5.4). Though, the setup did not allow for large amounts of water that could provide a continuous source of heat. Hence, the vertical temperature gradient diminishes over time until it has completely disappeared when all heat is conducted into the air at the snow-air interface. In case of lower air temperatures (Fig. 5.5) vertical gradients decline over a shorter period of time compared to higher air temperatures (Fig. 5.4). This is due to a more effective heat release into the air at colder temperatures. Profiles of other experiments show similar characteristics (see Fig. A.5 and Fig. A.4)

Water with lower salinity has a higher freezing point temperature than water with higher salinity and consequently provides a bigger heat source. Since the experiments have the same boundary conditions otherwise, there is more heat to release in the low-saline experiment. This results in longer preservation of the temperature gradient and more distinctive changes of the vertical temperature gradient over time compared to the high-saline experiment. Therefore, the experiment flooded by low-saline water develops a stronger temperature gradient (Fig. 5.4a; Fig. 5.5a) compared to the experiment flooded by high-saline water (Fig. 5.4b; Fig. 5.5b). The same characteristics appear if comparing the temperature evolution of the remaining Experiment 3–7 (Fig. A.4; Fig. A.5). It is also visible if comparing the change over time of the upper levels 13 cm and 15 cm for the low-saline (Fig. 5.3a) and high-saline (Fig. 5.3b) scenario.

Each experiment lasts at least 48 h after the point of flooding before I switched off the cold laboratory and thereby induced melting. With the so achieved 15 °C air temperature the melt-event appears as a significant drop over all levels in all experiments. The melt event is rather strong and from a temporal perspective not realistic. My focus is to investigate the rise of water and refreezing and rather have multiple experiments with different parameters than realising an ideal melt event. The latter might be relevant for another study and was already initiated by *Fuchs* (2017) who studied the impact of snow on the salinity of the sea ice.

5.3 Salinity evolution in flooded snow

In this section I provide and discuss the results of four exemplary experiments with varying air temperatures and salinities. The aim is to show that with the theory and calculations presented in Sec. 4 it is possible to retrieve reasonable results of the liquid fraction and bulk salinity evolution in snow. Both describe strong dependencies on the air temperature and the salinity of the flooding water and I provide a more detailed description below.

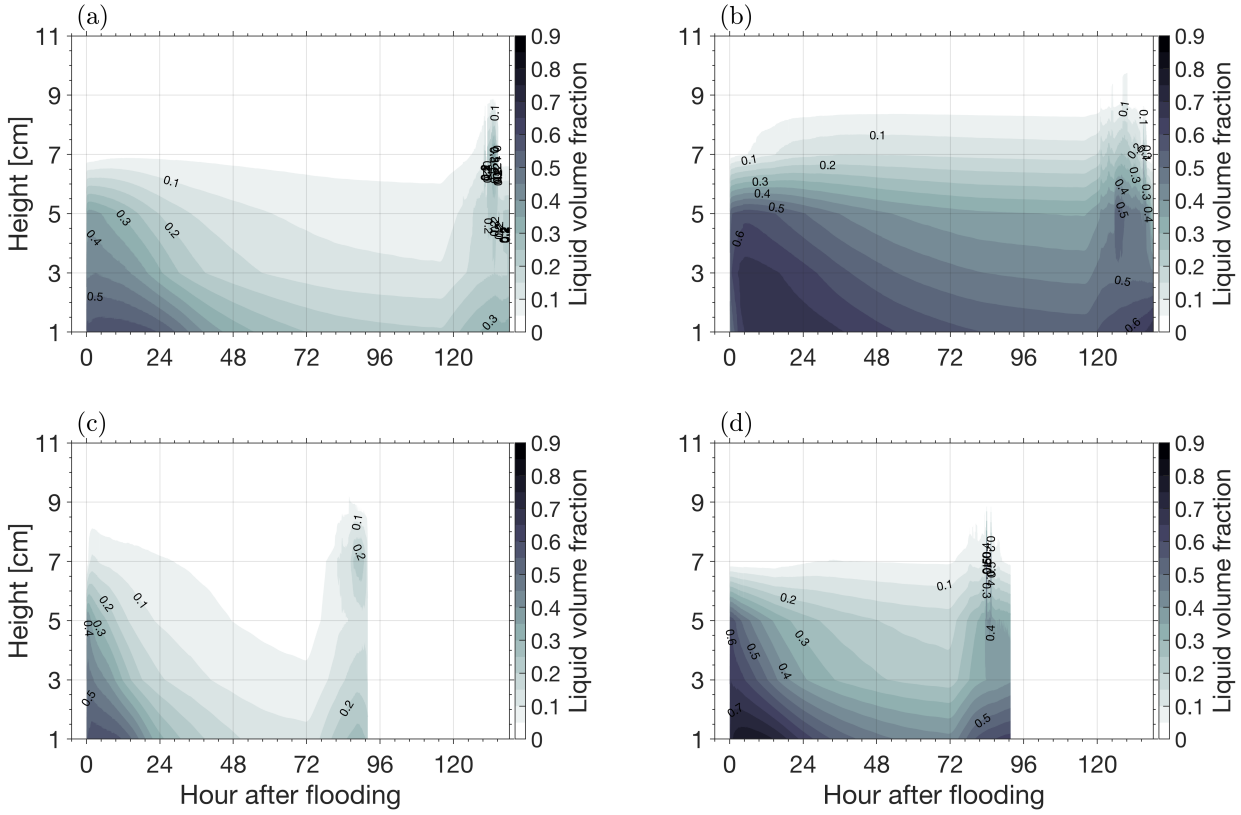

Figure 5.6 *The evolution of the liquid volume fraction $\phi_{l,v}$ of a) Experiment 1_{5L}, b) Experiment 1_{5H}, c) Experiment 2_{10L} and b) Experiment 2_{10H} estimated from salinity harp measurements at a vertical resolution of 2 cm and a temporal resolution of approximately 40 s. Removed data also appear as white areas.*

5.3.1 Results

From impedance measurements of the salinity harp it is possible to calculate the liquid volume fraction $\phi_{l,v}$ like described above (Sec. 3.1). Fig. 5.6 represents the evolution of $\phi_{l,v}$ for Experiment 1_{5L}, 1_{5H}, 2_{10L} and 2_{10H}. The data is based on measurements every 2 cm, starting at 1 cm with a temporal resolution around 40 s and values in between the measuring levels are linear interpolated.

Before the event of flooding no liquid or $\phi_{l,v} < 0.05$ is present in the snow in all experiments. Though, when flooded, liquid appears in the lower 7 cm of the profile. The maximum liquid volume fractions are in the beginning close to the 1 cm level with values up to 0.55 for Experiment 1_{5L} and 2_{10L} and up to $0.65 - -0.75$ for Experiment 1_{5H} and 2_{10H}. In the latter $\phi_{l,v} > 0.5$ up to the height of 5 cm whereas in the former only heights below 2 cm show $\phi_{l,v} > 0.5$. Experiment 1_{5L} and 2_{10L} were flooded with low-saline water and Experiment 1_{5H} and 2_{10H} with high-saline water. Furthermore, Experiment 1_{5L} and 2_{10L} are at high temperatures and Experiment 1_{5H} and 2_{10H} at low temperatures. All other parameters in all four experiments are the same.

In Experiment 1_{5L} the liquid fraction overall decreases with time in each level. There are only some contrary features in the beginning. Between 1–3 cm there is an indication that the liquid

fraction further increases in the initial 5 h and values above 5 cm remain constant within the initial 24 h. The decrease of $\phi_{\mathrm{l,v}}$ is strongest in the lower two thirds of the flooded snow between 1–5 cm. The liquid fraction rises in all levels at the moment of melting when I set the air temperature of the laboratory to 15 °C.

Comparing the results to Experiment $1_{5\mathrm{H}}$ which is flooded at higher salinity and identical parameters otherwise (Fig. 5.6b) the liquid fraction is higher in all levels by about 0.1. Below 6 cm values show similar characteristics like in the low saline experiment. The liquid fraction first increases within the initial 12 h and decreases afterwards until the moment of melting. Though, the behaviour above 6 cm is different to the low saline experiment. The liquid fraction remains almost constant throughout the whole experiment until the melt event in the end. During the latter values increase in all levels similar to Experiment $1_{5\mathrm{L}}$.

If using the same parameter setup but at an air temperature of −10 °C overall values are similar to the respective experiment at same salinity. Though, the characteristics of the evolution with time change for both, low saline (Fig. 5.6c) and high saline (Fig. 5.6d) experiments respectively. In the time after flooding no rise of the liquid fraction is present in the lower levels. Instead, the liquid fraction decreases in all levels with time right after flooding. The overall decay is stronger compared to the high temperature experiments. However, the same characteristics due to the different salinity of the flooding water are present. The low saline experiment (Fig. 5.6c) shows overall smaller liquid fractions than the high saline experiments (Fig. 5.6d). In addition, the liquid fraction remains almost constant above 6 cm in Experiment $2_{10\mathrm{H}}$. After the onset of higher air temperatures at 72 h both experiments show increasing increasing liquid fractions in all levels similar to the high temperature experiments.

Following the methods introduced in Sec. 4 it is possible to estimate the bulk salinity S_{bu} during the experiment at each wire pair of the respective salinity harp. I used the quintic approach Eq. 4.12 for the density profile of ρ_{iso} with $c = 7$, $\rho_{\mathrm{l}} = 1028\,\mathrm{kg\ m^{-3}}$ and $\rho_{\mathrm{iso}} = 900\,\mathrm{kg\ m^{-3}}$ at the grid-snow interface. For the density at the highest wire pair in snow I set $\rho_{\mathrm{iso}} = \rho_{\mathrm{sn}}$ with ρ_{sn} from the respective experiment in Tab. 5.1. Thus, by applying a linear interpolation between the measuring heights the evolution of S_{bu} for the covered snow profile is shown in Fig. 5.7. In all experiments the snow was not in contact with saltwater before the moment of flooding and for the whole profile covered by the salinity harp $S_{\mathrm{bu}} < 2\,\mathrm{g\,kg^{-1}}$ before the moment of flooding.

In the low salinity and high temperature experiment (Experiment $1_{5\mathrm{L}}$, Fig. 5.7a) the bulk salinity shows values around $16\,\mathrm{g\,kg^{-1}}$ between 1 cm and 5 cm after the initial flooding. Between 5 cm and 7 cm values decrease down to $S_{\mathrm{bu}} < 2\,\mathrm{g\,kg^{-1}}$ showing a strong vertical gradient compared to the levels below. Afterwards, within the initial 24 h the bulk salinity increases by 2–4 $\mathrm{g\,kg^{-1}}$ in the levels from 1 cm to 3 cm and then remain almost constant until the moment of melting. The layers from 3 cm to 6 cm show a decrease of the bulk salinity by about $2\,\mathrm{g\,kg^{-1}}$ until 24 h. Afterwards,

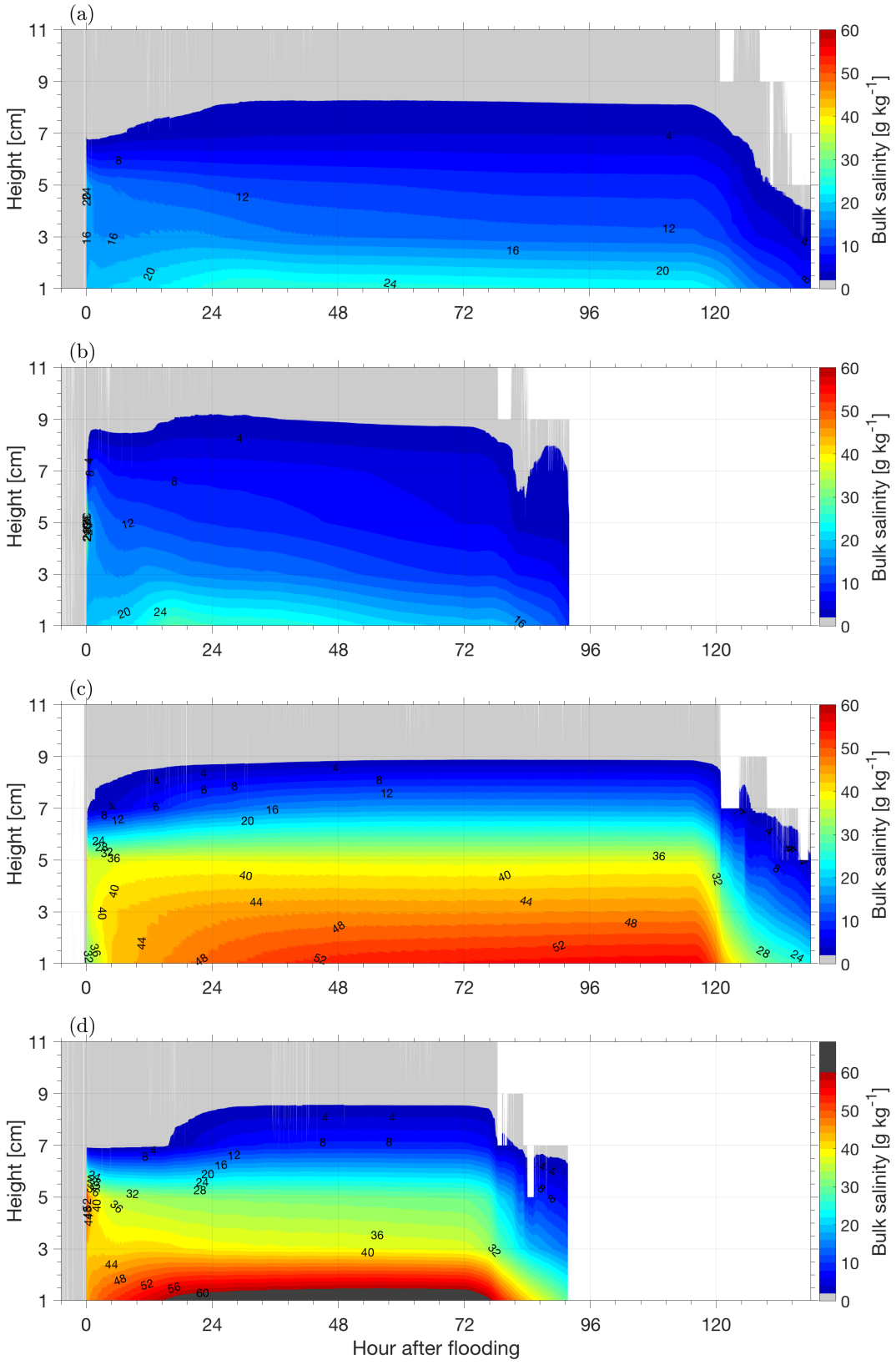

Figure 5.7 *The bulk salinity S_{bu} evolution of a) Experiment $1_{5\mathrm{L}}$, b) Experiment $2_{10\mathrm{L}}$, d) Experiment $1_{5\mathrm{H}}$ and b) Experiment $2_{10\mathrm{H}}$ measured by the salinity harp instrument at a vertical resolution of 2 cm and a temporal resolution of approximately 40 s. Data points with $S_{\mathrm{bu}} < 2\,\mathrm{g\,kg^{-1}}$ are coloured in grey for visual enhancement of the least and unaffected snow and removed data are marked as white areas.*

values decrease at lower rates until the melt event. The layers above 6 cm show almost constant values throughout the whole experiment between flooding and the moment of melting. Overall, the strongest vertical gradients appear between 5 cm and 7 cm in the initial 24 h and thereupon between 1 cm and 3 cm. With the onset of melting at around 115 h the bulk salinity decreases in all levels.

For lower air temperatures (Experiment 1_{5H}, Fig. 5.7b) the overall values are almost the same. Though, the initial decrease and rise between 1 cm and 3 cm takes place over a shorter period of time. Furthermore, only levels above 7 cm show almost constant values. In all other levels the bulk salinity decreases over time. The strongest vertical gradients are present between the 1 cm and 3 cm level.At the moment of flooding around 72 h the bulk salinity first remains constant in all levels for another 12 h. Afterwards, values decrease until the end of the experiment similar to the high temperature experiment (Fig. 5.7a)

In the high saline experiments (Fig. 5.7c,d) overall values of the bulk salinity are up to twice as high compared to the respective low saline experiment. Furthermore, vertical gradients are stronger throughout the duration of the experiment. They are strongest between 1 cm and 3 cm and between 5 cm and 7 cm. Both experiments show characteristics of increasing bulk salinities after flooding in the lower layers, similar to the low saline experiments. However, comparing respective low (Experiment 1_{5L} and 2_{10L}) to high saline experiments (Experiment 2_{10L} and 2_{10H}), the increase takes place over a longer period of time in the high saline case. Furthermore, the increase occurs up to a higher level of 5 cm in Experiment 2_{10L} (Fig. 5.7c). Instead, Experiment 2_{10H} (Fig. 5.7d) shows decreasing values between 3 cm and 5 cm, similar to the low saline experiments. Above 5 cm both high saline experiments present constant values throughout the experiment between the time of flooding and melting. Subsequent to the onset of melting the bulk salinity decreases in all experiments across all layers.

5.3.2 Discussion

The vertical resolution provided by the salinity harp is 2 cm. For the illustrations of the liquid volume fraction $\phi_{l,v}$ (Fig. 5.6) and the bulk salinity S_{bu} (Fig. 5.7) values in between are linearly interpolated. As to my knowledge literature does not provide any other suggestions on how to interpolate the liquid fraction or the bulk salinity between two layers in snow. It only provides values for the height the water reaches in snow (e.g. *Coléou et al.* (1999) for freshwater or *Massom et al.* (2001) for saltwater) and information about the profile of the liquid water content of the pore volume (*Coléou et al.*, 1999). From a mathematical perspective the linear approximation is the method with the least assumptions about the profile for the interpolation between two data points and thus the most appropriate to use in my case. Though, with the given 2 cm resolution features such as the height of the rising waterfront are likely to be overestimated by the linear interpolation. That is clearly visible at the 7 cm level in Fig. 5.7d for instance. As soon as $S_{bu} \geq 2\,\mathrm{g\,kg^{-1}}$ after 16 h

values are linearly interpolated to the measurement at 9 cm where $S_{\mathrm{bu}} < 2\,\mathrm{g\,kg^{-1}}$. The resulting strong ascend of the point $S_{\mathrm{bu}} < 2\,\mathrm{g\,kg^{-1}}$ does not match the development of the measurements at 7 cm before 16 h. Additionally, none of the measuring levels below suggests any rise that strong. Measurements at the 5 cm level even indicate decreasing values of the layers below. Thus, whereas it was reasonable to estimate a linear profile for the temperature evolution (see Sec. 5.2) the liquid volume fraction and bulk salinity profiles are not linear for the whole profile. Consequently, presented values and features between the measuring heights of $\phi_{\mathrm{l,v}}$ and S_{bu} need to be interpreted critically. The linear interpolation is a reasonable choice for the first guess of the profile. Though, further investigations or higher vertical resolutions for measurements are required to find a more appropriate interpolation method.

As mentioned earlier it is necessary to transfer the liquid volume fraction into the liquid mass fraction $\phi_{\mathrm{l,m}}$ to estimate the bulk salinity. Though, the liquid volume fraction is more appropriate when describing the presence of liquid in snow. One one hand, it is a more intuitive quantity that defines the space the liquid is claiming in the snow. On the other hand, for the derivation of $\phi_{\mathrm{l,m}}$ it is necessary to insert assumptions about the density of the profile as described in Sec. 4.2.2. Thus, the evolution of $\phi_{\mathrm{l,m}}$ is influenced by those assumptions and instead, $\phi_{\mathrm{l,v}}$ is the original quantity measured by the salinity harp, free of any assumptions.

In Sec. 4.2.2 I provided an approach to estimate $\phi_{\mathrm{l,m}}$ based on only the density at the bottom and at the top of the profile and the height of the water rise (c in Eq. 4.12). For ρ_{iso} at the bottom of the profile as well as for ρ_{l} and c I use the same values as discussed in Sec. 4.2.2. Therefore, the uncertainty incorporated in the definition of these three variables is the same for the results of all experiments. Due to practical reasons I was only able to measure the density at the top of the profile but not at the bottom. Furthermore, in my study I did not have a reliable method to quantify an exact value for c in every experiment. This is linked to the same problem as for the interpolation method of lacking exact information about the vertical profile in the snow. Again, a higher vertical measuring resolution or a higher quantity of different experiments may yield a better approximation of the vertical profile.

With the results I present in this section it is not possible to draw final conclusions on the effect of all different parameters on the evolution of $\phi_{\mathrm{l,v}}$ and S_{bu}. Though, if comparing the evolution of $\phi_{\mathrm{l,v}}$ in all experiments (Fig. A.6; Fig. A.7) it is possible to identify a trend for the impact of the air temperature T_{air} and the salinity of the flooding water S_{w}. At low salinity and temperature and constant experiment parameters otherwise (Fig. 5.6c; Fig. A.6a,c) the liquid volume fraction tends to decrease over a shorter period of time compared to the low salinity high temperature experiments (Fig. 5.6a; Fig. A.6b,d). The same characteristics appear in the high salinity experiments comparing the low temperature (Fig. 5.6d; Fig. A.7a,c) and high temperature (Fig. 5.6b; Fig. A.7b,d) experiments. At lower temperatures the flooding water freezes at higher rates compared to higher temperatures. That is due to the more effective heat release at colder

temperatures as discussed in Sec. 5.2. Freezing induces an increase of the solid fraction and a consequent decrease in the liquid fraction.

There is further evidence in the bulk salinity evolution. For the calculation of the bulk salinity both impedance and temperature evolution are incorporated in form of the liquid fraction and the brine salinity (see Sec. 2 and Sec. 3.1). Therefore, it defines an adequate representation of the interaction of both. This is also an explanation why the bulk salinity may be low even if the liquid fraction indicates the presence of large amounts of water. At lower temperatures (Fig. 5.7b,d; Fig. A.9a,c; Fig. A.10a,c) the onset of the bulk salinity decrease in the lower levels is at a shorter period of time compared to the high temperature case (Fig. 5.7a,c; Fig. A.9b,d; Fig. A.10b,d). Thus, dropping values of the bulk salinity in low temperature experiments indicate higher rates of freezing and subsequent brine release.

Furthermore, there is evidence for a trend caused by the impact of different S_{w} at otherwise constant parameters. In the high saline experiments (Fig. 5.6b,d; Fig. A.7) the liquid volume fraction tends to decrease at lower rates over time and along the whole profile compared to the high saline experiments (Fig. 5.6a,c; Fig. A.6). The same characteristics appear also at lower salinity differences with $S_{\mathrm{w}} = 45\,\mathrm{g\,kg^{-1}}$ (Fig. A.8a) and $S_{\mathrm{w}} = 55\,\mathrm{g\,kg^{-1}}$ (Fig. A.8b). Thus, if flooded by higher salinities, freezing in snow occurs at lower rates compared to flooding by lower salinities. There is further evidence in the evolution of the bulk salinity profile in the low saline (Fig. 5.7a,b; Fig. A.9) compared to the high saline experiments (Fig. 5.7c,d; Fig. A.10). The former shows an increase in the bulk salinity in the lower levels until around 24 h after flooding and decreasing values afterwards. Instead, the increase is present until the melt event in the end in almost all high saline experiments. This is due to the different rates of freezing and subsequent brine release at the bottom. I suggest that with low salinity the onset of freezing at lower levels appears at shorter time periods after flooding than for high salinities. I provide further explanations and draw final conclusions on the effect of different salinities and temperatures in the next section (Sec. 5.4.2).

During the initial rise of water in the moment of flooding both, $\phi_{\mathrm{l,v}}$ and S_{bu} show high values at the 1 cm level decreasing with height up to the 7 cm level. The high values at the bottom in all experiments are explained by the freeboard of $h_{\mathrm{f}} \leq -1cm$. As a result snow between the snow interface at the bottom and the waterline is soaked with water. Above the waterline water rises due to capillary suction as described for freshwater by *Coléou et al.* (1999). They find a decreasing liquid water content of the pore volume with height. Thus, less water is present with height which explains the decrease of the liquid fraction and the bulk salinity with height. From my own experiences and from reports by *Massom et al.* (2001) capillary suction is strongest at short time scales after flooding. Still, within approximately 12 h after flooding in the lower levels of most of the experiments the liquid fraction increases before dropping afterwards (e.g. Fig. 5.6; Fig. A.6). Similarly the bulk salinity initially decreases and increases afterwards (e.g. Fig. 5.7a,c,d; Fig. A.9). Thus, I suggest that after the initial flooding the subsequent rise in the liquid fraction and decrease

in the bulk salinity originates from a combination of release of less saline brine from upper layers and further rise of more saline brine from lower levels. I provide a concluding discussion on this in Sec. 5.4.2.

During the experiment the saltwater around the frame also froze. As a result the salinity of the water below the ice and the grid of the frame increased. This could lead to the infiltration of more saline water from below. However, the decrease of the liquid fraction over time and along the whole vertical profile for all experiments (e.g. Fig. 5.6) suggests that liquid is either freezing or draining off at the bottom. Hence, no water penetrates the snow from below after the initial flooding.

5.4 Drivers of water rise and freezing

In the previous section I used new theories and several assumptions to estimate the evolution of the bulk salinity profile from impedance measurements and the resultant liquid volume fraction. Here I use the raw data time series for the impedance Z. Every experiment features a different combination of the parameters S_w the salinity of the flooded water, T_air air temperature , D the dominating grain sizes and h_f the freeboard at flooding (see Tab. 5.1). For each experiment I set the parameters such that at least two experiments have one parameter in common. Hence, the impedance measurements during those experiments are comparable at each respective measuring height. Thus, I am able to compare all experiments per measurement height, further investigate the effects of the chosen parameters for each experiments and evaluate the features mentioned in Sec. 5.2 and Sec. 5.3. Furthermore, I draw final conclusions about all mentioned features and provide explanations for observed characteristics.

5.4.1 Results

In Fig. 5.8 the time series of Z during the initial 60 h after flooding are shown for all low saline (Fig. 5.8a) and high saline (Fig. 5.8b) experiments. At the lower three measuring heights (Fig. 5.8a[i–iii]; Fig. 5.8b[i–iii]) at 1 cm, 3 cm and 5 cm the impedance drops significantly down to $Z \approx 10\,\Omega$ at the moment of flooding. The absolute values of Z in the low saline experiments are higher by about 2–4 Ω than in the high saline experiments for each level. At 5 cm (Fig. 5.8a[iii]; Fig. 5.8b[iii]) the impedance immediately increases steadily and linear over time after the flooding for all experiments besides Experiment $5_{5\mathrm{H}}$. The rise is at higher rates for the low saline experiments than for the high saline experiments. A similar increase of Z is present at 3 cm (Fig. 5.8a[ii]; Fig. 5.8b[ii]) and 1 cm (Fig. 5.8a[i]; Fig. 5.8b[i]). Though, there is trend of a shifted onset by on average 8 h every −2 cm. The rise starts between 6 h and 18 h after flooding at 3 cm and between 12 h and 24 h at 1 cm. Furthermore, rates are lower with decreasing height and also lower in the high saline experiments compared to the low saline experiments in each level. At 3 cm the increase is only present in Experiment $2_{10\mathrm{H}}$, $4_{10\mathrm{H}}$ and $6_{10\mathrm{H}}$. Experiment $1_{5\mathrm{H}}$, $3_{5\mathrm{H}}$ and $5_{5\mathrm{H}}$ remain constant after flooding, also

in the 1 cm level. Thus, in the three lower measuring levels the high saline experiments show no or lower rates of increasing impedance than the high saline experiments. In terms of the shifted onset of freezing with decreasing height there are no major differences between the low and high salinity case . Within the 60 h after flooding $Z \leq 15\,\Omega$ at 1 cm and $Z \leq 30\,\Omega$ at 3 cm and 5 cm in the high saline experiments. In the low saline experiments $Z \leq 40\,\Omega$ at 1 cm, $Z \leq 70\,\Omega$ at 3 cm and $Z \leq 110\,\Omega$ at 5 cm.

In the 7 cm level (Fig. 5.8a[iv]; Fig. 5.8b[iv]) the same differences between low and high saline experiments occur. Though not all experiments show a drop during flooding and a subsequent increase in impedance. In the low saline experiments only Experiment 2_{10L}, 4_{10L}, 5_{5L} and 6_{10L} show a similar behaviour like in the 5 cm level. Values initially drop significantly and $10\,\Omega \leq Z \leq 50\,\Omega$. The increase afterwards appears at rates similar to the rates at the 5 cm level. However, Experiment 1_{5L} and 3_{5L} are not revealing any distinct characteristics similar to the behaviour at lower levels. They show decreasing impedance around 12 h and 24 h respectively. Though, $Z \geq 140\,\Omega$ for the former and $Z \geq 90\,\Omega$ for the latter. For both there is an indication for similar increasing rates afterwards like at the 5 cm level. A similar behaviour appears in the high saline experiments (Fig. 5.8b[iv]). Not all experiments show characteristics analogue to the heights below. Only Experiment 5_{5H} and 6_{10H} feature a distinct drop of impedance down to $20\,\Omega \leq Z \leq 30\,\Omega$ in the moment of flooding. While in Experiment 5_{5H} the impedance remains rather constant it increases steadily in Experiment 6_{10H}. Experiment 1_{5H} also shows a drop of impedance but over a longer period of time. In the beginning $Z \approx 160\,\Omega$ and subsequently it further decreases non-linearly. In Experiment 2_{10H} and 4_{10H} the impedance drops at around 12 h and 24 h respectively. For both the impedance steadily increases afterwards at higher rates compared to the 5 cm level. Experiment 3_{5H} does not appear within the range of Z in this illustration.

In Fig. 5.9 the same experiments are illustrated in a different arrangement. Here experiments are grouped according to same air temperatures $T_{\mathrm{air}} = -10\,^{\circ}\mathrm{C}$ (Fig. 5.9a) and $T_{\mathrm{air}} = -5\,^{\circ}\mathrm{C}$ (Fig. 5.9b). In addition the impedance time series for Experiment $7_{5L(i)}$ and $7_{5H(i)}$ are included. They also show a significant drop of impedance down to $Z \approx 10\,\Omega$ in the three lower measuring heights 1 cm, 3 cm and 5 cm at the moment of flooding like the other experiments (Fig. 5.9a[i–iii]); Fig. 5.9b[i–iii]). Afterwards the impedance increases, starting at different periods of time since flooding and at various rates similar to characteristics described for different S_{w} (Fig. 5.8). However, in the representation of the impedance evolution here it is possible to directly compare parameter setups at different air temperatures. In all three levels at 1 cm, 3 cm and 5 cm the low temperature experiments (Fig. 5.9a) show a significantly stronger rise of impedance than the respective experiment (indicated by same colours) at high temperature (Fig. 5.9b). The rates show a stronger increase with increasing height in the low temperature experiments compared to the high temperature experiments. Additionally, a lower temperature leads to a stronger increase of impedance in the low saline experiments (Experiment 1_{5L}, 2_{10L}, 3_{5L}, 4_{10L}, 5_{5L} and 6_{10L}) than in the high saline experiments (Experiment 1_{5H}, 2_{10H},

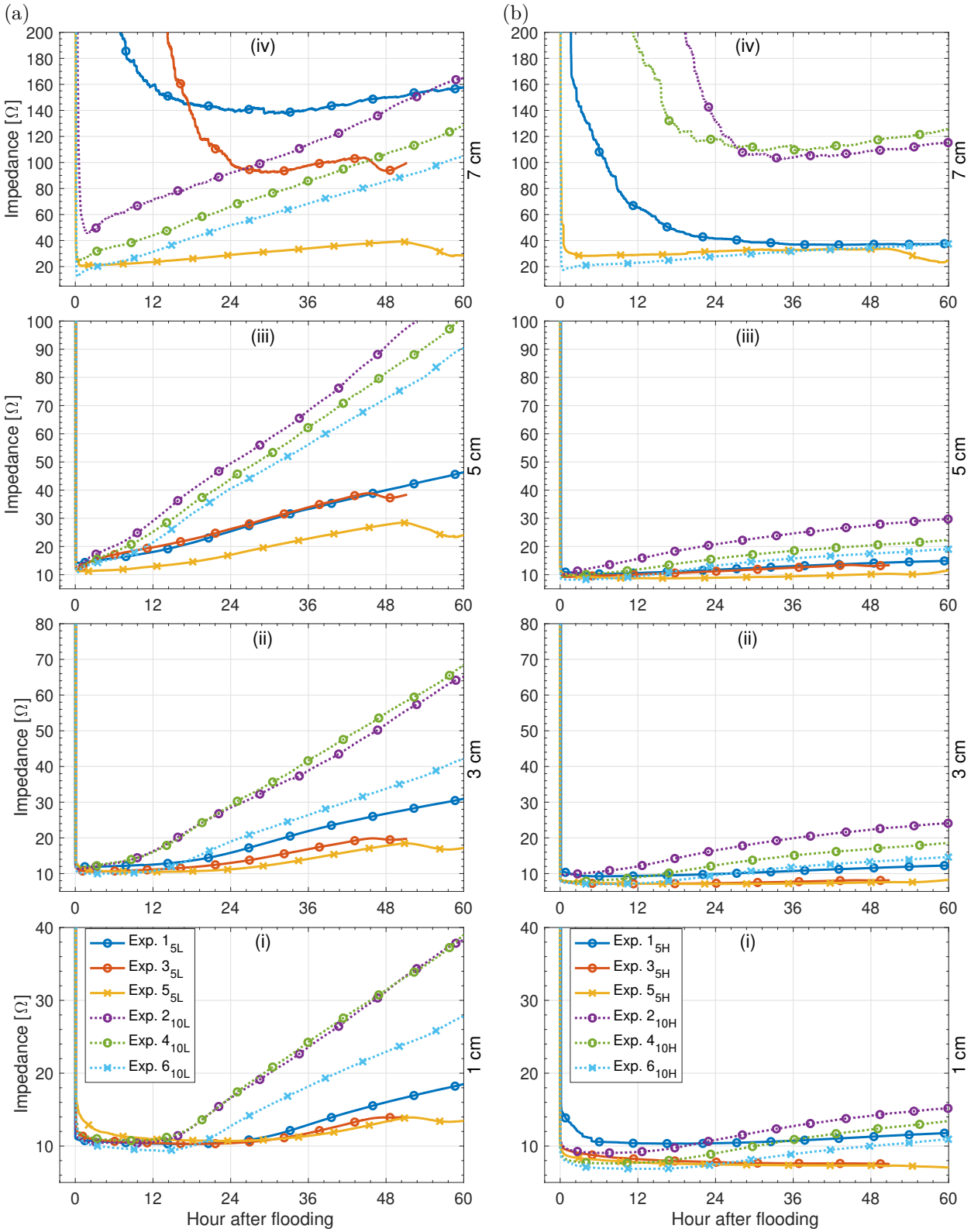

Figure 5.8 *Comparison of the impedance Z per height i) 1 cm, ii) 3 cm, iii) 5 cm and iv) 7 cm with a) $S_w \approx 34\,g\,kg^{-1}$ and b) $S_w \approx 68\,g\,kg^{-1}$. Note different y-scales. The line colour refers to the same parameters besides S_w, the line style refers to similar air temperatures T_{air} and the type of marker to the same freeboard.*

3_{5H}, 4_{10H}, 5_{5H} and 6_{10H}). Furthermore the shift of the onset with decreasing height starting at the 5 cm level is different for the high and low temperature experiments. In the former experiments the impedance either immediately rises after flooding or remains constant at the 5 cm level. In the low temperature setups all experiments show an immediate rise of impedance after flooding. At 3 cm the impedance starts to rise between approximately 6–12 h in the low temperature experiments. In the same level the onset of the increase is either around 24 h or values are constant in the high temperature experiments. At 1 cm the onset is located around 12–24 h in the low temperature experiments and around 24–36 h in the high temperature experiments. Hence, the shift with decreasing height is about 1.5–2 times larger over the heights from 5 cm down to 1 cm at higher temperatures compared to lower temperatures.

Similar characteristics for respective experiments at either high or low temperature appear in the 7 cm level. For instance Experiment 2_{10L}, 4_{10L}, 6_{10L} and 6_{10H} (Fig. 5.9a[iv]) at lower temperature indicate higher rates for the increase of impedance after the initial drop compared to the respective parameter setup at higher temperature in Experiment 1_{5L}, 3_{5L}, 5_{5L} and 5_{5H} (Fig. 5.9b[iv]). In addition, the drop of impedance takes place at a later period of time in the high temperature Experiment 1_{5L} and 3_{5L} compared to the respective low temperature Experiment 2_{10L} and 4_{10L}. However, Experiment 1_{5H} and Experiment 2_{10H} show a behaviour contrary to that.

The two experiments that were flooded by water with salinities at intermediate values (Experiment $7_{5L(i)}$ and $7_{5H(i)}$) indicate an impedance evolution as a composition of both sets of low and high saline characteristics. Similar to the low saline experiments the impedance increases after flooding at all heights showing a similar delay with decreasing height. Though, rates are smaller and values range between the constant impedance evolution of the high saline experiments and the impedance evolution of the low saline experiments. At the 7 cm no overall characteristic of one experiment group is dominant. However, the impedance measurements in Experiment $7_{5L(i)}$ and $7_{5H(i)}$ describe similar characteristics as Experiment 5_{5L} but with up to 40 Ω higher absolute values.

In all heights (Fig. 5.8; Fig. 5.9) the experiments with $h_f = -2$ cm (Experiment 5_{5L}, 5_{5H}, 6_{10L} and 6_{10H}) show the lowest impedance measurements compared to the experiments with $h_f = -1$ cm (all others) at same T_{air} or S_w. Furthermore, all $h_f = -2$ cm experiments show values in the 7 cm (e.g. Fig. 5.9a[iv],b[iv]) level with characteristics similar to the 5 cm level. During flooding the impedance drops down to the lowest values of impedance in the 7 cm level compared to the other experiments and steadily increases afterwards.

5.4.2 Final discussion

In Sec. 5.2 and Sec. 5.3 I already initiated conclusions on the temperature and salinity effect on the evolution of the temperature, liquid volume fraction $\phi_{l,v}$ and bulk salinity S_{bu} profile in flooded snow. However, I described tendencies based on the results of mainly four experiments and it

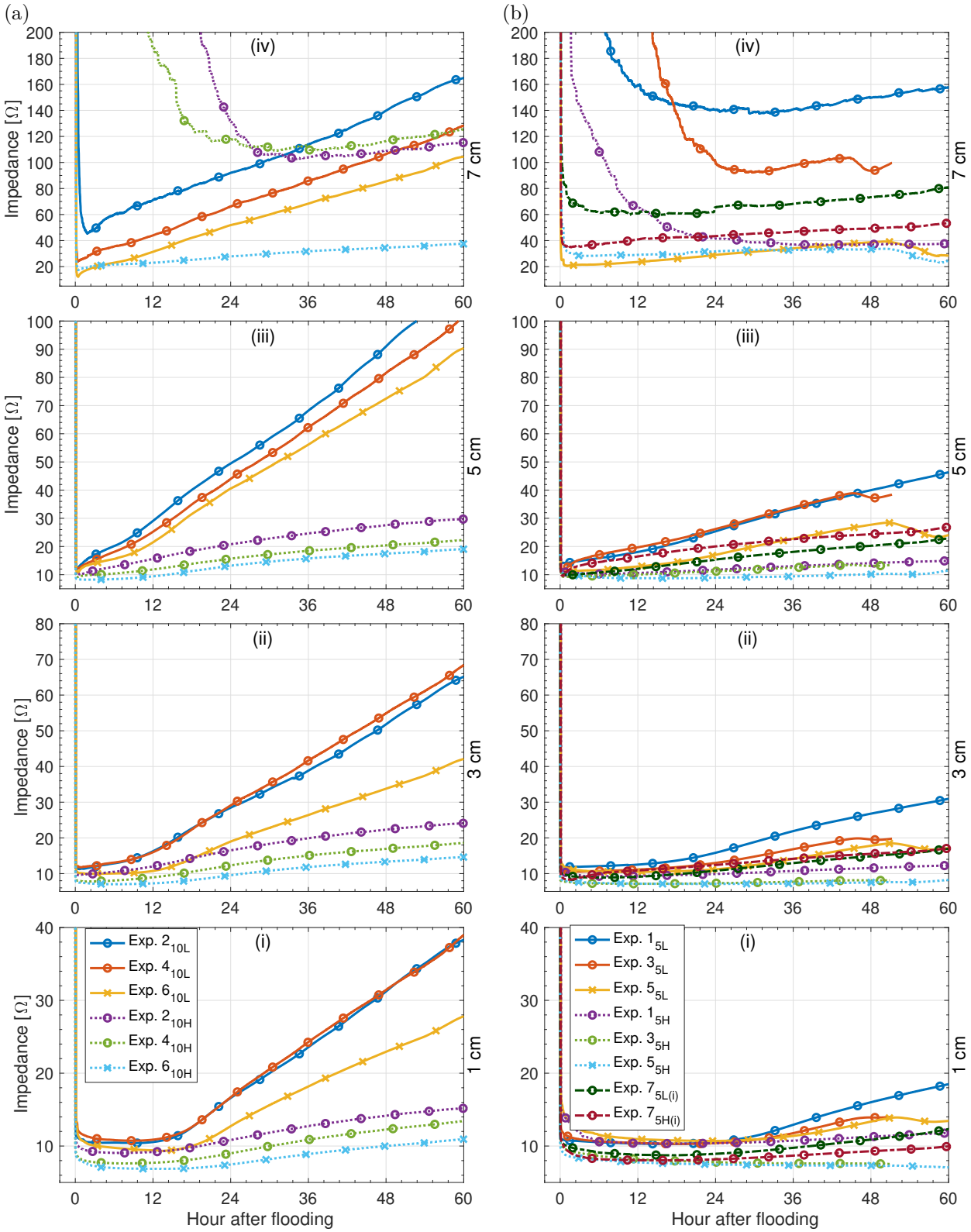

Figure 5.9 *Comparison of the impedance Z per height i) 1 cm, ii) 3 cm, iii) 5 cm and iv) 7 cm at a) $T_{\mathrm{air}} = -10\,°C$ and b) $T_{\mathrm{air}} = -5\,°C$. Note different y-scales. The line colour refers to the same parameters apart from T_{air}, the line style refers to similar salinities S_{w} (Experiment $7_{5\mathrm{L(i)}}$ and $7_{5\mathrm{H(i)}}$ considered as intermediate salinities) and the marker to the same freeboard.*

was difficult to draw certain final conclusions on the effect of all varied experiment parameters. Thus, in this section I compare the raw impedance data to confirm findings from before and to not only discuss the effect of air temperature T_{air} and salinity of the flooding water S_{w} but also the freeboard h_{f} and grain size D. Therefore, I am able to draw final conclusions without the restriction of incorporated assumptions that go into the calculation of the bulk salinity profile for instance.

INTERPRETATION OF IMPEDANCE MEASUREMENTS

First of all, as mentioned earlier absolute values of impedance may already be influenced by small changes in the spacing of the wires or impurities on the wires for instance. Thus, in every experiment absolute values of the impedance can differ even if the conditions of the measurement volume may be identical. Though, this effect is in the dimension of 1 Ω. If differences are larger by at least one dimension the absolute values of impedance yields information about the different properties of the measuring volume. Lower absolute values yield a lower solid/isolating fraction and a higher liquid fraction. Furthermore, the impedance is related to the salinity and temperature of the liquid fraction which both have an effect of the conductivity (Fig. 4.1; Fig. A.2). Though, if salinity and temperature does no change significantly differences are at smaller dimensions compared to the change of the liquid to isolating fraction ratio. Furthermore, the relative change of impedance forms the basis of the liquid volume fraction calculation as presented above (Sec. 3.1). The impedance is strongly related to the fraction of ice that surrounds the wire pair (*Notz et al.*, 2005) or here the isolating fraction (see Sec. 4). Thus, the rate of decline or increase of impedance yields information on the melting or freezing respectively. The type of illustration I present in this section is appropriate to compare the overall effect of the respective parameters. For instance, it is possible to compare the effect of the salinity of the flooding water S_{w} by comparing respective experiments at low salinity (Fig. 5.8a) to experiments at high salinity (Fig. 5.8a). In the presentation in this section I only compare the 1 cm, 3 cm, 5 cm and 7 cm level because the water did rarely reach heights above 9 cm or show a change in impedance in this level.

FREEBOARD

In the 7 cm level (e.g. Fig. 5.9a[iv],b[iv]) there is an indication that besides the already mentioned effects of the salinity and the air temperature the freeboard h_{f} may also affect the impedance. Even though the absolute values are not as important as mentioned above there is an explanation for the overall lower values for experiments at $h_{\mathrm{f}} = -2$ cm (Experiment $5_{5\mathrm{L}}$, $5_{5\mathrm{H}}$, $6_{10\mathrm{L}}$ and $6_{10\mathrm{H}}$). At a more negative freeboard the hydrostatic pressure on the water in the bottom of the snow is higher compared to a less negative freeboard. Furthermore by definition the waterline reaches up to a higher level in the snow. If the freeboard is −1 cm it is likely that the water completely covers the lower 1 cm in the snow and that water rise above 1 cm is mainly induced by capillary suction. Thus, if the freeboard is 2 cm this interface is moved up by 1 cm. That means, more water is present in

the lower 2 cm of the snow and the profile induced by capillary suction is also moved up by 1 cm. However, this is not strictly true as there are other parameters that influence the rise of water as well. Nevertheless, there is evidence for this theory such that only experiments at −2 cm freeboard show an evolution of impedance in the 7 cm similar to the characteristics of the levels below. This is visible if comparing Experiment 5_{5L}, 5_{5H}, 6_{10L} and 6_{10H} to Experiment 3_{5L}, 3_{5H}, 4_{10L} and 4_{10H} respectively (Fig. 5.8; Fig. 5.9; Fig. A.12) where only the freeboard differs and all other parameters are identical.

SNOW AND GRAIN SIZE

To identify the effect of the grain size it is appropriate to compare experiments with varying grain size $D = 0.5$–1 mm (Experiment 1_{5L}, 1_{5H}, 2_{10L} and 2_{10H}) to the respective experiments with $D = 1$–2 mm (Experiment 3_{5L}, 3_{5H}, 4_{10L} and 4_{10H}) at identical parameters otherwise (Fig. 5.8; Fig. 5.9; Fig. A.13). Different to the other three parameters the grain size does not have as strong effects on the impedance. However, in the experiments I realised I was not able to use a huge variety of different snow. Based on the explanations above (Sec. 5.1) the snow only varied in grain size and not in density or bonding and strength. Prior to flooding the snow was at about same temperatures. Metamorphism in such type of snow leads to rounding of grains and increase of snow strength (*Massom et al.*, 2001). Thus, I expect same conditions in all snow which I used in the experiments here. To draw more reliable conclusions about the effect of snow grains it is necessary to conduct further experiments at different types of snow and with respect to various densities and bonding. For example *Sturm et al.* (1998) reports grain size in the Amundsen and Ross Seas varying from 1.1 ± 0.6 mm in new snow to 2.0 ± 0.9 mm in depth hoar and snow density varying from $210\,\mathrm{kg\,m^{-3}}$ for depth hoar to $410\,\mathrm{kg\,m^{-3}}$ for hard slabs. These values can be an appropriate guideline for further experiments and the investigation of the effect of snow density, grain size and type on impedance measurements in flooded snow. Furthermore, by using instruments like the blade hardness gauge (Sec. 3.2) it is possible to introduce a better scientific representation of the snow hardness and grain bonding into the investigation of saltwater rise in snow.

SALINITY AND AIR TEMPERATURE

In all experiments the differences in T_{air} and S_{w} created the largest impact on impedance measurements. Features were also present in the evolution of the liquid fraction and the bulk salinity (Sec. 5.3) as well as in the temperature evolution (Sec. 5.2). However, one reason why in my study T_{air} and S_{w} describe the largest impact is because I used a large interval for values of both. The air temperature varies by 5 K with −10 °C and −5 °C and the salinity of the flooding water is different by double the salt concentration at $S_{\mathrm{w}} \approx 34\,\mathrm{g\,kg^{-1}}$ and $S_{\mathrm{w}} \approx 68\,\mathrm{g\,kg^{-1}}$. Though, I chose these four values based on experienced temperatures and salinities I found at the ice-snow interface in the field to investigate the extremes rather than values in between.

SALINITY INDUCED MELTING AND FREEZING IN SNOW

To understand the effect of saltwater on snow there are two main processes to describe. First, the liquid fraction increases due to the presence of water independent of its salt concentration. Second, the interface between the snow grains and the saltwater is defined by a dynamic equilibrium between the ice and the liquid phase (*Kim and Yethiraj*, 2008). Salt prevents water from freezing and thus lowering the freezing point. Conversely, salty water melts ice until the equilibrium is reached. The more saline the water the more ice is melted. Though, this is strongly dependent on the temperature difference between the flooding water and the snow. At a lower salinity the freezing point is higher. Thus, even if the flooding water is at its respective freezing point the temperatures differ at different salinities. Less saline flooding water is warmer and high saline water is colder. According to *Notz* (2005) the interface between brine and solid ice must always be in in phase equilibrium. Thus, if there is no temperature difference between a salt solution and adjacent ice it means that both are in equilibrium i.e. the local temperature of the ice equals the freezing temperature of the water. One example are brine pockets in sea ice. Applying this to the case of flooded snow no melting occurs if the flooding water is at same temperatures like the snow. Prior to flooding the snow was at temperatures close to the set air temperature. Thus, there is evidence if comparing Experiment 1_{5H}, 3_{5H} and 5_{5H} with freezing temperatures of the flooding water closest to the air temperature (Tab. 5.1) to experiments with larger deviations (all others, excluding Experiment $7_{5L(i)}$ and $7_{5H(i)}$ because of different salinities). The experiments at small deviations show the lowest values for the impedance in the measuring levels between 1 cm and 5 cm (e.g. Fig. 5.8b[i–iii]) and also the lowest or no rates of increasing impedance with time. Thus, only little or no freezing occurs subsequent to flooding. Furthermore, the temperature gradients are smaller in Experiment 1_{5H}, 3_{5H} and 5_{5H} (Fig. 5.4b; Fig. A.5b,d). Hence, salinity is the controlling quantity to describe the flooding of snow by saltwater which confirms results by *Jutras et al.* (2016). It is linked to the freezing point of the flooding water which defines the potential for freezing or melting during the rise in snow dependent on the temperature deviation to the penetrated snow. I suggest that rising water will always be at its freezing temperature, independent to the fact if it is the brine within sea ice or ocean water from below the sea ice that is flooding the snow. Thus, it is more appropriate to describe characteristics depending on its deviation to the temperature of the penetrated snow. Therefore, I draw final conclusions with respect to the "5H"-experiments (Experiment 1_{5H}, 3_{5H} and 5_{5H}) and the remaining experiments (apart from Experiment 7 which I discuss separately in the end of this section).

DEVIATING TEMPERATURES OF FLOODING WATER AND SNOW

The experiments with deviating temperatures between the flooding water and the snow show similar characteristics in the evolution of temperature, liquid fraction, bulk salinity and impedance. To outline the main features I focus on the evolution of the unbiased impedance (Fig. 5.8; Fig. 5.9) and the upon assumptions derrived bulk salinity (Fig. 5.7;Fig. A.9–Fig. A.11). Even if assumptions are incorporated in the calculation of the bulk salinity, it represents the interaction of temperature

and impedance i.e. brine salinity and liquid fraction. In the discussion here I follow results of Experiment 1_{5L}, but features are present in all experiments with deviating temperatures and can be transferred to results of other experiments. The larger the difference between the temperatures of the flooding water and the snow the shorter the period of time of the described features and the less prominent. Furthermore, overall values of the bulk salinity are larger if the salinity of the flooding water is higher but characteristics of the evolution stay the same.

Initial rise

In the beginning water gets soaked up into the snow and less water is present with height, similar to work by *Coléou et al.* (1999) for freshwater rise in snow. The rise of water explains the dropping impedance in layers up to at least 5 cm in the moment of flooding (Fig. 5.8; Fig. 5.9). The effect of capillary rise is strongest over short time scales of a few hours like also reported by *Massom et al.* (2001). This explains the bulk salinity profile in the moment of flooding (Fig. 5.7a). On one hand the bulk salinity decreases with height because of less water reaching the higher layers. On the other hand, the rising water is relatively warmer than the snow it penetrates into. Thus, where in contact with the snow grains at lower temperature the liquid and solid phase is not in equilibrium. Consequently, melting is induced which cools and further freshens the water an so decreases the brine salinity with height resulting in lower bulk salinities in the upper layers. *Matt* (2014) already found this to be a dominant effect in the horizontal flooding of snow.

Upper layer above 5 cm

Afterwards, the upper levels of the flooded snow start to freeze. Evidence is present in the increase of impedance at 5 cm almost immediate after the moment of flooding (e.g. Fig. 5.9a[iii],b[iii]). This is due to the more effective heat release closer to the snow surface. Since the liquid and solid phase must always be in equilibrium (*Notz*, 2005) with colder temperatures the freezing point of the liquid also decreases which leads to an increase in brine salinity. The brine becomes more dense which implies gravity drainage (*Notz and Worster*, 2009) similar to desalination processes in sea ice. As to my knowledge, there are no studies about pathways of brine in flooded snow. However, I expect that brine follows similar pathways which also led to the capillary suction in the first place. This also explains the short time scale of only a few hours of this process. Thus, the bulk salinity in the upper layers of the flooded part in the snow decreases. In case of Experiment 1_{5L} (Fig. 5.7a) this is only the case in the initial few hours after flooding whereas the same is more dominant in Experiment 2_{10L} for instance. Afterwards, the bulk salinity in the upper layers stays almost constant. This is due to the entrapment of brine forming brine pockets similar to entrapped brine in sea ice.

Middle layer between 3 cm and 5 cm

A similar freshening is present in the middle part of the flooded snow around 3–5 cm. Although, the values of impedance do not show any significant increase right after flooding at the 3 cm level (Fig. 5.9a[ii],b[ii]). Thus, I suggest characteristics different to the features in the layers above and

freshening is related to brine draining from upper layers into the layers below. The brine is still less saline than the brine in the middle layers of the flooded snow. In the example of Experiment 1_{5L} these characteristics are the dominant within the initial 6 h after flooding. After that initial period the middle layers show increasing bulk salinity until 24 h in case of Experiment 1_{5L} (Fig. 5.7a). This can only be due to further rising of more saline water from lower levels. Hence, with time the middle layers represent a transition from initial effects of relatively fresher brine drainage towards more saline brine rising afterwards.

Subsequently, there is evidence that with time freezing occurs at lower heights. This is indicated by the increasing impedance in the 3 cm level at a later time than in the 5 cm level, in case of Experiment 1_{5L} after 12 h since flooding. Consequently, brine is released to lower levels due to the same reasons as already described. In Experiment 1_{5L} freezing is dominating the bulk salinity evolution after 24 h in the middle layers. From this time on no further significant increase of bulk salinity is present and values only decrease at smaller rates compared to the characteristics between 0–24 h. This is related to the already described effects of formation of brine pockets and brine release.

Lower layer between 1 cm and 3 cm

In the lower level no freshening is present after the moment of flooding. Furthermore, the onset of freezing as shown in the impedance measurements is after the largest period of time compared to the layers above. Thus, the increase of bulk salinity in the beginning is due to further saltier water rising from below. It is the dominating effect in the beginning until freezing becomes more prominent. The latter leads to formation of brine pockets and brine release over time and consequently constant or decreasing bulk salinities with time. Thus, the lower section describes a transition from further rising of more saline water in the beginning towards freezing. In case of Experiment 1_{5L} this is visible within the initial 24 h after flooding (Fig. 5.7a).

Freezing rates

Higher rates of increasing impedance in layers further up in the snow indicate different rates of freezing (Fig. 5.8; Fig. 5.9). This provides further evidence for the presented theory. In the upper layers of the flooded snow less water at lower salinities is present. Furthermore, the heat release is more efficient close to the colder snow surface. Thus, freezing occurs at higher rates further up in the snow which inversely leads to the same conclusions about the characteristics as presented above. Moreover, if the deviations between snow and flooding water temperature are larger freezing rates are higher. For instance, this follows by comparing Experiment 2_{10L}, 4_{10L} and 6_{10L} characterised by larger deviations in snow and flooding water temperature to Experiment 2_{10H}, 4_{5H} and 6_{10H} described by lower deviations.

Liquid fraction

In addition, the evolution of the liquid fraction also fits into this theory. With time the upper layers

show decreasing values almost immediate after flooding. This is related to the characteristics of freezing initiating from the top. Moreover, evidence is also present in the lower levels. First increasing and then decreasing liquid fractions within the initial 24 h in case of Experiment 1_{5L} (Fig. 5.6a) fit to the theory of the transition from more water rising to freezing.

SIMILAR TEMPERATURES OF FLOODING WATER AND SNOW

If the temperatures of snow and flooding water are similar no transition from effects of brine release to water rising from the bottom are present. Moreover, such characteristics only originate from the larger temperature deviations between snow and flooding water in the beginning. Thus, if the deviations are small like in the 5H-experiments (Experiment 1_{5H}, 3_{5H} and 5_{5H}) characteristics suggest that no brine release occurs across the whole profile. Instead, rise of more saline water from below is the dominating process.

Evidence is present in the evolution of the impedance for the 5H-experiments (Fig. 5.9b). Values are almost constant indicating no or only very little freezing. This is similar to impedance values of experiments at larger temperature deviations in the lower layer during the initial 24 h (e.g. Fig. 5.9a[i]). Thus, I suggest that it is the same process of more saline water rising which is dominant in the 5H-experiments. Moreover, it defines the characteristics of the whole profile post flooding. Further evidence lays in the bulk salinity evolution of Experiment 1_{5H} for instance (Fig. 5.7c). The flooding water that penetrates the snow is almost same temperatures as the surrounding ice. On one hand, only little or no melting occurs during the capillary rise in the moment of flooding. Consequently, lower values in the bulk salinity with height are mainly dependent on less water transported up to the higher levels like described by *Coléou et al.* (1999) for freshwater. More water gets soaked into the snow afterwards, increasing the liquid fraction (Fig. 5.6b) and providing more water at higher salinity. As a result, the bulk salinity increases continuously. On the other hand, the similar temperatures define only little potential for freezing. Hence, as soon as the water rise stabilised no freezing and subsequent brine release occurs and the bulk salinity and liquid fraction remain almost constant. This is the case in the layers above 5 cm (Fig. 5.6b; Fig. 5.7c).

However, in Experiment 1_{5L} temperatures were not exactly the same like in the snow. Thus, I expect only the water at higher levels is cooled down to almost same temperatures like the snow by the time it reached its final height. Instead in the lower parts a small temperature deviation is present. Thus, the liquid fraction evolution indicates rates of freezing related to reducing values over time between 1 cm and 5 cm (Fig. 5.6b). However, the duration of the experiment is too short to reach the point where freezing is strong enough to counter the rise of more saline water by brine release. Hence, the bulk salinity in the lower layers increases until melting in the end of the experiment. If temperatures of snow and flooding water were the same in the beginning I would not expect such a behaviour. Following the suggested theory the characteristics would only depend

on the rise of water due to capillary suction.

SNOW ICE

In my experiments the snow was defined by almost constant temperatures across the whole vertical profile prior to flooding. Though, in reality snow and sea ice are defined by a vertical temperature gradient which describes the transition from the cold air temperatures at the snow surface to the freezing point temperature at the ice-ocean interface. Thus, if water rises it will always be warmer than the new surrounding. Consequently, in the ice-snow interface temperature deviations between flooding water and snow are small and increase with height. Thus, following the described characteristics above, in any scenario flooded snow initially is defined by a combination of capillary suction and brine release i.e. rise of saltier water from below and higher rates of freezing from above. With time, and if cooling persists I find the latter to be dominant in all flooded layers.

Snow which is flooded by water is commonly referred to as slush and as snow ice if the slush is frozen. Correspondingly and with the results described in this section, I suggest the transition from slush to snow ice to be the moment of onset of freezing and subsequent brine release. At this time the growth of new ice is similar to sea ice growth (*Notz*, 2005) and the resulting ice is a combination of newly grown ice and snow grains i.e. snow ice.

THE HEIGHT OF SALTWATER RISE

Additionally, there is a tendency that the lower the deviations between temperatures of snow and flooding water the higher the water rises. This is related to the higher freezing rates in experiments at larger deviations, slowing down the water rise with height like discussed above. Evidence is present if comparing experiments at same freeboard of -1 cm for instance. Only Experiment $2_{10\mathrm{L}}$ and $4_{10\mathrm{L}}$ show an initial drop of impedance due to capillary suction during flooding at the 7 cm level (Fig. 5.9a[iv]). Instead, Experiment $2_{10\mathrm{H}}$ and $4_{10\mathrm{H}}$ at lower deviations show decreasing impedance values more than 12 h later and at higher values. Furthermore, evidence for this theory is present the overall higher absolute values of the impedance in experiments with small deviations (5H-experiments) compared to higher deviations (all other experiments) in the 1–5 cm layer (e.g. Fig. 5.8a[i–iii];b[i–iii]).

INTERMEDIATE EXPERIMENTS

To find further evidence for the discussed features above I realised Experiment $7_{5\mathrm{L(i)}}$ and $7_{5\mathrm{H(i)}}$ at intermediate salinities. Due to technical reasons of high varying temperatures in the cold lab (Fig. 5.3) it was not possible to realise a reliable experiment at intermediate temperatures. If comparing Experiment $7_{5\mathrm{L(i)}}$ and $7_{5\mathrm{H(i)}}$ to experiments at the same temperature they show an evolution of impedance in between values of the lower and higher salinity experiments (Fig. 5.9a). Furthermore, if comparing results for temperature, liquid fraction and bulk salinity evolution (Fig. A.5e,f; Fig. A.8; Fig. A.11), results fit into the theory of deviating temperatures like described above.

5.5 Summary

In this section I introduced a simplified experimental setup to study the saltwater rise in snow as part of more complex processes involved during snow-ice formation. I designed the setup for the application of the salinity harp into snow to measure the temperature and impedance evolution. However, depending on the desired measurement parameters other instruments may be used as well. The main simplifications compared to a scenario in the field are the unlimited water supply in the bottom of the snow and the disregard of any existing temperature gradient in the snow prior to flooding. I realised 14 different experiments at varying parameter setups of the air temperature T_{air}, the salinity of the flooding water S_{w}, the freeboard H_{f} and the snow-grain size D. An overview of the used values is listed in Tab. 5.1.

Exemplary for all realised experiments within my study I described four experiments at low and high salinity and low and high temperature. I find that the lower the temperature the stronger the vertical temperature gradient in the snow and the higher the rate of decay over time. Furthermore, if the salinity of the flooding water is lower the freezing point is higher which leads to a higher source of heat when flooding. Consequently, the vertical temperature gradient is stronger and the decay over time is at higher rates comparing low saline experiments to high saline experiments. Results suggest higher rates of freezing at low salinity and temperature compared to high salinity and temperature.

Based on the impedance measurements of the salinity harp I determined the evolution of the liquid volume fraction $\phi_{\mathrm{l,v}}$ and the bulk salinity S_{bu} in the snow profile. Values in between the measuring heights are linearly interpolated. The linear interpolation method proves to be not satisfactory but a good first guess with least assumptions about the snow profile. Higher vertical measuring resolutions or further experiments at different parameter setups may yield not only better assumptions for the interpolation method. It may also improve assumptions in terms of the density profile used to calculate the liquid mass fraction. The liquid fraction, derived from impedance measurements decreases over time in all experiments, indicating freezing over time after the initial flooding. This indicates that after the initial flooding and capillary suction no further water enters the snow. The bulk salinity calculation combines impedance and temperature measurements. Therefore, its evolution represents the interaction of both. Results of the liquid fraction and bulk salinity evolution both confirm the already suggested theory of higher freezing rates in flooded snow at lower salinity and temperature.

Comparing all experiments with respect to the impedance evolution I find salinity to be the relevant quantity to describe the rise of saltwater in snow. The salinity of the flooding water is directly related to the freezing temperature of the water. I suggest that water rising into snow is always at its freezing point, no matter if it is brine from sea ice or ocean water from below. If

deviations between the temperatures of the flooding water and the snow are larger I find described characteristics are less prominent. On one hand, for large deviations results suggest a transition from effects of continuing water rise with time due to capillary suction to effects of brine release. This is connected to the higher rates of freezing from the top. On the other hand, if temperatures of snow and flooding water are similar I find the continuing rise of water due to capillary suction to be the dominant effect after flooding. In case of snow on sea ice in nature a vertical temperature gradient is present different to my experiments where snow was at constant temperatures prior to flooding. Thus, I propose that in any scenario flooded snow initially is defined by a combination of capillary suction and brine release i.e. rise of saltier water from below and higher rates of freezing from above. With time, and if cooling persists I find the latter to be dominant in all flooded layers. Additionally, I suggest the transition from slush to snow ice to be the moment of onset of freezing and subsequent brine release. Furthermore, I find that in in case of less temperature deviations between flooding water and snow the water rises higher to higher layers the snow. This is linked to higher potential of freezing, slowing down capillary suction if temperature deviations are larger. Experiments at intermediate values of the flooding water salinity provide further evidence for suggested theories.

6 A new laboratory method to study snow-ice formation on thin ice

In the former section (Sec. 5) the experimental setup is designed to partly investigate the process of snow-ice formation. Within this section I present a more complex method to not only study the rise and refreezing of water in snow but to represent the whole process of snow-ice formation in a laboratory environment. Whereas the goal in Sec. 5 was to simplify the setup, here I developed a method to include all processes and match the real scenario in the field as best as possible. In Sec. 6.1 I describe and explain the experimental setup and in Sec. 6.2 I discuss results of one exemplary continuous experiment. The used equipment is partly tailored to the UNIS cold laboratory. However, I only used easy accessible and cost-effective materials and devices and by that ensure that it is possible to adapt the method to any other cold laboratory. The here described method is the final result of many shorter experiments that I improved over time to come to this experimental setup. Due to time limiting reasons I was only able to conduct one full experiment run with the experimental setup as described in this section.

6.1 Experimental setup

In order to investigate the rise of saltwater in snow on sea ice I developed a setup to represent floating sea ice in a laboratory environment (Fig. 6.1). The cold lab in UNIS facilitates an ice tank which I filled with seawater. At the bottom I installed a pump system that continuously mixes the water in the tank. In the height of the water surface I placed a Lexan frame fixed to vertical movable sliders to adjust the height of the frame in the water. The frame is smaller than the tank such that there is water around the frame between the ice tank walls and the frame. In this open water I installed a heating system that guarantees ice free water around the frame. The walls of the Lexan frame have horizontal cuts to ensure ice sticking to the wall during freezing. Furthermore, I installed two salinity harps inside the frame, two temperature sensors above the whole setup in the air and a salinometer in the water below the frame. Then, I set the temperature of the cold lab to negative temperatures such that the water in the tank cooled down and sea ice started to grow at the water surface. Ice only grows within the Lexan frame. As soon as it reached the desired thickness I deployed snow on top. After letting the snow stabilise for at least 24 h I adjusted the height of the Lexan frame to push the ice-snow interface below the water level. Because of the design water can not flood the snow from the sides but rather through the ice. Measurements of all instruments provide information about the change in physical properties of the sea ice and snow.

Detailed description

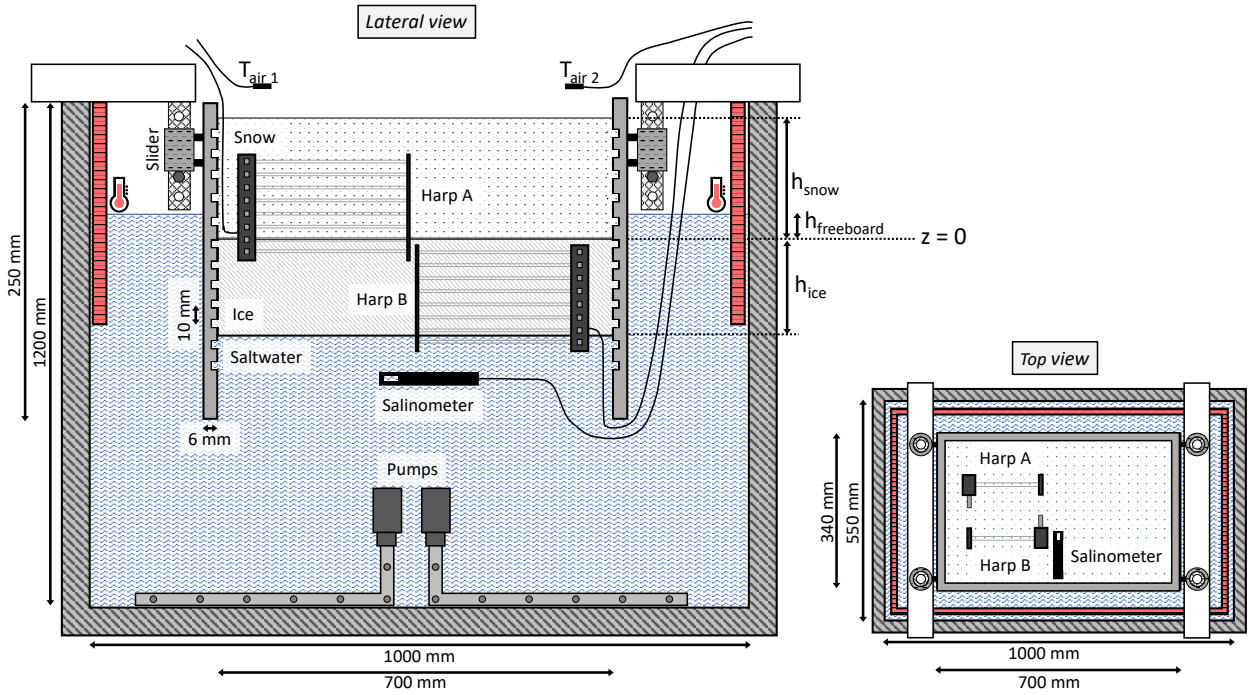

Figure 6.1 *Sketch of the experimental setup for the ice tank experiment. Note that dimensions are not true to scale.*

In Fig. 6.1 the sketch of the experimental setup is illustrated. I used the FRYSIS ice tank at the UNIS cold laboratory (Fig. 6.2a). The tank has a volume of 600 l and is 100 cm long, 50 cm wide and 120 cm deep. I filled the tank with seawater from Adventfjorden at an initial salinity of $34.2\,\mathrm{g\,kg^{-1}}$.

Reducing the dimension of the experiment to the limits of a cold laboratory increases the prominence of small scale effects. Thus, it is crucial to avoid these in order to represent snow on sea ice at large scale. As already explained in **??** it is necessary to get a negative freeboard in order to get sea ice flooded. Horizontal flooding is the dominant process at cracks, smaller ice floes or close to the ice edge of larger floes and was already investigated by *Matt* (2014). Hence, I wanted to focus on the vertical movement of water and achieve that water percolates vertically through the ice to flood the snow from below rather than from the side. Suppressing a piece of sea ice inside the used water tank below the water level would flood the ice rather horizontally than vertically. Hence, I designed a frame out of Lexanglas to block all horizontal ways. The frame has a wall thickness of 6 mm. Every 1 cm in vertical direction I created a 3 mm high and 3 mm deep cut on the inside of the frame. These cuts form one continuous horizontal channel along the frame wall for each vertical step. During its growth sea ice forms in those channels making the ice stuck to the wall due to the increased wall roughness. Thereby water is prevented from rising at the boundary of

the frame between ice and frame wall. I attached the frame with sliders to mounts that are fixed to the ice tank wall. The sliders enable the frame to freely move in a vertical direction. Additionally, I placed holes in the slider mount every 1 cm enable the possibility of locking the frame at different heights. The $z = 0$ level is defined relative to the frame i.e. moving the frame in vertical direction only changes the height of water relative to the frame creating a postive or negative freeboard.

Inside of the frame I used two salinity harps to cover a vertical range of 28 cm. The lowest wire pair of Harp A was below the water level and the second lowest was at the water-air interface. The highest wire pair of Harp B was at the same level as the lowest of Harp A to get a seamless transition. I attached the upper harp to mounts from above and the lower harp to mounts from below (Fig. 6.2b). In doing so there exists no vertical pathway between the water under the ice and the ice-snow interface inside the frame. Below the lowest harp I placed a WTW Multi 340i hand-held salinometer. It records the temperature and salinity of the water below the ice-water interface with a 30 min temporal resolution. Furthermore, I installed two TinyTag temperature sensors above the frame on each side to measure the air temperature with a temporal resolution of 10 min. All instruments inside the frame are located in one half of the frame (see Fig. 6.1 top view; Fig. 6.2b) and the other half is accessible for characterisation of the snow and ice. It is only possible to cut the ice in the end of the experiment. Before it would open an artificial pathway for the seawater below to reach the ice-snow interface. To measure the ice thickness during the ongoing experiment I equipped the frame with a scale on the outside of the frame. It enables to visually measure the ice thickness by lowering an underwater camera for instance. As soon as the desired ice thickness is reached I sieved snow on top of the ice (Fig. 6.2c).

The final step is to ensure that the boundary conditions are as close to nature as possible. The first condition is to keep grown ice floating and not getting jammed between the ice tank walls. Outside of the frame there is open water between the ice tank wall and frame which would also freeze. After Archimede's Principle more water would be replaced by ice and increase the water level in the tank and thus unintentionally cause a negative freeboard. In addition, since ice is expanding during growth the ice would start to build up horizontal pressure against the wall, get stuck and don't float on the water anymore. Hence, I installed a second frame out of wood close to the ice tank wall and wrapped a thin isolated wire around it. The wire had an effective cross section of 0.25 mm^2 and I created a short-circuit by connecting both ends to a power source. Consequently the wire heats up dependant on the chosen amperage at the power source. The resulting energy P is calculated by the following equation:

$$P = U \cdot I \tag{6.1}$$

where U denotes the voltage and I the amperage. For an exemplary air temperature of $-15\,°C$ and the here described setup in the FRYSIS ice tank I found 100 W an ideal energy input to keep the ice floating. Furthermore this value prevented too strong warming, which would have created

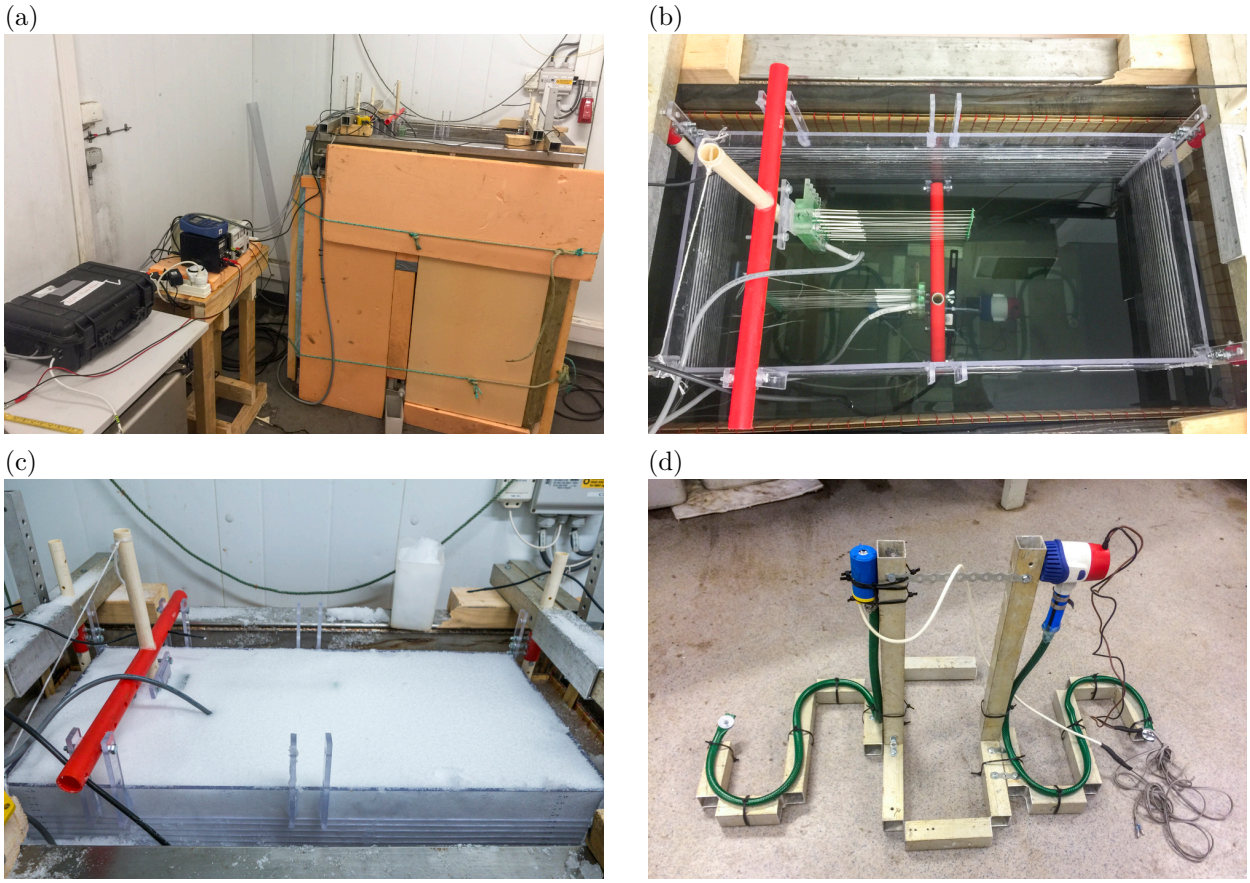

Figure 6.2 *a) The FRYSIS ice tank in the UNIS cold laboratory. b) Top view on tank showing the frame with harp A outside of the water and harp B below the water surface. Below the water surface it is also possible to see the WTW Multi 340i and the pump system at the bottom of the tank. On the left and right hand side of the picture the placement of the TinyTag temperature sensors is visible. Next to the ice tank wall the heat frame is installed. c) The pump system which is installed at the bottom of the ice tank. d) Frame filled with a layer of 10 cm thick snow as soon as the ice reached the desired thickness.*

a circulation cell in the water that could eventually enter the inner frame from below and influence the ice growth. Fur further experiments I recommend to arrange the wires in a horizontal way around the wood and not in a vertical as in the setup here. This prevents horizontal differences in heat and if the spacing of the wires is not sufficient ice will still stick to the wall.

The second boundary is the underlying water. As described above (Sec. 2.2) during the ice growth salt is released. The water at the ice-water interface gets heavier and sinks down to the bottom of the tank resulting in a strongly stratified salinity profile inside of the tank. Instead I developed a pump system to keep the water in the tank mixed (Fig. 6.2d). Two pumps take in water from approximately 30 cm above the tank bottom. They pump the water through two hoses down to the middle of the tank bottom. From there I built a construction to install them in a meandering pattern until they cover the complete bottom. The end of the hoses are blocked and along the hoses I drilled small holes such that no hole is pointing upwards in vertical direction of the tank. Both pumps are controlled by a power source. I chose the voltage so that both transport

a similar amount of water which in my case was approximately $10.5\,\mathrm{l\,min^{-1}}$. During testings this value proved to be adequate in causing sufficient mixing but no strong currents or circular flow patterns which could affect the ice growth. In addition I used a time switch to activate them only every 45 min for 15 min to avoid any stationary circulation patterns inside the tank that could impact the ice growth. The pump system uses two processes. On the one hand, less saltier and thus lighter water from higher up in the tank gets pumped down to the ground. There it replaces heavier water making the water column unstable and creates convection. On the other hand, turbulence is created by spreading the water through the small holes in the hoses with high velocities.

So far the described settings were dependant on the overall circumstances I had in the UNIS cold lab. They may differ to another cold laboratory and ice tank. For instance the energy used for the heat frame is different for another ice tank and for another chosen air temperature. The same goes for the used water in the tank. The salinity of the water, the air temperature and the dimensions of tank and frame define the energy required for the heat frame and the power for the pumps to keep the desired boundary conditions.

Finally, the presented method has two limitations to keep in mind. First, with the growth of sea ice and linked brine release the salinity of the water in the tank steadily increases during the performance of any freezing experiment. Due to the connection between salinity and freezing temperature (Eq. 2.2) the latter also decreases over time. Second, the frame has to be vertically fixed in the beginning to not sink and thus holds initial growing ice in a steady vertical position. As a result during ice growth displaced water leads to an increase of the total water level in the tank. Consequently, a negative freeboard develops which leads to early cycles of flooding and refreezing on top of the bottom.

Both limitations are complex to fix. Realistically, the seawater salinity under sea ice would not change that drastically and sea ice would float on top of seawater. Although, I maintained the latter condition by taking out water of the tank twice a day to ensure a positive freeboard.

6.2 Characteristics of an exemplary experiment configuration

In the end I was able to realise one experiment over 21 days. Within this section I present results of the temperature, impedance, liquid fraction and bulk salinity evolution. The aim is to show the possibilities this experimental setup provides. Within this study I was able to realise one exemplary parameter setup. which is not sufficient to to draw reliable conclusions out of the comparison to the snow-frame experiments. Instead, results

6.2.1 Results

The seawater from Adventfjorden I used to freeze sea ice in the tank had an initial salinity of $34.2\,\mathrm{g\,kg^{-1}}$. I set the air temperature of the cold lab to $-15\,^{\circ}\mathrm{C}$ and to $-10\,^{\circ}\mathrm{C}$ after around hour 380 of the experiment. When ice started to form the wire pairs of the salinity harp closest to the water surface were situated approximately 1 cm above and below. The lowermost wire pair of the salinity harp installed below the water surface was at $-17\,\mathrm{cm}$ and the uppermost at $-3\,\mathrm{cm}$. The lowermost wire pair of the salinity harp installed across the waterline was at $-3\,\mathrm{cm}$ and the uppermost at $z = 11\,\mathrm{cm}$. As soon as the ice thickness reached 10 cm I sieved snow through a grid with 2 mm mesh size and evenly filled up the upper part of the frame to a final snow cover of 10 cm thickness. I waited 24 h to let the snow metamorphose and stabilise before I pushed the frame down to reach a freeboard of approximately $-1\,\mathrm{cm}$. Prior to the negative freeboard creation the snow grain size was in the range of $D = 1 \pm 0.5\,\mathrm{mm}$ and the density at approximately $447\,\mathrm{kg\,m^{-3}}$. Furthermore, the hardness of the snow showed a blade hardness index above 30 N. Thus, following the discussion above (Sec. 5.1) I assumed well-bonded grains in the deployed snow and did not further specify the properties of the snow. Both salinity harps were measuring at a temporal resolution of approximately 40 s and vertical resolution of 2 cm. Due to a technical defect no measurements are available between 168 h and 192 h of the experiment for the upper salinity harp. Furthermore, the heat frame failed after hour 330 due to an irreparable technical defect. In the end, 408 h after the start of the experiment I set the air temperature 15 °C.

Temperature

The air temperature during the realisation of the experiment was always close to the set temperatures $-15\,^{\circ}\mathrm{C}$ and $-10\,^{\circ}\mathrm{C}$ (Fig. 6.3a). It shows variations by up to $\pm 2\,\mathrm{K}$ and an oscillating pattern at an amplitude of $\pm 1\,\mathrm{K}$ and a period of around 8 h. The evolution of the temperature recorded by the salinity harps shows distinct differences between above the waterline and below (Fig. 6.3b). Above the waterline temperatures are around $-12\,^{\circ}\mathrm{C}$ from the beginning until the moment of snow deploayment at 144 h.Water temperature steadily decreases with time to values below $-1\,^{\circ}\mathrm{C}$ at 60 h in all levels between $-17\,\mathrm{cm}$ and $-1\,\mathrm{cm}$. Afterwards, temperatures further decrease continuously with time and depth. At the time of the snow deployment at 144 h all layers between $-12\,\mathrm{cm}$ and $-1\,\mathrm{cm}$ are below $-2\,^{\circ}\mathrm{C}$ linearly decreasing to the coldest temperature at the $-1\,\mathrm{cm}$.

After the deployment of snow at 144 h a linear temperature gradient appears in both, above and below the waterline. The gradient is stronger above the waterline and below reaches down until the $-12\,\mathrm{cm}$ level. In the moment of artificial creation of a negative freeboard at 168 h no date is available above $-3\,\mathrm{cm}$ until 192 h. Below the waterline the vertical temperature gradient is shifted up by about 1–1.5 cm in the moment of negative freeboard creation. Afterwards the same cooling behaviour continues like before with decreasing temperatures over time and depth. As soon as the upper harp is measuring again temperatures show almost constant values above the waterline until

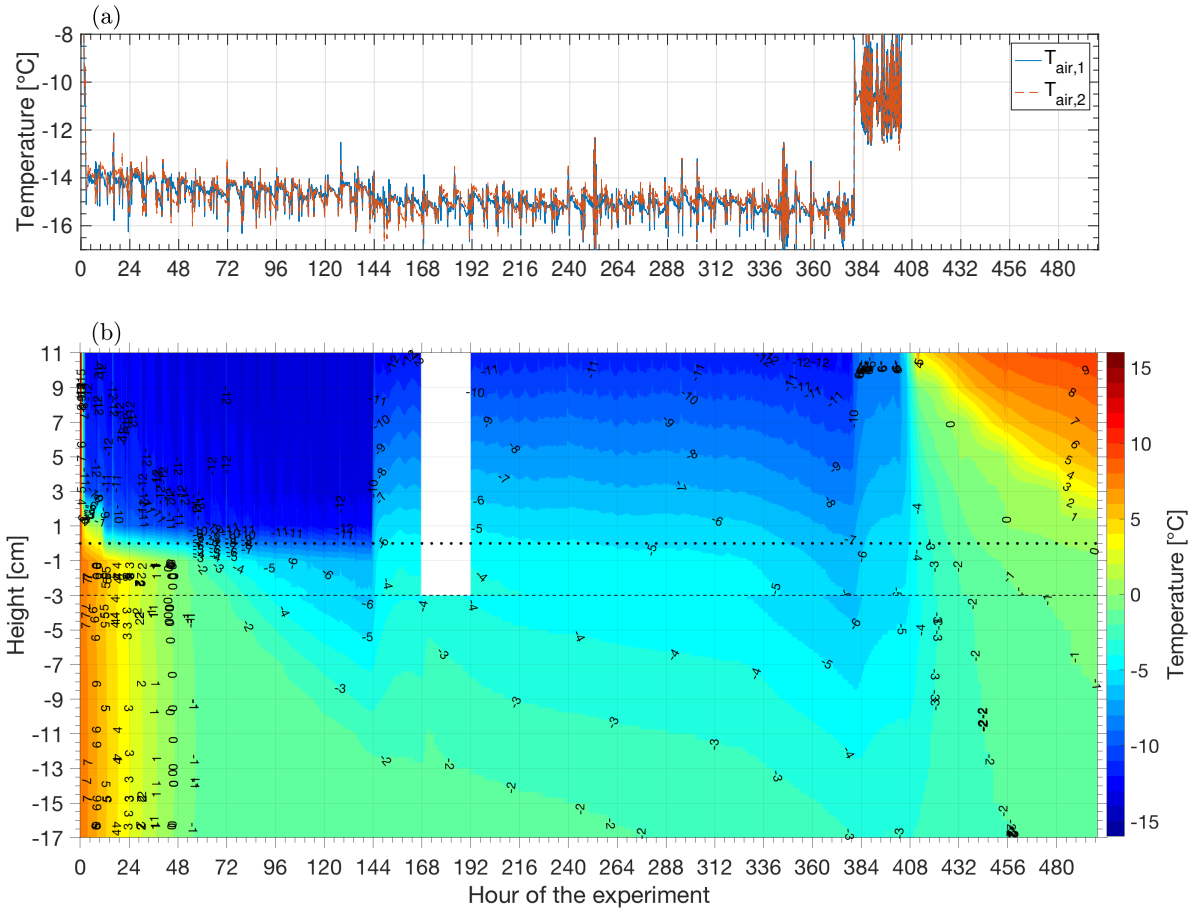

Figure 6.3 *a) The air temperature T_{air} measured by the TinyTag sensors above the experiment setup (see Fig. 6.1). Values after setting $T_{air} = 15\,°C$ are not shown in this figure. b) The evolution of the temperature of the ice-tank experiment. Values are based on Harp A and B meeting at the −3 cm level (indicated by the dashed line). Measurements are at a temporal resolution of approximately 40 s and at a vertical resolution of 2 cm starting at −17 cm for Harp B and at −3 cm for Harp A. The dotted line indicates the z = 0 cm level.*

hour 330. Only between 0–3 cm there is an indication of a vertically shifter temperature gradient by about 0.5 cm. Furthermore, values between 0–5 cm decrease by less than 0.5 K until hour 330.

From the moment of the defect heating system at hour 330 to hour 384 temperature decreases at higher rates in all levels between −17 cm and 11 cm. At 384 h I changed the air temperature to −10 °C and afterwards all levels show an increase in temperatures. The rates increase after hour 408 when setting the air temperature to 15 °C. Temperatures below the waterline increase at almost the same rates in all levels. Above the waterline a strong signal of warmer temperatures evolves from the top.

Impedance

Instead of providing a detailed description of the impedance evolution I focus on the relative changes. The impedance evolution for the upper harp (Fig. 6.4a) and the lower harp (Fig. 6.4b) shows the lowest values for the wire pairs below 0 cm until hour 60. Afterwards, over time an increase of impedance with depth appears starting at −1 cm at 60 h until it is present in −13 cm at 144 h.

Afterwards, overall values for wire pairs below 0 cm further increase. Though, the measurements by the harp installed below the water level (Fig. 6.4b) show some deviating features. In the moment of negative freeboard creation impedance values in all levels show a sudden rise before continuing to increase at approximately same rates afterwards. Furthermore, the −3 cm and −5 cm level show decreasing impedance after around hour 192 until 330 h. Subsequent to the moment of setting air temperature to 15 °C at 408 h impedance decreases in all levels below 0 cm for both harps.

Impedance measurements by the upper harp (Fig. 6.4a) for heights above 0 cm show values close to the 17 000 Ω line until the technical defect at 168 h. The 17 000 Ω line marks the upper limit at which data has to be interpreted as noise or as not reliable due to the technical properties of the salinity harp (Sec. 3.1). After hour 192 the impedance at −1 cm and −3 cm has increased compared to the values before the technical defect. Furthermore, the impedance dropped significantly in the 1 cm and 3 cm. Until 408 h values between −3 cm and 3 cm stay almost constant. Though, the wire pairs at higher levels show decreasing impedance with time and height. Starting after hour 192 first the impedance in the 5 cm level significantly decreases until at around 372 h the impedance of the 11 cm level decreases. After hour 408 the impedance above 0 cm first significantly drops and then increases again up to measurements that have to be defined as noise.

Liquid volume fraction and bulk salinity

With the presented theory above (Sec. 3.1; Sec. 4) I calculated the liquid volume fraction from impedance measurements (Fig. 6.4c). Moreover, by including the temperature i.e. brine salinity and transferring $\phi_{\mathrm{l,v}}$ to $\phi_{\mathrm{l,m}}$ I am able to calculate the bulk salinity in each level (Fig. 6.4d). I provide a discussion of the calculation in Sec. 6.2.2.

During the whole experiment until the moment of metling after 408 h no change in liquid fraction is present above 0 cm. Below 0 cm the evolution of the liquid fraction shows constant values at 1 within the initial 60 h. Afterwards values significantly decrease over time and depth. The lowest values below the 0 cm level appear between −9 cm and 0 cm from around hour 168 to hour 456. Significant features that vary from the overall evolution of the liquid fraction occur in the moment of snow deployment at 144 h and negative freeboard creation at 168 h. In both moments, layers between −9 cm and 0 cm show higher rates of decreasing liquid fraction over a time of about 5 h. In the former moment, values afterwards are constant for about 10 more hours and then further decrease at rates similar to rates before the snow deployment. Furthermore, the layers between −3 cm and 0 cm show an increase of liquid fraction after the deployment of snow.

Similar characteristics are present in the bulk salinity evolution. If the liquid fraction equals 1 the salinity data are based on the salinometer. Similar to the liquid fraction evolution the bulk salinity shows decreasing values with depth and time after hour 60 and the lowest values between −9 cm and 0 cm from hour 168 to hour 456. Furthermore, analogue features in the moment of snow deployment (144 h) and negative freeboard creation (168 h) are present. In both moments

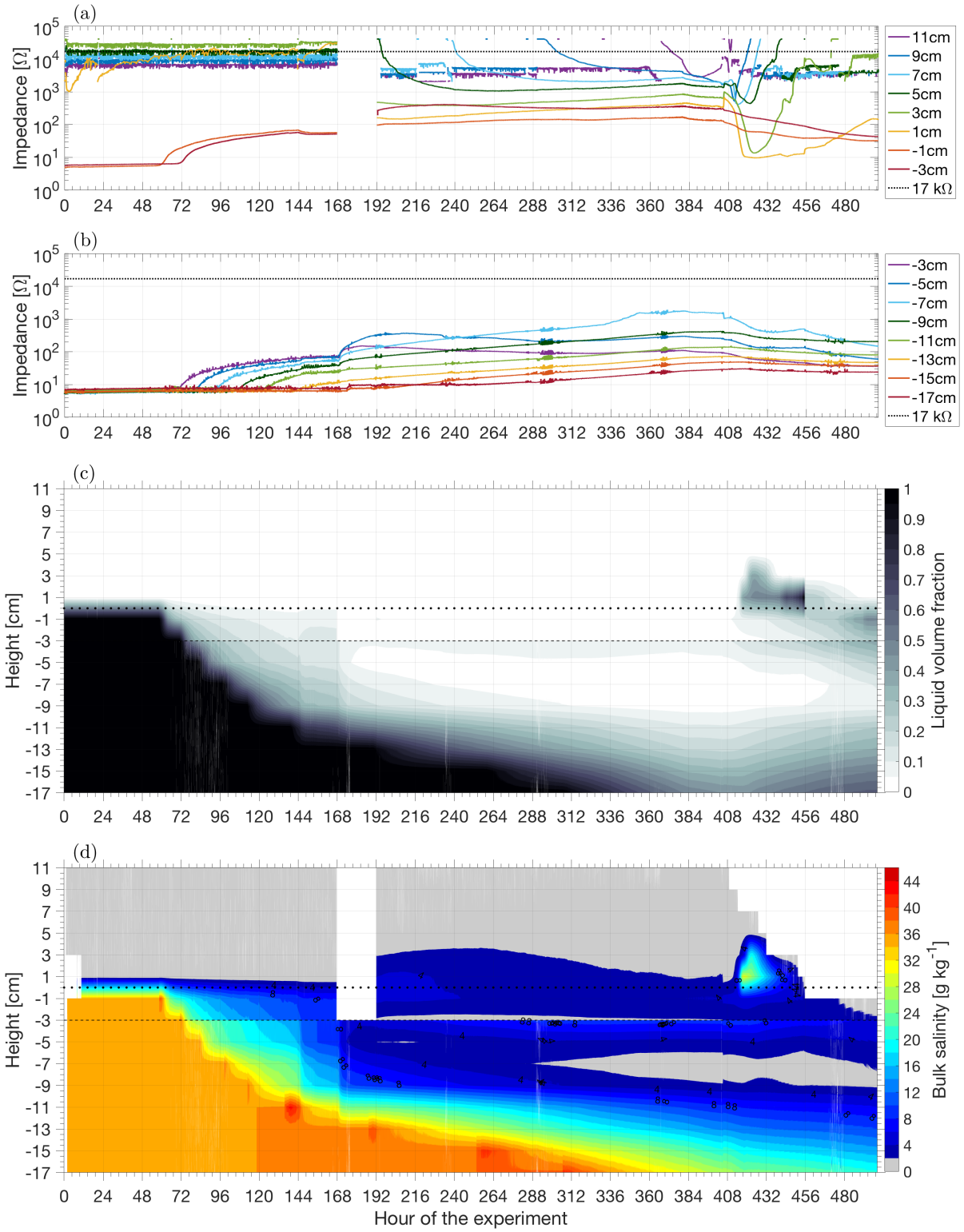

Figure 6.4 *Time series of the impedance Z for a) Harp A and b) Harp B. c) The evolution of the liquid volume fraction $\phi_{l,v}$ and d) the evolution of the bulk salinity S_{bu}. Results in c) and d) are based on Harp A and B meeting at the −3 cm level (dashed line). If $\phi_{l,v} = 1$ the bulk salinity data is taken from the salinometer. Measurements are at a temporal resolution of approximately 40 s and at a vertical resolution of 2 cm starting at −17 cm for Harp B and at −3 cm for Harp A. The dotted line in c) and d) indicates the $z = 0$ cm level. Data points with $S_{bu} < 2\,g\,kg^{-1}$ are coloured in grey for visual enhancement of the least and unaffected snow and removed data appear as white areas. (Experimental setup: Fig. 6.1; Fig. 6.2b)*

the layers between −9 cm and −3 cm indicate indicate strong freshening by about 6 g kg^{-1} over short times in the dimension of a few hours. Above 0 cm the bulk salinties only increases after the technical defect at 192 h. Values are around 4 g kg^{-1} at the most around 1 cm and subsequent to hour 240 results indicate a decrease of bulk salinity with time between 0–3 cm. Furthermore, there is a distinct discrepancy between measurements in the −3 cm level bei the upper harp and the lower harp. In both the initial decrease is at the same moment around 72 h. Though, afterwards the measurements by the lower harp show constantly higher values until the end of the experiment.

6.2.2 Discussion

The temperature, impedance, liquid fraction and bulk salinity evolutions indicate distinct features during the deployment of snow and negative freeboard creation. Below, I provide theories based on linking of the behaviour of each quantity in the respective event to explain the overall characteristics. Furthermore, results indicate further potential of this method to investigate processes of saltwater rise from sea ice into snow and subsequent snow-ice formation.

INTERPRETATION OF IMPEDANCE – SUPPLEMENTS FOR SNOW

In Sec. 5.4.2 already explained how to interpret changes in impedance. Results in this section indicate why it is important to also consider the raw impedance data for interpretations and not only the products of it like the liquid fraction. For instance, after the negative freeboard creation the liquid fraction evolution indicates very little or no liquid in the snow (Fig. 6.4c). One one hand, this is due to the chosen coarse colour scale. Though, a colour scale at smaller intervals smooths the differences in the profile which makes it more difficult to identify features. On the other hand, even at a finer colour scale the liquid fraction evolution did not provide any characteristics of the layers above 1 cm. Instead, the impedance evolution (Fig. 6.4a) indicates a drop in impedance with height and time, even though it may not show an increase of the liquid fraction. Still, I explain this drop of impedance with time by the presence of water vapour in the snow which rises over time similar to the formation of surface hoar (e.g. *Hachikubo and Akitaya* (1997)). Thus, even though water did not significantly rise in the snow the changes due to the presence of water at the ice-snow interface affect the snow layers above. Consequently, impedance measurements are influenced by these changes. However, to quantify the effect of presence of water on impedance measurements of the salinity harp further investigations of impedance measurements are necessary. The experimental setup described in Sec. 5.1 may provide an appropriate measurement principle.

CALCULATIONS

For the calculation of the liquid mass fraction of measurements below 0 cm I used the same method as proposed by *Notz et al.* (2005) and *Fuchs* (2017). To calculate $\phi_{\mathrm{l,v}}$ above 0 cm in snow I used the theory developed in Sec. 4. I determined Z_0 by using Eq. 4.6 where I estimated S to be the brine salinity (Eq. 2.4) of the −1 cm level as I expect that this would be the water rising into

snow. Though, the temperature changes with time (Fig. 6.3b) as does the brine salinity due to the connection via Eq. 2.4. However, subsequent to the negative freeboard creation the temperature around 0 cm does not change significantly. The respective brine salinities values range from about $70\,\mathrm{g\,kg^{-1}}$ to $90\,\mathrm{g\,kg^{-1}}$ between hour 168 and 360. If calculating the respective value for Z_0 differences are in the range of 1 %. Thus, I calculated Z_0 based on the brine salinity at 168 h. I suggest this to be sufficient if the brine salinity does not change significantly over time.

DEPLOYMENT OF SNOW

The deployment of snow affects the ice below. Snow on top of sea ice acts as an isolator (*Massom et al.*, 2001). Consequently, with the deployment of snow a strong vertical temperature gradient establishes in the snow (Fig. 6.3b). As a result the top of the sea ice is not in contact to the cold air anymore. Hence, the whole column of the sea ice gets warmer (where the ice thickness can be derived from $\phi_{\mathrm{l,v}} < 1$). According to *Martin* (1979) brine channels in warming ice grow. As a consequence brine is released more efficiently from sea ice. This explains the decreasing liquid fraction and bulk salinity in the moment of snow deployment (Fig. 6.4c,d).

NEGATIVE FREEBOARD

By lowering the frame system I created a negative freeboard with respect to snow-ice interface. Consequently, the pressure of the saltwater on the ice from below increased. Thus, warmer and fresher saltwater is pushed up into the sea ice, displacing the colder and more saline brine. Evidence is present in the significant rise of temperatures after hour 168 between −12 cm and −3 cm. Furthermore, the freshening explains the bulk salinity decrease in that moment (Fig. 6.4d). Moreover, it implies a higher potential for freezing which leads to stronger rates of impedance increase (Fig. 6.4b) and decreasing liquid fraction (Fig. 6.4c).

Comparing the impedance measurements of each level the increasing rates are strongest in the 5 cm level. This is because of the bulk salinity distribution in the sea ice prior to the intrusion of the warmer and fresher saltwater. Similar to reports from work of others (e.g. *Notz* (2005)) the ice describes a “C”-shaped salinity profile. The denomination refers to a profile where more salt is in the upper and lower layers of the ice compared to the layers in between. The shape is related to brine entrapment during the growth of the sea ice (*Notz*, 2005). I find the same type of profile in my work with the bulk salinity minimum around the 5 cm level (Fig. 6.4d). The least brine is present i.e. it is the layer at the least liquid fraction (Fig. 6.4c). Thus, the mass of liquid replaced by the warmer and fresher rising liquid is smaller compared to the other levels. Consequently, less heat loss is required for freezing which explains why freezing is strongest in this level.

The replaced brine is pushed further up in the ice until it reaches the snow-ice interface and subsequently floods the snow. Evidence is present in the dropping impedance in the 1 cm and 3 cm levels after the negative freeboard onset (Fig. 6.4a). The bulk salinity evolution in this time provides a more comprehensible illustration (Fig. 6.4d). As already mentioned above this wettening

of the lower snow layers induces further effects in the snow which over time leads to a decrease of impedance in higher levels. I expect the whole process of liquid rising to be dependent on two properties. First, if the pressure under the ice is higher i.e. the freeboard is lower then the potential for more water rise is increased. Second, if the freezing rates with height in the ice i.e. the strength of the vertical temperature gradient are stronger it prevents more water from rising.

EXPERIMENTAL SETUP EVALUATION

Several discussed aspects provide evidence that the experimental setup I developed provides a reliable representation for investigations of floating sea ice at negative freeboard. However, some of the features described in Sec. 6.2.1 may not occur in the same way in nature. First, the air temperature shows an oscillating pattern which is related to the cooling system of the cold laboratory as already discussed above (Sec. 5.2). Furthermore, the wire pairs and temperature sensors of both harps in the same height of $-3\,\mathrm{cm}$ indicate different measurements in both, impedance and temperature. One explanation for this are the inhomogeneities in sea ice growth. For instance, one harp may be in contact to more brine channels than the other. Furthermore, due to the experimental setup horizontal differences in sea-ice growth may occur. This can be related to distinct flow patterns within the ice tank created by the pumping system or the heat frame. Though, as already described in Sec. 6.1 I aimed to reduce these effects as best as possible.

Moreover, the heat frame defect provided an unintended effect of more cooling of the whole system. Results show that temperatures in the whole ice-snow profile decrease if less heat is applied to the water in the ice tank (Fig. 6.3b). This may provide a foundation for future work to investigate ocean heat flux differences. For example, one could install another heating system into the experimental setup below the ice and induce a heating at constant or changing rates.

6.3 Summary

Within this section I presented a experimental setup to investigate vertical flooding of snow on top of floating sea ice in a laboratory environment. To avoid effects of strong stratification in the used water tank I introduced a pump system that keeps the water mixed. Furthermore, I designed a frame which I installed at the water surface and which is adjustable with height. Thus, I am able to control the freeboard of the growing sea ice inside the frame. To prevent ice growth around the frame I designed a heat frame that ensures open water and vertical manoeuvrability of the frame. It is possible to adjust several parameters of the setup to investigate various processes related to vertical rise of saltwater in sea ice, subsequent flooding of snow and snow-ice formation.

Results of one exemplary experiment demonstrate the capability of the experimental setup. I find dominant characteristics in the sea during the deployment of snow and the creation of a negative freeboard. The former implies warming of the ice which leads to effects of increased brine release

and freshening of the sea ice. The latter shows evidence of saltwater from below the ice is infiltrating the sea ice, displacing saltier brine and thus freshening the ice. Displaced brine is pushed further up and appears at the ice-snow interface where it floods the snow. I suggest the rise of water to be depending on the freeboard and temperature profile in the sea ice and snow. With the set of parameters I chose I did not achieve strong flooding of the snow. To ensure more distinct rise of water lower air temperatures, alternative types of snow, different ice thickness and variations in the negative freeboard are appropriate. Together with the theory I developed (Sec. 4) the experimental setup defines a promising method to future studies of saltwater rise and snow-ice formation on top of sea ice.

7 Conclusions

The aim of my study was to develop a reliable method to investigate the different processes of saltwater rise in snow on and subsequent freezing with respect to salinity and temperature evolution. I provided adaptions to existing theories in sea-ice investigations to utilise the salinity harp for measurements of impedance and temperature in snow.

Results from 14 different snow frame flooding experiments yield salinity of the flooding water to be the predominating quantity to describe the rise of saltwater in snow. I find a transition from effects of capillary rise to effects of freezing and brine drainage within the initial 24 h after flooding if temperatures between flooding water and snow differed.

Furthermore, I designed a cost-effective experimental setup to represent floating sea ice in cold laboratory environment. Results of an exemplary experiment highlight the capability of the setup and indicate reliability to mimic the situation found in nature. They also indicate that deployment of snow leads to increased gravity drainage and that negative freeboard creation induces upward moving brine. The latter is pushed up to the ice-snow interface where it wets the snow.

Together with the findings in the snow frame experiments I provide a set of theory and methods which provides a promising foundation for further investigations of saltwater rise in snow on sea ice and subsequent freezing. In follow-up studies a variation at smaller intervals for the salinity of the flooding water would be appropriate to find a possible parametrisation of the features I presented in this study. Furthermore, to optimise the presented results for the bulk salinity evolution it is crucial to find a better observation of the height of water rise. Overall a higher vertical resolution of the salinity harp would improve the identification of prominent features like the location of the waterfront of the rising water. Such results would provide more appropriate information to estimate the characteristics of the vertical profile. Consequently, this would improve the quality of the bulk salinity calculation and may yield satisfactory information on how to interpolate between measuring sticks.

A Appendix

A.1 Snow crystal classification

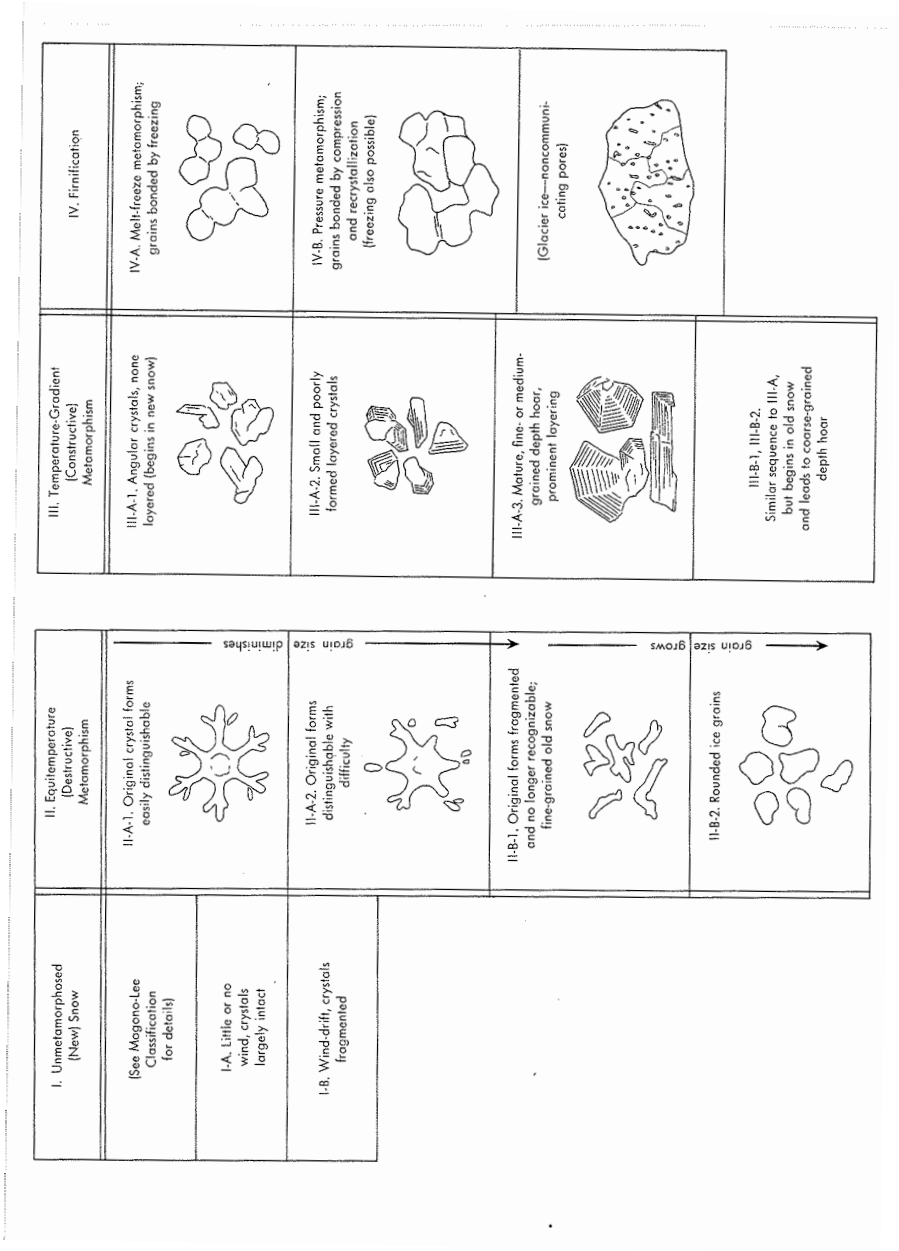

Figure A.1 *Snow crystal classification (from* Halfpenny and Ozanne *(1989), based on work by* Sommerfeld and LaChapelle *(1970)).*

A.2 Conductivity dependeny on temperature

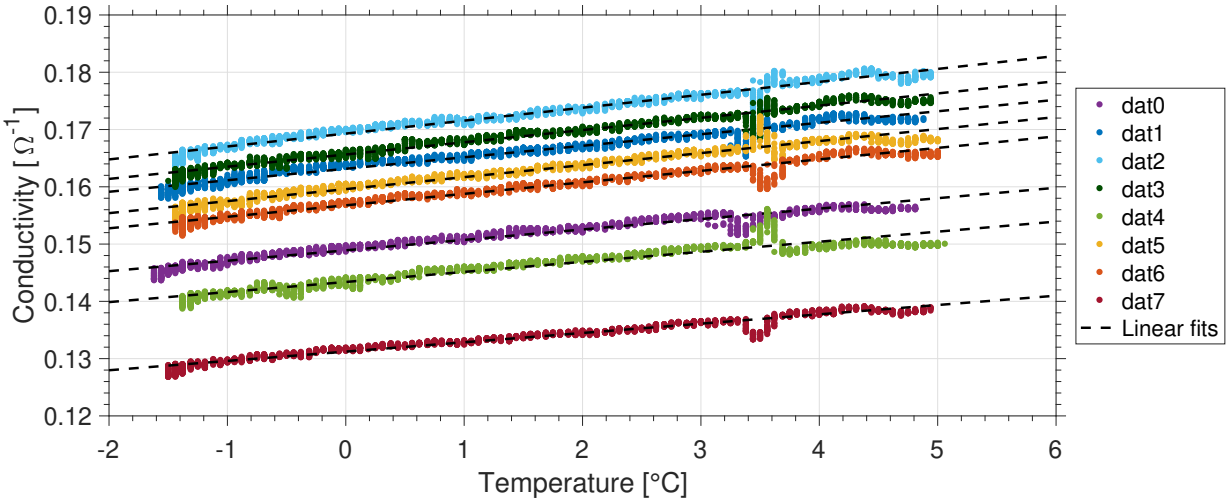

Figure A.2 *The dependency of conductivity on temperature at a salinity of* $34.45 \pm 0.25\,g\,kg^{-1}$ *represented by values of salinity Harp A and respective linear fits.*

Table A.1 *The slope coefficients (b) of the linear fit* ($y = a + b \cdot (T_{\mathrm{ref}} - x)$) *to the conductivity values shown in Fig. A.2 for each wire pair (dat0 – dat7) of salinity Harp A.*

	dat0	**dat1**	**dat2**	**dat3**	**dat4**	**dat5**	**dat6**	**dat7**	**Mean**
Slope	-0.0018	-0.0020	-0.0023	-0.0021	-0.0018	-0.0021	-0.0020	-0.0016	-0.00196

A.3 Matlabtool

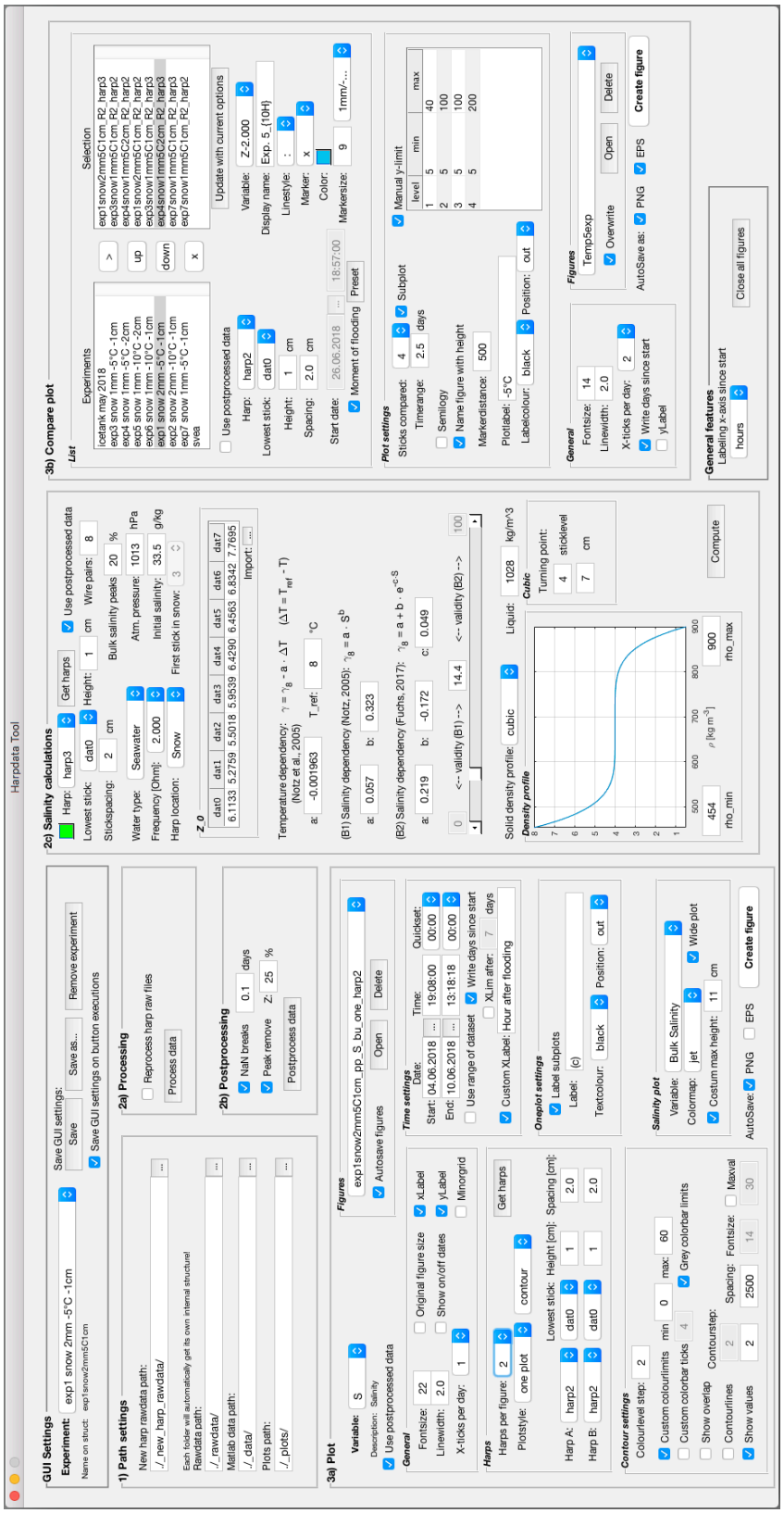

Figure A.3 *The Matlab graphical user interface that is used for the processing and plotting of the salinity harp data.*

A.4 Temperature evolution of snow frame experiments

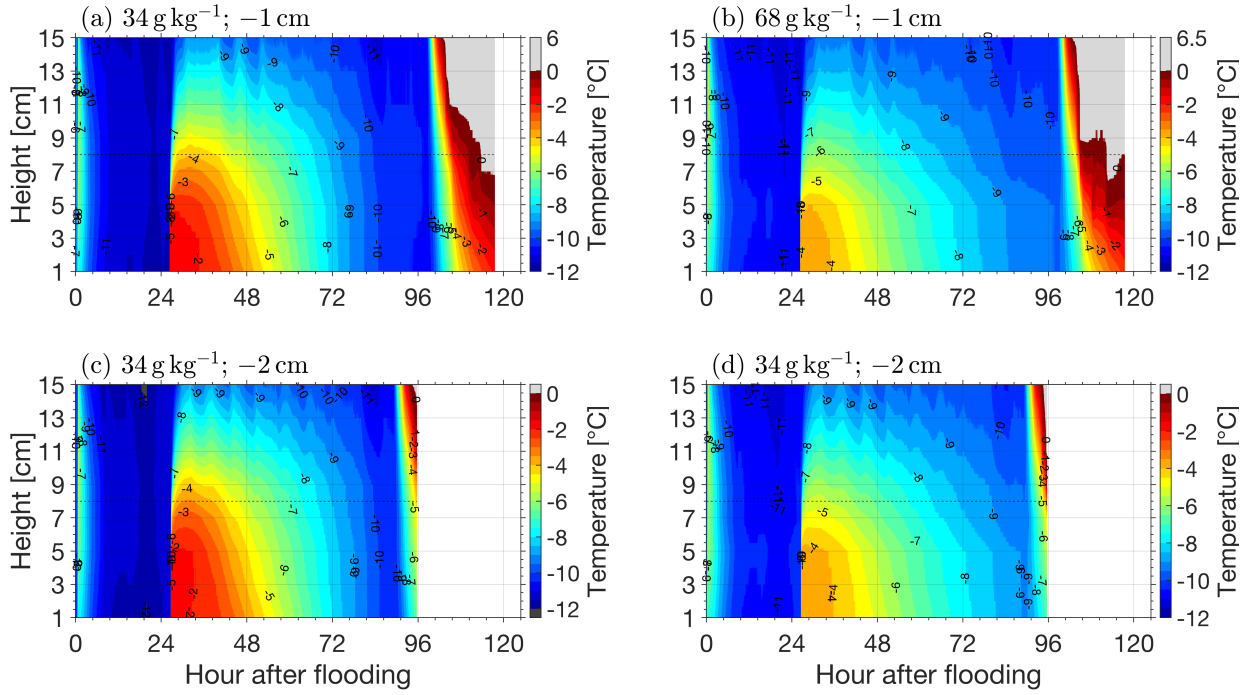

Figure A.4 *The temperature evolution of experiments at* $T_{\text{air}} = -10\,°C$ *and* $D = 0.5 - -1\,mm$*, measured by the salinity harp instrument at a vertical resolution of 2 cm and a temporal resolution of approximately 40 s With reference to Tab. 5.1: a) Experiment* $4_{10\text{L}}$*, b) Experiment* $4_{10\text{H}}$*, c) Experiment* $6_{10\text{L}}$ *and d) Experiment* $6_{10\text{H}}$*. Values for the respective salinity* S *and freeboard* h_{f} *are indicated above each panel. By reason of comparability temperature values below 0 °C are shaded in grey. Removed data or data points after the end of the experiment appear as white areas.*

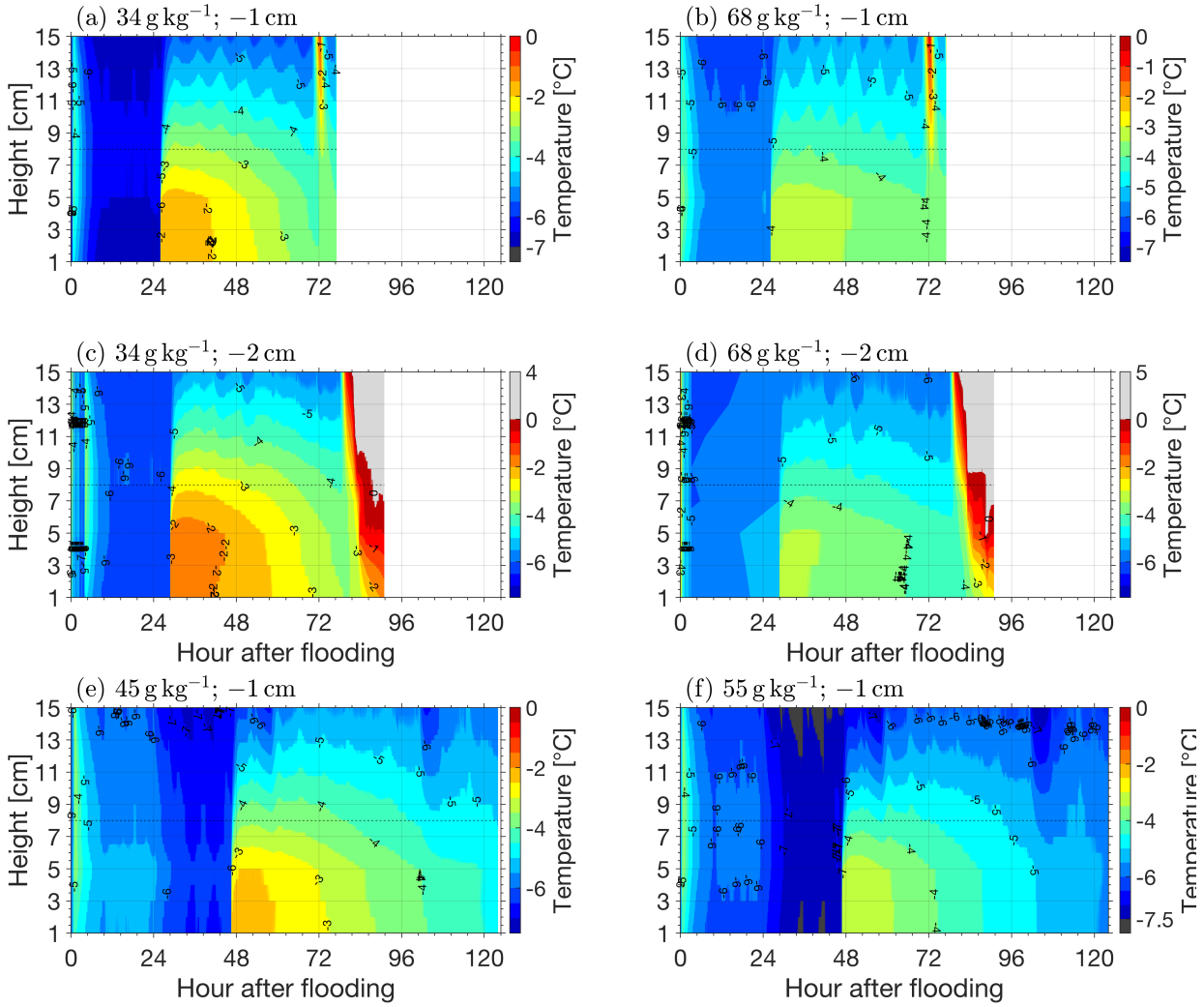

Figure A.5 *The temperature evolution of experiments at* $T_{\mathrm{air}} = -5\,°C$ *and* $D = 0.5$–$1\,mm$*, measured by the salinity harp instrument at a vertical resolution of* $2\,cm$ *and a temporal resolution of approximately* $40\,s$*. With reference to Tab. 5.1: a) Experiment* $3_{5\mathrm{L}}$*, b) Experiment* $3_{5\mathrm{H}}$*, c) Experiment* $5_{5\mathrm{L}}$*, d) Experiment* $5_{5\mathrm{H}}$*, e) Experiment* $7_{5\mathrm{L(i)}}$ *and f) Experiment* $7_{5\mathrm{H(i)}}$*. Values for the respective salinity of the flooding water* S_{w} *and freeboard* h_{f} *are indicated above each panel. By reason of comparability temperature values above* $-7.5\,°C$ *and below* $0\,°C$ *are shaded in dark and light grey. Removed data or data points after the end of the experiment appear as white areas.*

A.5 Liquid volume fraction evolution of snow frame experiments

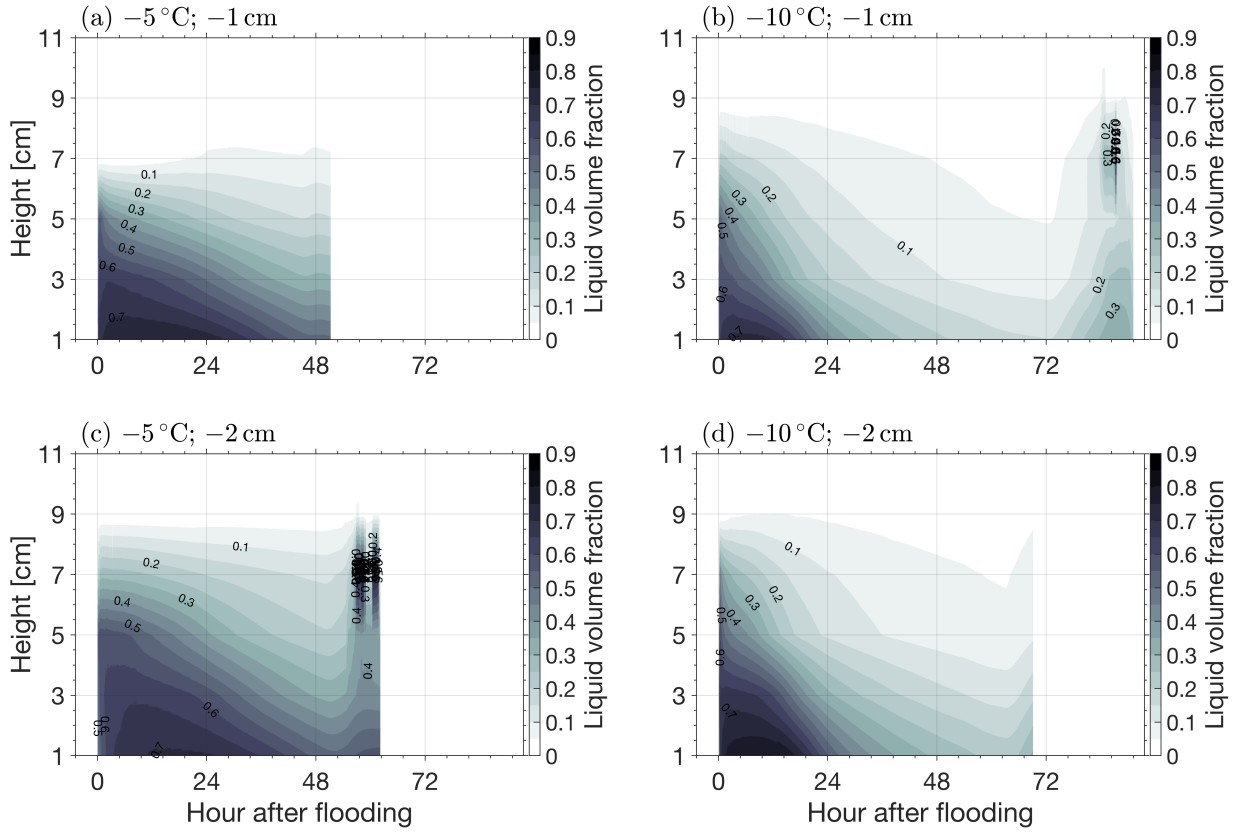

Figure A.6 *The liquid volume fraction $\phi_{\mathrm{l,v}}$ evolution of all experiments flooded with low saline saltwater at $S_{\mathrm{w}} = 34\,g\,kg^{-1}$ and $D = 0.5$–$1\,mm$, based on impedance measurements by the salinity harp instrument at a vertical resolution of 2 cm and a temporal resolution of approximately 40 s. With reference to Tab. 5.1: a) Experiment $3_{5\mathrm{L}}$, b) Experiment $4_{10\mathrm{L}}$, c) Experiment $5_{5\mathrm{L}}$ and d) Experiment $6_{10\mathrm{L}}$. Values for the respective air temperature T_{air} and freeboard h_{f} are indicated above each panel. Removed data or data points after the end of the experiment appear as white areas.*

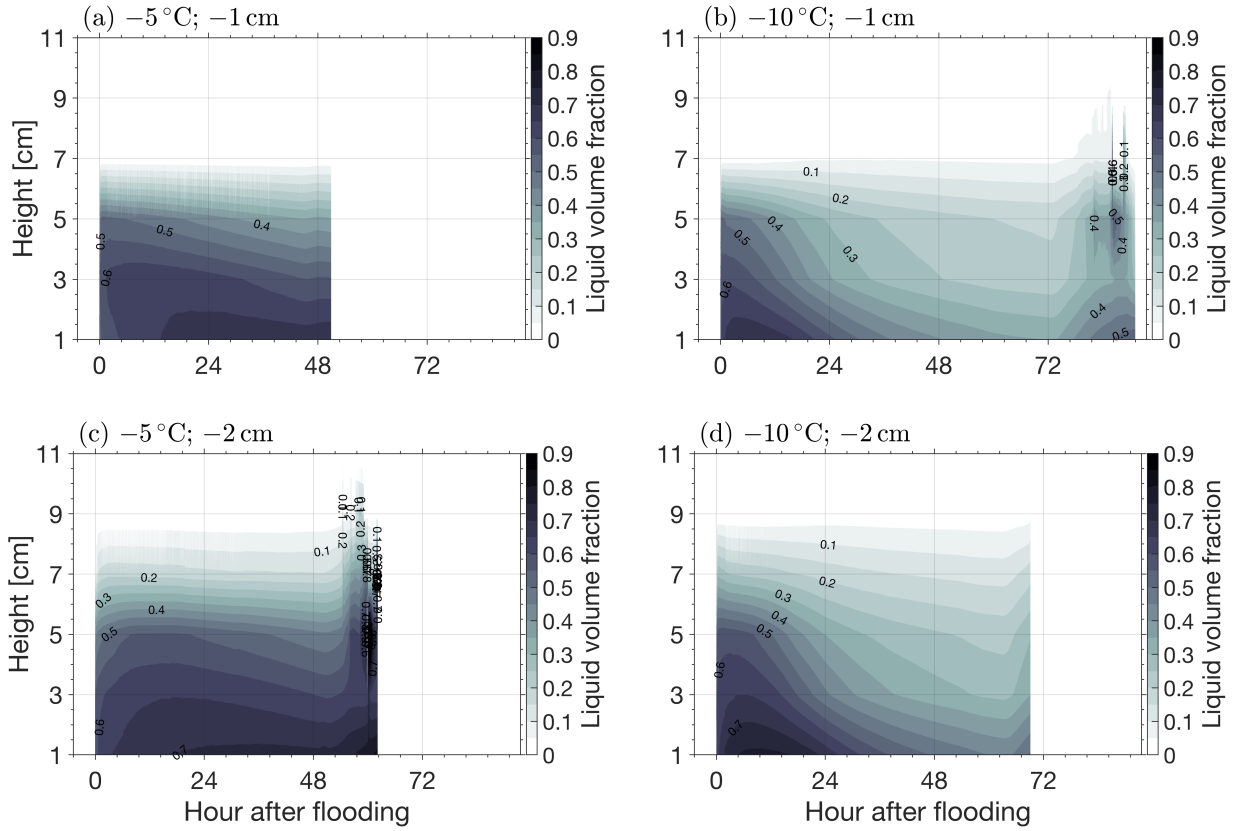

Figure A.7 *The liquid volume fraction $\phi_{\mathrm{l,v}}$ evolution of all experiments flooded with high saline saltwater at $S_{\mathrm{w}} = 68\,g\,kg^{-1}$ and $D = 0.5$–$1\,mm$, based on impedance measurements by the salinity harp instrument at a vertical resolution of 2 cm and a temporal resolution of approximately 40 s. With reference to Tab. 5.1: a) Experiment $3_{5\mathrm{H}}$, b) Experiment $4_{10\mathrm{H}}$, c) Experiment $5_{5\mathrm{H}}$ and d) Experiment $6_{10\mathrm{H}}$. Values for the respective air temperature T_{air} and freeboard h_{f} are indicated above each panel. Removed data or data points after the end of the experiment appear as white areas.*

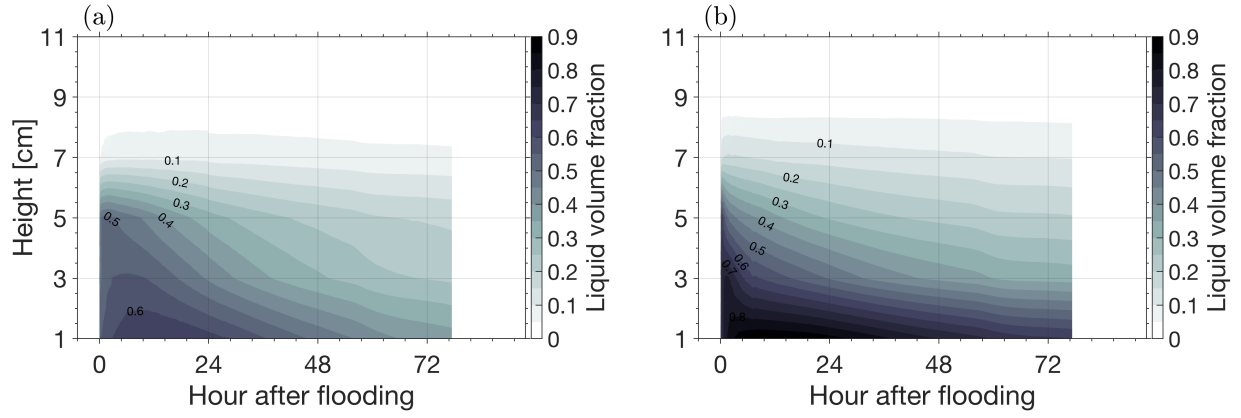

Figure A.8 *The liquid volume fraction $\phi_{\mathrm{l,v}}$ evolution of all experiments flooded with intermediate saline saltwater at a) $S_{\mathrm{w}} = 55\,g\,kg^{-1}$ and b) $S_{\mathrm{w}} = 45\,g\,kg^{-1}$, based on impedance measurements by the salinity harp instrument at a vertical resolution of 2 cm and a temporal resolution of approximately 40 s. With reference to Tab. 5.1: a) Experiment $7_{5\mathrm{L(i)}}$ and b) Experiment $7_{5\mathrm{H(i)}}$. In both experiments $D = 0.5$–$1\,mm$, $T_{\mathrm{air}} = -5\,°C$ and $h_{\mathrm{f}} = -1\,cm$. Removed data or data points after the end of the experiment appear as white areas.*

A.6 Salinity evolution of snow frame experiments

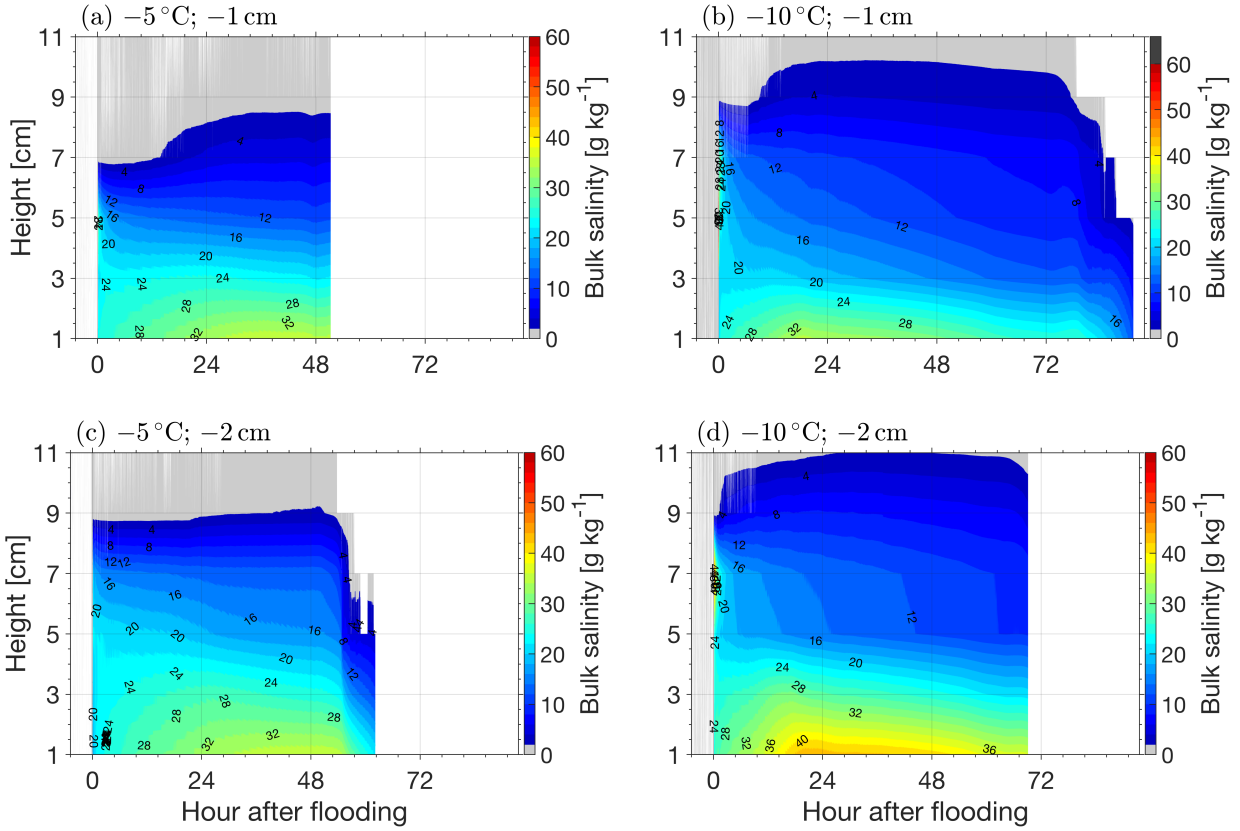

Figure A.9 *The bulk salinity S_{bu} evolution of all experiments flooded with low saline saltwater at $S_w = 34\,g\,kg^{-1}$, based on impedance measurements by the salinity harp instrument at a vertical resolution of 2 cm and a temporal resolution of approximately 40 s. With reference to Tab. 5.1: a) Experiment 3_{5L}, b) Experiment 4_{10L}, c) Experiment 5_{5L} and d) Experiment 6_{10L}. Values for the respective dominating grain size D, air temperature T_{air} and freeboard h_f are indicated above each panel. By reason of comparability values with $S_{bu} > 60\,g\,kg^{-1}$ are shown in grey. Data points with $S_{bu} < 2\,g\,kg^{-1}$ are coloured in grey for visual enhancement of the least and unaffected snow and removed data or data points after the end of the experiment appear as white areas.*

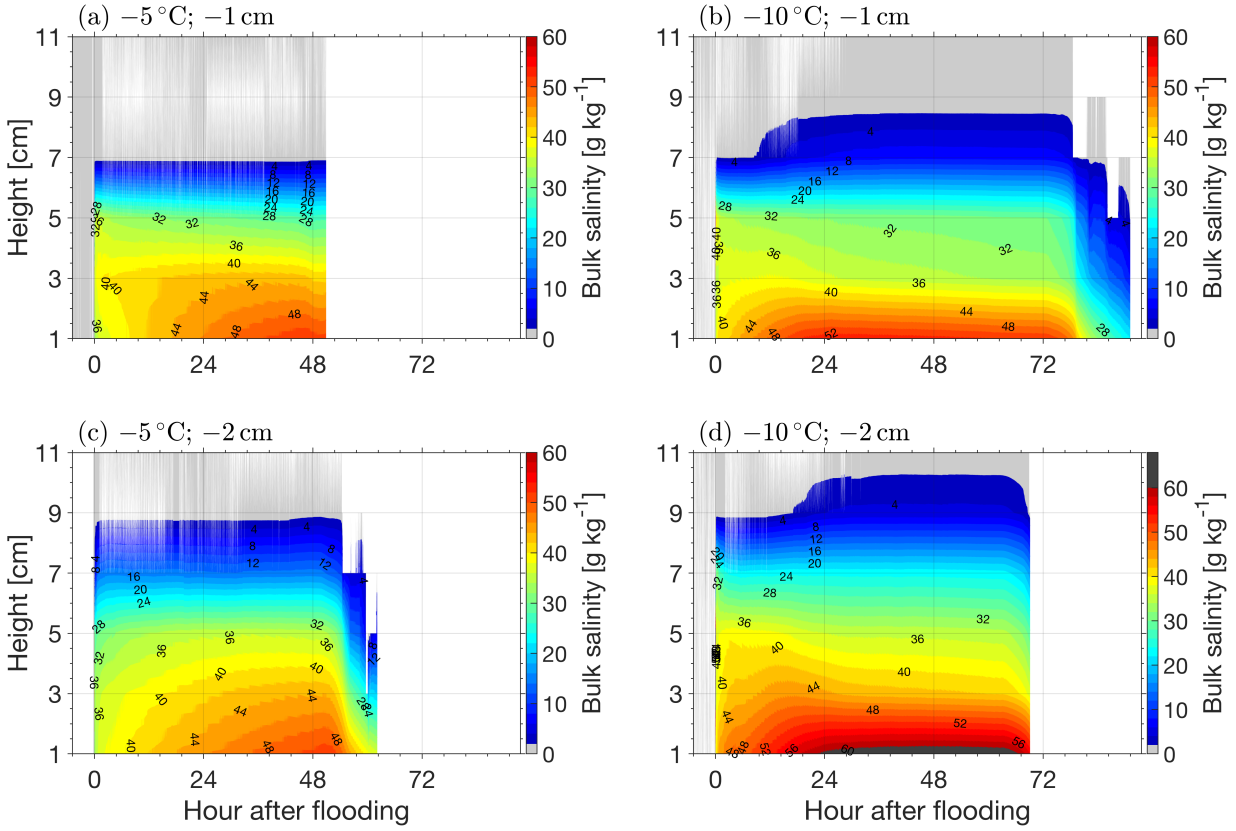

Figure A.10 *The bulk salinity S_{bu} evolution of all experiments flooded with high saline saltwater S_w = 68 g kg^{-1}, based on impedance measurements by the salinity harp instrument at a vertical resolution of 2 cm and a temporal resolution of approximately 40 s. With reference to Tab. 5.1: a) Experiment 3_{5H}, b) Experiment 4_{10H}, c) Experiment 5_{5H} and d) Experiment 6_{10H}. Values for the respective dominating grain size D, air temperature T_{air} and freeboard h_f are indicated above each panel. By reason of comparability values with S_w > 60 g kg^{-1} are shown in grey. Data points with S_{bu} < 2 g kg^{-1} are coloured in grey for visual enhancement of the least and unaffected snow and removed data or data points after the end of the experiment appear as white areas.*

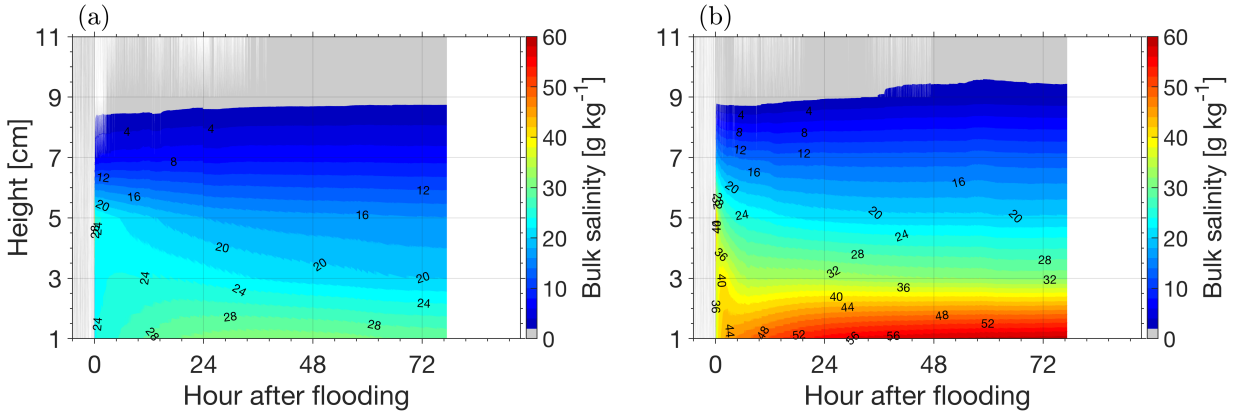

Figure A.11 *The bulk salinity S_{bu} evolution of all experiments flooded with intermediate saline saltwater at a) S_w = 45 g kg^{-1} and b) S_w = 55 g kg^{-1}, based on impedance measurements by the salinity harp instrument at a vertical resolution of 2 cm and a temporal resolution of approximately 40 s. With reference to Tab. 5.1: a) Experiment $7_{5L(i)}$ and b) Experiment $7_{5H(i)}$. In both experiments D = 0.5–1 mm, T_{air} = −5 °C and h_f = −1 cm. Data points with S_{bu} < 2 g kg^{-1} are coloured in grey for visual enhancement of the least and unaffected snow and removed data or data points after the end of the experiment appear as white areas.*

A.7 Impedance comparison

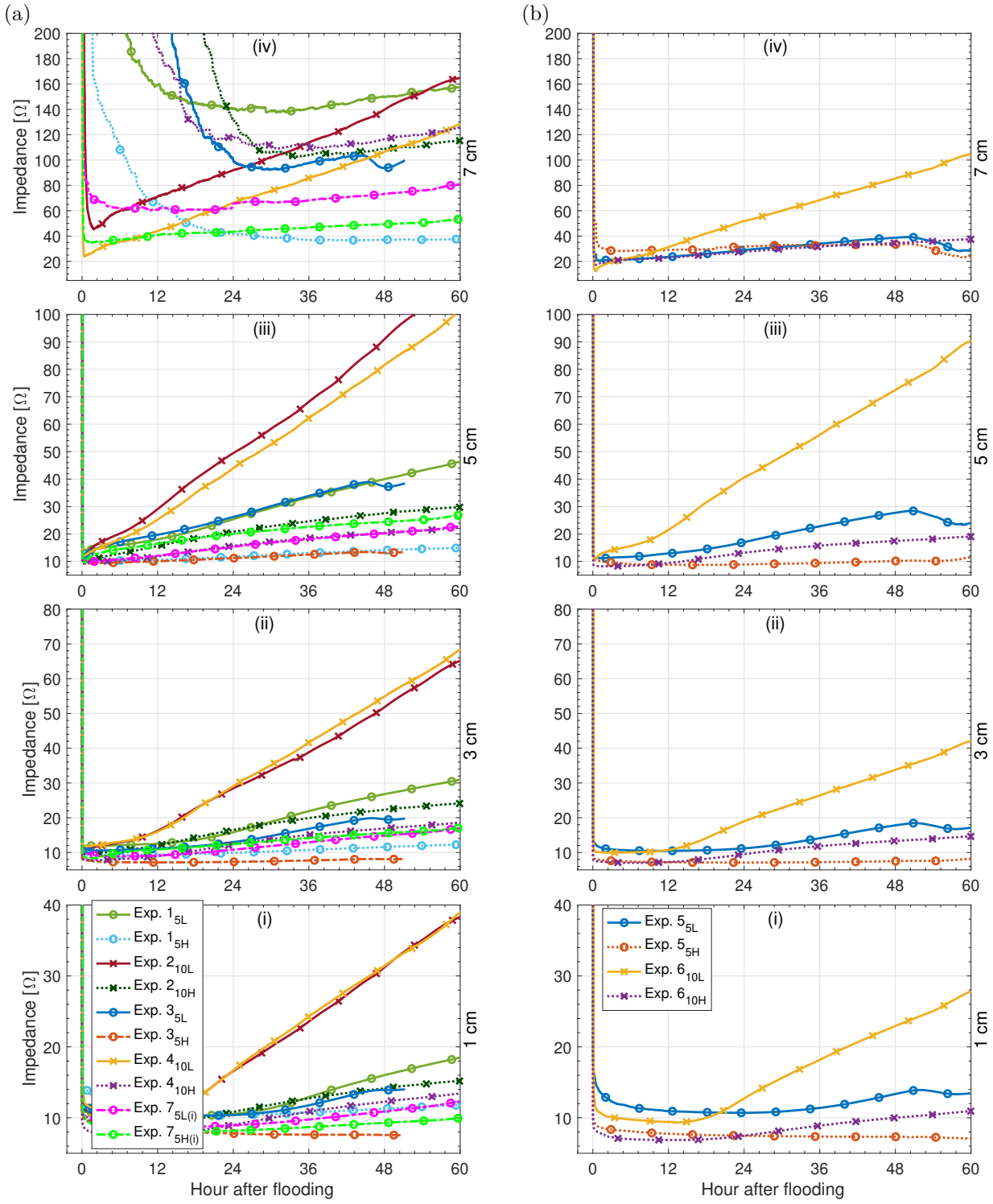

Figure A.12 *Comparison of the impedance Z per height i) 1 cm, ii) 3 cm, iii) 5 cm and iv) 7 cm at a) $h_f = -1$ cm and b) $h_f = -2$ cm . Note different y-scals. The line colour refers to the same parameters apart from h_f, the line style refers to similar salinities S_w (Experiment $7_{5L(i)}$ and $7_{5H(i)}$ considered as intermediate salinities) and the marker to the same T_{air}.*

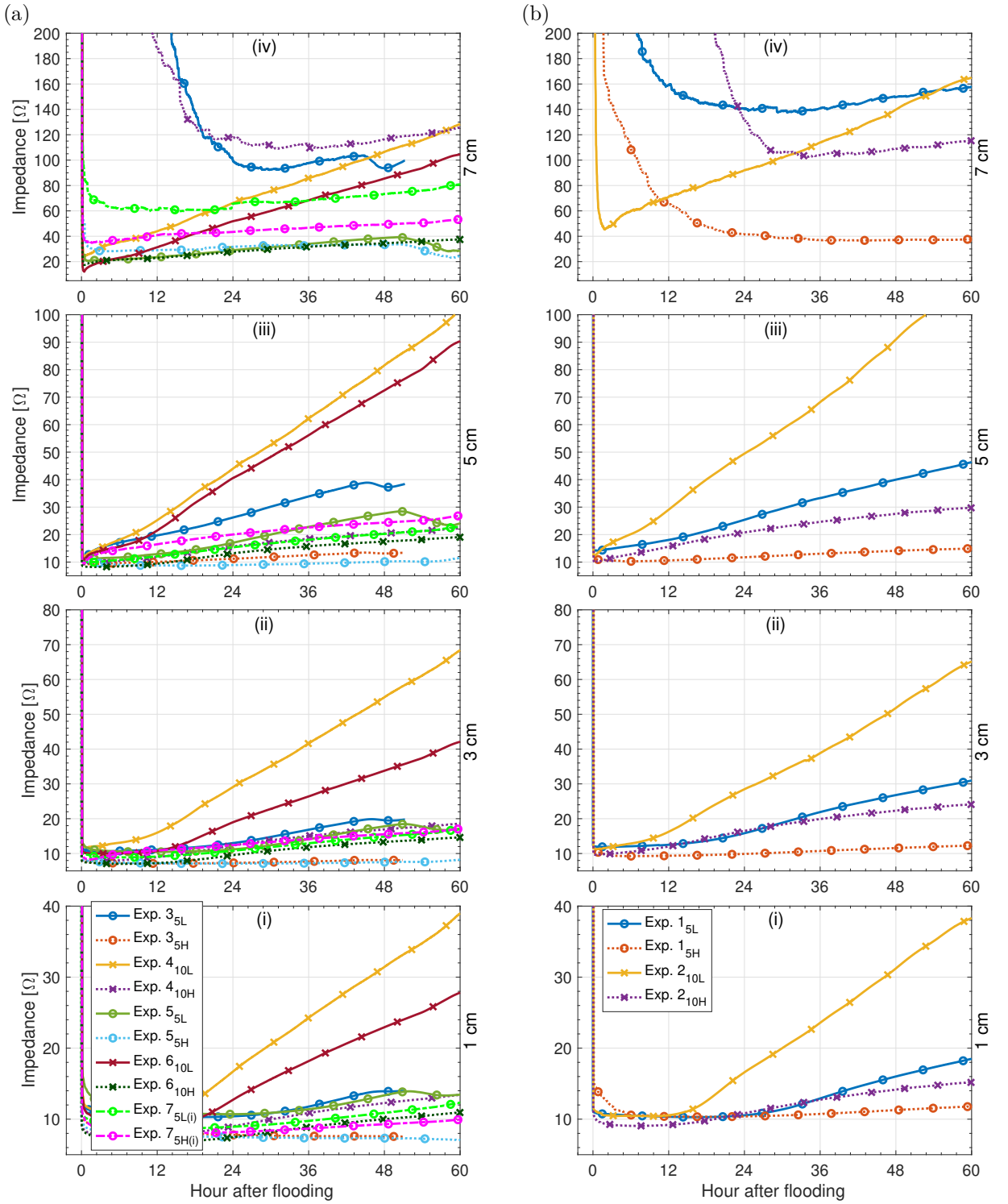

Figure A.13 *Comparison of the impedance Z per height i) 1 cm, ii) 3 cm, iii) 5 cm and iv) 7 cm at a) D = 0.5–1 mm and b) D = 1–2 mm . Note different y-scales. The line colour refers to the same parameters apart from D, the line style refers to similar salinities S_w (Experiment $7_{5L(i)}$ and $7_{5H(i)}$ considered as intermediate salinities) and the marker to the same T_{air}.*

Bibiliography

Aagaard, K., L. Coachman and E. Carmack (1981). On the halocline of the Arctic Ocean. *Deep Sea Research Part A. Oceanographic Research Papers*, **28**(6), 529 –545. doi:https://doi.org/10.1016/0198-0149(81)90115-1.

Assur, A. (1958). Composition of sea ice and its tensile strength. *Arctic sea ice*, **598**, 106–138.

Borstad, C. and D. McClung (2011). Thin-blade penetration resistance and snow strength. *J. Glaciol.*, **57**(202), 325–336. doi:10.3189/002214311796405924.

Coléou, C., K. Xu, B. Lesaffre and J.-B. Brzoska (1999). Capillary rise in snow. *Hydrol. Process.*, **13**(12-13), 1721–1732. doi:10.1002/(SICI)1099-1085(199909)13:12/13<1721::AID-HYP852>3.0.CO;2-D.

Crocker, G. and P. Wadhams (1989). Modelling Antarctic fast-ice growth. *J. Glaciol.*, **35**(119), 3–8. doi:10.3189/002214389793701590.

Doherty, B. T. and D. R. Kester (1974). Freezing-point of seawater. *J. Mar. Res.*, **32**(2), 285–300.

Eicken, H., M. A. Lange and P. Wadhams (1994). "Characteristics and distribution patterns of snow and meteoric ice in the Weddell Sea and their contribution to the mass balance of sea ice". *Annales Geophysicae*. Vol. 12. 1. Springer, 80–93.

Evans, S (1965). Dielectric properties of ice and snow–a review. *J. Glaciol.*, **5**(42), 773–792.

Fofonoff, N. P. and R. Millard Jr (1983). Algorithms for the computation of fundamental properties of seawater.

Fuchs, N. (2017). The impact of snow on sea-ice salinity. Masterthesis. Universität Hamburg.

Granskog, M. A., A. Rösel, P. A. Dodd, D. Divine, S. Gerland, T. Martma and M. J. Leng (2017). Snow contribution to first-year and second-year Arctic sea ice mass balance north of Svalbard. *J. Geophys. Res. Oceans*, **122**(3), 2539–2549. doi:10.1002/2016JC012398.

Hachikubo, A. and E. Akitaya (1997). Effect of wind on surface hoar growth on snow. *Journal of Geophysical Research: Atmospheres*, **102**(D4), 4367–4373.

Halfpenny, J. C. and R. Ozanne (1989). *Winter: an ecological handbook*. Big Earth Publishing.

Jutras, M., M. Vancoppenolle, A. Lourenço, F. Vivier, G. Carnat, G. Madec, C. Rousset and J.-L. Tison (2016). Thermodynamics of slush and snow–ice formation in the Antarctic sea-ice zone. *Deep Sea Research Part II: Topical Studies in Oceanography*, **131**, 75–83.

Kim, J. S. and A. Yethiraj (2008). The effect of salt on the melting of ice: A molecular dynamics simulation study. *The Journal of chemical physics*, **129**(12), 124504.

Lindsay, R. and A. Schweiger (2015). Arctic sea ice thickness loss determined using subsurface, aircraft, and satellite observations. *TC*, **9**(1), 269–283. doi:10.5194/tc-9-269-2015.

Martin, S. (1979). A Field Study of Brine Drainage and Oil Entrainment in First-Year Sea Ice. *J. Glaciol.*, **22**(88), 473–502. doi:10.3189/S0022143000014477.

Massom, R. A., H. Eicken, C. Hass, M. O. Jeffries, M. R. Drinkwater, M. Sturm, A. P. Worby, X. Wu, V. I. Lytle, S. Ushio, *et al.* (2001). Snow on Antarctic sea ice. *Rev. Geophys.*, **39**(3), 413–445.

Matt, F. (2014). Movement of sea-water front through snow: Model and experiment. Masterthesis. Universität Hamburg.

Millero, F. J. and W. H. Leung (1976). "Thermodynamics of seawater at one atmosphere". *Am. J. Sci.*

Notz, D. (2005). Thermodynamic and fluid-dynamical processes in sea ice. PhD thesis. University of Cambridge.

– (2012). Challenges in simulating sea ice in Earth System Models. *Wiley Interdiscip. Rev. Clim. Change*, **3**(6), 509–526. doi:10.1002/wcc.189.

Notz, D. and M. G. Worster (2008). In situ measurements of the evolution of young sea ice. *J. Geophys. Res. Oceans*, **113**(C3).

– (2009). Desalination processes of sea ice revisited. *J. Geophys. Res. Oceans*, **114**(C5).

Notz, D., J. S. Wettlaufer and M. G. Worster (2005). A non-destructive method for measuring the salinity and solid fraction of growing sea ice in situ. *J. Glaciol.*, **51**(172), 159–166.

Provost, C., N. Sennéchael, J. Miguet, P. Itkin, A. Rösel, Z. Koenig, N. Villacieros-Robineau and M. A. Granskog (2017). Observations of flooding and snow-ice formation in a thinner Arctic sea ice regime during the N-ICE2015 campaign: Influence of basal ice melt and storms. *J. Geophys. Res. Oceans*. doi:10.1002/2016JC012011.

Rösel, A., P. Itkin, J. King, D. Divine, C. Wang, M. A. Granskog, T. Krumpen and S. Gerland (2018). Thin Sea Ice, Thick Snow, and Widespread Negative Freeboard Observed During N-ICE2015 North of Svalbard. *J. Geophys. Res. Oceans*, **123**(2), 1156–1176.

SABIC (2018). *LEXAN RESIN 103*. Tech. rep. Saudi Basic Industries Corporation (SABIC).

Saloranta, T. M. (2000). Modeling the evolution of snow, snow ice and ice in the Baltic Sea. *Tellus A*, **52**(1), 93–108. doi:10.1034/j.1600-0870.2000.520107.x.

Shirtcliffe, T., H. E. Huppert and M. Worster (1991). Measurement of the solid fraction in the crystallization of a binary melt. *J. Crystal Growth*, **113**(3), 566 –574. doi:https://doi.org/10.1016/0022-0248(91)90092-J.

Sommerfeld, R. and E LaChapelle (1970). The classification of snow metamorphism. *J. Glaciol.*, **9**(55), 3–18.

Sturm, M. (1991). *The role of thermal convection in heat and mass transport in the subarctic snow cover*. Tech. rep. Cold Regions Research *and* Engineering Laboratory Hanover NH.

Sturm, M., K. Morris and R. Massom (1998). The winter snow cover of the West Antarctic pack ice: its spatial and temporal variability. *Antarctic sea ice: physical processes, interactions and variability*, 1–18. doi:https://doi.org/10.1029/AR074p0001.

Sturm, M., D. K. Perovich and J. Holmgren (2002). Thermal conductivity and heat transfer through the snow on the ice of the Beaufort Sea. *J. Geophys. Res. Oceans*, **107**(C10).

Talley, L. D. (2011). *Descriptive physical oceanography: an introduction*. Academic press.

Timco, G. and R. Frederking (1996). A review of sea ice density. *Cold Reg. Sci. Technol.*, **24**(1), 1–6.

Weast, R. C., M. J. Astle, W. H. Beyer, *et al.* (1989). *CRC handbook of chemistry and physics*. Vol. 1990. CRC press, Boca raton FL.

Acknowledgements

My first and deepest thanks go to my supervisors Chris Borstad, Dirk Notz and Frank Nilsen. I am very glad that I got all of you involved into this project after I met you first at UNIS in 2016. Thank you Chris for all your constructive feedback, an always open door for discussions and all the help for organising fieldwork, writing applications and general bureaucratic problems.
I would also like to sincerely thank you Dirk! You enabled the whole project through the supply of the salinity harps. Even though communication was remote I had helpful conversations which led me in the right direction.
My participation in the AGF-211 cruise would not have been possible without the support from Frank. Thank you very much for the possibility to join the cruise as teacher in the sea-ice group. Also thank you for the instruments and tools which I needed for the realisation of my experiments.

A particularly big thanks goes to Leif Riemenschneider. I could always call you for technical support, even from a $-20\,^{\circ}\mathrm{C}$ cold stormy measurement field on sea ice in Svalbard.
Without the funding through Arctic Field Grant by the Norwegian Research Council all my field work on Van Mijenfjorden in Svea would not have been possible. I really appreciated the opportunity, even though field measurements did not turn out as planned due to technical defects.
Furthermore, I want to thank the Geophysical Institute in Bergen (GFI) for giving me the possibility to carry out this project and to allow me to extend my master studies by acknowledging external further scientific education. I am grateful to UNIS that I could spent one year at the Geophysical Department and use the cold lab facility. Sincerely thanks the whole Geophysics department in UNIS. They were always welcoming and supportive. Thanks to all who lend me all the needed equipment to realise my laboratory experiments In this connection a huge thanks to the Logistics department for giving me access to the workshop, for your flexibility and the construction materials I was allowed to use to build all my experimental setups. I especially thank Dag Furberg Fjeld and Kåre Johansen for their helpfulness and company during a overnight session to Svea to rescue my instruments from the sea ice. I also want to thank Stefan Claes for the electrical support.

Thank you Niels Fuchs and Steffi Arndt for helpful discussions and provided material. Thank you Chris, Dirk, Bonnie and Niels for feedback on my thesis and the great suggestions and advices.

Finally, I am extremely thankful for the support of my family and the best parents in the world! Without you it would not be possible to take all these chances. Thank you Bonnie, for being the best field assistant and polar bear watch I know. I don't know what I would have done without you. You always encouraged me to continue even though things went wrong. Also thank you for all encouragement from all my friends!

Thank you! / Tusen takk!